Discovery of Small Molecule: Regulates the Cryptochrome Stability and Controls Blood Glucose Levels in Diabetic Mice

by

Saliha SÜRME

A Dissertation Submitted to the
Graduate School of Sciences and Engineering
in Partial Fulfillment of the Requirements for
the Degree of

Doctor of Philosophy

in

Molecular Biology and Genetics

KOÇ ÜNİVERSİTESİ

July, 2023

Discovery of Small Molecule: Regulates the Cryptochrome Stability and Controls Blood Glucose Levels in Diabetic Mice

Koç University

Graduate School of Sciences and Engineering

This is to certify that I have examined this copy of a doctoral dissertation by

Saliha SÜRME

and have found that it is complete and satisfactory in all respects,
and that any and all revisions required by the final
examining committee have been made.

Committee Members:

Prof. İ. Halil Kavaklı

Prof. Alper Okyar

Prof. Metin Türkay

Asst. Prof. Serkan Kır

Asst. Prof. Mehmet Tardu

Date: 27 July 2023

To my beloved family, you are the foundation upon which my life is built. Your unwavering love, presence, and support have shaped me into the person I am today. I am eternally grateful for the countless memories we have created together, and I cherish the bond we share that withstands the test of time. Mom, Dad and Burki...

ABSTRACT

Discovery of Small Molecule: Regulates the Cryptochrome Stability and Controls Blood Glucose Levels in Diabetic Mice

Saliha SÜRME

Doctor of Philosophy in Molecular Biology and Genetics

July, 2023

The circadian rhythm controls the behavioral, biochemical, and physiological variables in most living organisms, from bacteria to mammals. The circadian rhythm is an endogenous, the most well-known biological rhythm, and refers to a 24-hour cycle that regulates various physiological processes like hormone secretion, food intake, sleep-wake cycles, body temperature regulation, and metabolism. These rhythmic oscillations are maintained by the internal biological clocks.

The mammalian circadian clock mechanism is endogenous, although it is synchronized with the environmental cues through the suprachiasmatic nuclei (SCN) located in the anterior part of the hypothalamus. Circadian clock disruption influences metabolic health and is closely associated with many diseases, including sleep disorders, neurological conditions, immune dysregulation, obesity, diabetes, and cancer.

Cryptochromes (CRYs), one of the core clock proteins, are transcriptional repressors of the circadian clock in mammals. The stability of CRYs is important because of the ability to alter the period and amplitude of the circadian rhythm.

The gluconeogenesis pathway is regulated by a variety of factors, including hormones such as glucagon and insulin and the circadian clock mechanisms. On the molecular level, CRY interacts directly with the glucagon-mediated G-protein coupled receptors, in turn, inhibits the gluconeogenesis pathway that controls glucose metabolism.

Therefore, we aimed to discover small organic molecules which increase the stability of CRYs and inhibit gluconeogenesis. Such molecules could be used as anti-diabetic drugs, which control blood glucose levels. To this end, we used a structure-based drug design approach against the primary pocket of CRY, which is responsible for their degradation.

Around 2 million small molecules with non-characterized functions were screened through molecular docking in silico. The candidate small molecules with binding free energy lower than -8.5 kcal/mol were tested for cellular toxicity and their effects on CRYs stability, circadian clock, and gluconeogenesis.

We identified a novel molecule, TW68, which increases the stability of both CRY1 and CRY2, lengthens the period of circadian rhythm, and represses gluconeogenic genes in further characterization of pre-clinical studies. In transgenic and fat-induced diabetic animal models, TW68 regulated the fasting blood glucose levels in biochemical and physiological studies. These results signify the therapeutic potential of TW68, a CRY stabilizer, on the circadian clock – gluconeogenesis-related metabolic diseases, including type 2 diabetes mellitus.

ÖZETÇE

Küçük Molekülün Keşfi: Diyabetik Farelerde Kriptokrom Kararlılığını Düzenler ve Kan Şekeri Seviyesini Kontrol Eder

Saliha SÜRME

Moleküler Biyoloji ve Genetik, Doktora

Temmuz, 2023

Sirkadiyen ritim, bakterilerden memelilere kadar çoğu canlı organizmada davranışsal, biyokimyasal ve fizyolojik değişkenleri kontrol eder. Sirkadiyen ritim içsel bir biyolojik ritimdir ve hormon salgılanması, besin alımı, uyku-uyanıklık döngüleri, vücut ısısının düzenlenmesi ve metabolizma gibi çeşitli fizyolojik süreçleri düzenleyen 24 saatlik bir döngüyü ifade eder. Bu ritmik salınımlar biyolojik saat tarafından control edilir.

Memeli sirkadiyen saat mekanizması, hipotalamusun ön kısmında yer alan suprakiazmatik çekirdek (SCN) aracılığıyla çevresel ipuçlarının varlığında senkronize olur. Sirkadiyen saatin bozulması metabolizmayı etkiler ve uyku bozuklukları, nörolojik hastalıklar, bağışıklık sisteminde düzensizlik, obezite, diyabet ve kanser gibi birçok hastalığın oluşmasına neden olabilir.

Çekirdek saat proteinlerinden biri olan kriptokromlar (CRY'ler), memelilerde sirkadiyen saatin transkripsiyonel baskılayıcılarıdır. CRY'lerin stabilitesi, sirkadiyen ritmin periyodunu ve genliğini değiştirebilme özelliği nedeniyle önemlidir. Glikoneogenez yolağı; glukagon ve insülin gibi hormonlar ve sirkadiyen saat mekanizması dahil olmak üzere çeşitli faktörler tarafından düzenlenir. Moleküler düzeyde CRY, doğrudan glukagon aracılı G-protein bağlı reseptörlerle etkileşime girer ve ardından glikoz metabolizmasını kontrol eden glukoneogenez yolağını inhibe eder.

Bu nedenle biz bu çalışmada, CRY'lerin stabilitesini artıran ve glukoneogenezi inhibe eden küçük organik molekülleri keşfetmeyi amaçladık. Bu tür moleküller, kan şekeri seviyelerini kontrol eden anti-diyabetik ilaçlar olarak kullanılabilir. Karakterize edilmemiş işlevlere sahip yaklaşık 2 milyon küçük molekül, hesaplamalı çalışmalar aracılığı ile tarandı. Bağlanma enerjisi -8.5 kcal/mol'den daha düşük olan aday moleküller, hücresel toksisite CRY stabilitesi, sirkadiyen saat ve glukoneogenez üzerindeki etkileri açısından test edildi.

Hem CRY1 hem de CRY2'nin stabilitesini artıran, sirkadiyen ritim periyodunu uzatan ve klinik öncesi karakterizasyon çalışmalarında glukoneojenik genleri baskılayan özgün bir molekül olan TW68 keşfedildi. Genetik ve yağlı beslenmeye dayalı diyabetik hayvan modellerinde yapılan biyokimyasal ve fizyolojik çalışmalarda TW68 insülin seviyesini azaltmış ve açlık kan şekeri seviyesini düzenlemiştir. Bu sonuçlar ile, CRY stabilizatörü olan TW68'in, tip 2 diyabet de dahil olmak üzere sirkadiyen saat ve glukoneogenez ile ilişkili metabolik hastalıklar üzerindeki terapötik potansiyeli olduğu gösterilmiştir.

ACKNOWLEDGEMENTS

Completing a Ph.D. thesis is a challenging task that requires years of hard work, dedication, and a strong mindset. This accomplishment could not have been possible without the contributions and support of many people, and I would like to take this opportunity to express my sincere gratitude to all of them.

First and foremost, I would like to express my deepest appreciation to my advisor Prof. İ. Halil Kavaklı, for providing me with guidance, support, and encouragement throughout my research journey. I would like to thank my supervisor Asst. Prof. Şeref Gül, for invaluable insights, constructive feedback, and support. Your mentorship since the day I arrived has been instrumental to me, and I am sincerely grateful.

I would also like to thank the members of my thesis committee, Prof. Alper Okyar, Prof. Metin Türkay, Asst. Prof. Serkan Kır, and Asst. Prof. Mehmet Tardu, for their insightful feedback and critical comments on my research. Your contributions have greatly enriched my research, and I appreciate your time and effort in evaluating my work.

I am also grateful to the former and current Kavaklı Lab members who have supported me in various ways, including providing feedback on my research, sharing their expertise, and offering me their friendship along with the opportunity to be myself. Your support, friendship, and contributions have made this journey even more enjoyable and memorable, and I am thankful for your presence in my life.

My research would not have been possible without the generous funding provided by TÜBİTAK (KBAG 116Z312 and SBAG 217S027) and Koç University. I am grateful for their support, which allowed me to carry out my research.

I would also like to thank my family for their unconditional love and support throughout my academic journey. Their encouragement, understanding, and sacrifices have been a constant source of my motivation, and I am lucky to have you.

TABLE OF CONTENTS

LIST OF TABLES

LIST OF FIGURES

ABBREVIATIONS

AMP Adenosine monophosphate

AMPK AMP-activated protein kinase

ARNTL Aryl hydrocarbon receptor nuclear translocator-like protein

ATP Adenosine triphosphate

bHLH Basic helix-loop-helix

BMAL1 Component Brain and muscle Arntl-1 like

cAMP Cyclic adenosine monophosphate

CCE Clock-controlled elements

CCG Clock-controlled genes

CK1 Casein kinase 1

CLOCK Circadian locomotor output cycles kaput

CR Circadian Rhythm

CRSD Circadian Rhythm Sleep Disorders

CRE Cyclic AMP response element

CREB CRE-binding protein

CRY Cryptochrome

CT Circadian Time

DBP D-box binding protein

DKO Double knockout

DMEM Dulbecco's modified Eagle's Medium

DMSO Dimethyl sulfoxide

DSPD Delayed sleep phase disorder

DYRK1A Dual-specificity tyrosine-phosphorylated and regulated kinase 1A

DXM Dexamethasone

EC50 Half maximal effective concentration

FAD Flavin adenine dinucleotide

FASPS Familial advanced sleep phase syndrome

FBS Fetal bovine serum

FBXL F-box/LRR-repeat protein

G6pc Glucose-6-phosphatase

GPCR G-protein-coupled receptor

GSK-3β Glycogen synthase kinase 3β

Glut2 Hepatic glucose transporter 2

HEK293T Human embryonic kidney HEK293T cell line

HEPES N-2-hydroxyethylpiperazine-n'-2-ethanesulfonic acid

HRP Horseradish peroxidase

i.p. Intraperitoneal

ISWR Irregular sleep-wake rhythm

LD Light-dark

LUC Luciferase

MAPK Mitogen-activated protein kinase

MTD Maximum tolerated dose

MTT 3-(4,5-dimethylthiazol-2-yl)-2,5-diphenyltetrazolium bromide

NIH3T3 Mouse embryo fibroblast NIH3T3 cell line

NPAS2 Neuronal PAS domain protein 2

PAS Per-Arnt-Single-minded

PBS Phosphate-buffered saline

PER Period

PHR Photolyase homology region

PIC Protease inhibitor cocktail

Pck1 Phosphoenolpyruvate carboxykinase

p.o. Per os, orally

REM Rapid eye movement

REV-ERB Nuclear receptor subfamily 1, group D

ROR Retinoic acid-related orphan nuclear receptors

RT-qPCR Real-time – quantitative polymerase chain reaction

SCN Suprachiasmatic nuclei

SDT Single dose toxicity

SDS-PAGE Sodium dodecyl sulfate - Polyacrylamide gel electrophoresis

SEM Standard error of the mean

SKP1 S-Phase kinase associated protein 1

SUMO Small ubiquitin-like modifier

TBS Tris-buffered saline

TTFL Transcriptional-translational feedback loop

U2OS Human osteosarcoma U2OS cell line

WT Wild type

ZT Zeitgeber time

Chapter 1

INTRODUCTION

Biological rhythms are fundamental for the proper functioning of various physiological and behavioral processes in organisms. The circadian rhythms regulate the daily routine of metabolic activities such as hormone release, sleep-wake cycles, immune response, and numerous other physiological activities. There are other biological rhythms besides the circadian rhythm, ultradian, and infradian rhythms. The ultradian rhythms refer to occur more frequently than once per day, such as heartbeat, breathing rate, and feeding behavior. The infradian rhythms, on the other hand, refer to occurring less frequently than once per day, such as the menstrual cycle, hibernation, seasonal changes in behavior and physiology.

The circadian rhythm is regulated by the circadian clock, which is in the suprachiasmatic nucleus (SCN) of the hypothalamus. The SCN is responsible for synchronizing the circadian rhythms throughout the body via neuronal, hormonal, and metabolic signaling pathways as well as environmental changes. The circadian clock mechanism is composed of a transcriptional-translational regulatory feedback loop (TTFL) at the molecular level. Through a loop, the transcription factors BMAL1 (Brain and muscle Arnt-like protein-1) and CLOCK (circadian locomotor output cycles kaput) activate the transcription of core clock genes, including *CRY1*, *CRY2, PER1,* and *PER2*. CRY (Cryptochrome) and PER (Period) proteins interact in the cytoplasm and then translocate back to the nucleus, where they suppress the activity of BMAL-1:CLOCK and, subsequently, their own expression.

The stability of CRY proteins plays an important role in the period and amplitude of the circadian rhythm. The ubiquitin ligases SCF-FBXL3 and SCF-FBXL21 maintain the stability and degradation of the CRY1 and CRY2 proteins in the nucleus and cytoplasm, respectively. Previous research has shown that the process of glucagon-induced gluconeogenesis and cAMP production is inhibited by increasing CRY1 protein levels in mammals. The relationship between CRY proteins and the gluconeogenesis pathway can be taken advantage of to identify small organic compounds for the treatment of type 2 diabetes and other disorders linked to glucose metabolism.

In this thesis, small molecules that regulate CRY stability were discovered by utilizing the structure-based drug design method, and one best fit, CRY stabilizer, TW68, was further characterized for its effects on the circadian clock and gluconeogenesis in vivo. The TW68 stabilized both CRY1 and CRY2, lengthened the period in cell-based circadian rhythm analysis, was well tolerated by C57BL/6J mice, and showed an excellent pharmacokinetic profile when orally administrated.

Furthermore, TW68 reduced the blood glucose levels in transgenic Lep ob/ob and fat-induced diabetic mice under fasting conditions by increasing the stability of CRYs and reducing the transcriptional levels of gluconeogenetic genes, *Phosphoenolpyruvate carboxykinase 1* (*Pck1)* and *Glucose-6-phosphatase* (*G6pc)*. All these results showed that TW68 has anti-diabetic effects in both in vitro and in vivo and indicated the therapeutic potency of TW68 in order to control fasting blood glucose levels in diabetes mellitus.

In Chapter 2, background information about the biological rhythms, the molecular mechanism of the mammalian circadian clock, its importance, and the diseases associated with circadian clock impairment were reviewed.

Chapter 3 provides all the materials and methods that were used in this thesis. Statistical analysis, in vitro and in vivo experimental procedures were explained in detail.

In Chapter 4, all the results obtained in this thesis were presented, and these results were discussed in Chapter 5 with concluding remarks, and potential therapeutic usage of TW68.

Chapter 2

LITERATURE REVIEW

2.1. Biological Rhythms and Clock

During the rotation of the Earth around its own axis and the sun, different parts of the planet are exposed to sunlight, which causes daylight in some areas and darkness in others. This cycle of light creates the 24-hour day and night cycle and contributes to the generation of tidal, lunar, and seasonal cycles [1]. Organisms have developed biological rhythms [2, 3] to adapt to the light and temperature changes in nature and utilize the available resources in the most efficient way [4, 5]. Light and temperature are the most dominant time-givers, also known as zeitgeber in German, which entrains the circadian clock mechanism. The timing, duration, and intensity of light exposure can affect biological rhythms [6, 7].

Approximately 24-hour rhythms govern a wide range of physiological and behavioral processes in organisms ranging between bacteria and fungi to humans [8]. The circadian rhythm is a biological mechanism that underlies these 24-hour periodic processes [9]. The main function of the circadian rhythm is to coordinate the phase of biological events to a specific feature of the environmental cycle and to ensure that the phase of multiple rhythmic events within the organism is appropriately coupled [10]. There are other biological rhythms alongside the circadian rhythm, which are ultradian and infradian rhythms.

Ultradian rhythms that occur with a frequency of more than one cycle in 24 hours [11], such as the sleep cycle of non-rapid eye movement (NREM) and rapid eye movement (REM) sleep stages that occur in cycles of around 90-120 minutes throughout the night, body temperature fluctuations, heartbeat, breathing rate, and the feeding cycle which occur several times a day. Infradian rhythms that occur with a frequency of less than one cycle in 24 hours, typically with a cycle length of days, weeks, or months such as the

menstrual cycle [12], seasonal changes in breeding behavior [13], hibernation, and migration [14, 15].

Circadian rhythms are generated by the body's internal clock, the suprachiasmatic nucleus (SCN), located in the brain and synchronized with external cues [16], such as light-dark cycles, temperature changes, and social cues [17, 18]. All these biological rhythms are important for maintaining homeostasis and regulating the timing of numerous physiological processes, such as sleep-wake cycles, immune response, hormone release, and metabolism [19, 20]. Circadian rhythms get the most attractive to researchers in the last decades among these types of biological rhythms.

2.2. Characteristics of Circadian Rhythm

There are three primary features of circadian rhythms: period, amplitude, and phase, which describe the duration, variation, and timing of the different phases of the cycle. Circadian rhythm requires fitting with some characteristic features that maintain the endogenous oscillations with 24-hour periods even though the absence of environmental [21] and social cues, compensating the changes in physiological temperature [22], and entraining by the environmental signals such as light exposure, feeding behavior, emotional mood, and social interactions which reset the cycle [23, 24].

Period refers to the amount of time it takes for one complete cycle of the circadian rhythm. In humans, the typical period is about 24.2 hours, which is also known as free running when they are isolated from the environment; on the other hand, it is around 23.5 hours in mice [25]. This discrepancy is corrected by exposure to external cues, such as light and social interaction, which help to reset the internal clock and keep it synchronized with the external environment. In some cases, however, the period may be shorter or longer than 24 hours, which can lead to circadian rhythm disorders, including delayed sleep phase syndrome or non-24-hour sleep-wake disorder [26, 27].

Amplitude indicates the degree of variation in a particular physiological or behavioral process over the course of a 24-hour period. For example, the amplitude of the sleep-wake cycle refers to the difference between the amount of time spent asleep versus awake

during a 24-hour period. The amplitude of circadian rhythms can be influenced by a variety of factors, including genetics, age [28], and environmental cues.

Timing, length, and quality of sleep are just a few of the numerous changes associated with aging. To control the organization of human sleep, the circadian timing system works in conjunction with a sleep-wake homeostatic system [29, 30]. In general, a healthy circadian rhythm will have a strong amplitude, meaning that there is a clear distinction between the different phases of the cycle.

Phase can be explained as the timing of a particular physiological or behavioral process within the 24-hour circadian cycle. The phase of the sleep-wake cycle refers to the time of day when humans are most likely to fall asleep and wake up. The phase of circadian rhythms can be regulated by external cues such as light and social interaction, as well as internal factors such as hormone release and metabolism.

The scientific discipline of chronobiology investigates adaptations to geophysical cycles [31]. Chronobiology frequently uses a unique timing system named Circadian Time (CT) is a special timing commonly used in chronobiology [32]. It is used to describe the free-running endogenous timing of the organism unaffected by external cues (zeitgebers). For humans, the active phase begins at CT 0, which is the light phase, whereas in nocturnal species like mice, the active phase begins at CT 12, which is the dark phase. Another system that is defined in relation to environmental cues is Zeitgeber Time (ZT). The light phase of this system begins with sunrise (ZT 0) and lasts until sunset (ZT 12), which is the dark phase. When the internal clock is out of sync with the external environment, it may lead to circadian rhythm disorders such as jet lag or shift work disorder [33]. Understanding these features is essential for maintaining a healthy circadian rhythm and preventing circadian rhythm disorders.

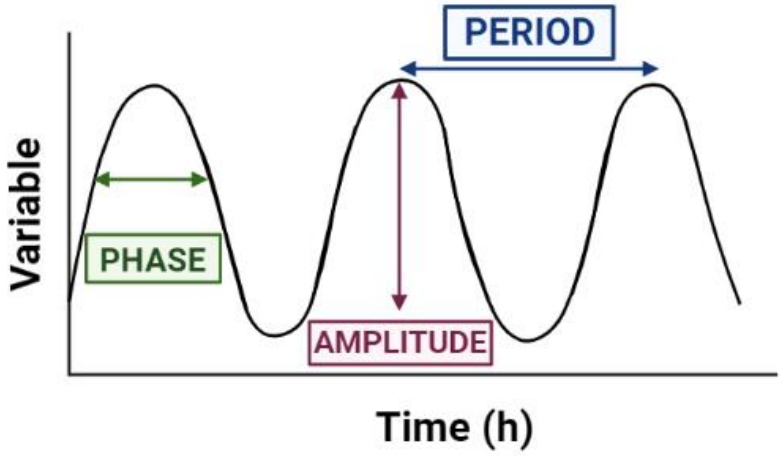

Figure 2. 1: Period, amplitude, and phase are the main characteristics of Circadian Rhythm. This figure was created with BioRender: Scientific Image and Illustration Software, BioRender.com.

2.3. Importance of Circadian Clock

The term "circadian" is derived from the Latin word "circa diem," which means "about a day," indicating that this clock is a 24-hour cycle. The circadian clock is a biological mechanism that controls the timing of various physiological and behavioral processes in most living organisms, including humans [34].

One of the most crucial roles of the circadian clock is the regulation of the sleep-wake cycle. As diurnal mammals, our bodies are naturally programmed to feel sleepy at night and alert during the day. The circadian clock synchronizes the secretion of the hormone melatonin, which is responsible for promoting sleep, with the natural light-dark cycle [35, 36]. When the circadian rhythm is disrupted, such as during shift work or jet lag, our sleep patterns are disrupted, leading to fatigue, insomnia, and other sleep disorders [37]. Chronic disruption of the circadian clock has also been linked to an increased risk of several diseases, including obesity, diabetes, cardiovascular disease, and cancer.

The circadian clock also plays an important role in regulating metabolism. Many metabolic processes, including glucose uptake [38] and insulin secretion [39], are synchronized with the circadian rhythm. Disruption of the circadian clock has been associated with a high risk of obesity and type 2 diabetes, as well as other metabolic disorders.

Another important aspect of the circadian clock is its role in regulating the immune system. The circadian clock controls the timing of immune cell migration, cytokine release, and other immune functions, helping to optimize immune responses and defend against infections. Disruption of the circadian clock can lead to an increased susceptibility to infections [40], inflammatory diseases, and other immune-related disorders [41, 42].

Moreover, the circadian clock is also essential for cognitive functions such as learning, memory, and attention. Studies have shown that the circadian rhythm affects cognitive performance, and disruption of the circadian clock can lead to impaired cognitive function [43], including decreased attention, memory [44], and learning ability [45]. It is essential to maintain a healthy circadian rhythm to prevent various diseases and promote overall well-being.

2.4. The Central and Peripheral Circadian Clocks in Mammals

In mammals, there are two primary components of the circadian clock: the central clock and the peripheral clock. The central clock, also known as the master clock, is located in the suprachiasmatic nucleus (SCN) of the anterior part of the hypothalamus in the brain. The SCN serves as the primary regulator of the circadian rhythm. It receives input from specialized cells in the retina that detect light through hypothalamic photoreceptors and transmit the signals to the brain, helping to synchronize the clock with the 24-hour light-dark cycle [46]. After the information reaches the SCN, behavioral and physiological changes occur in the organism by changing the expression of certain genes, affecting certain hormones and behavioral patterns. This can be explained by exposure to bright light in the morning can help reset the clock and improve sleep quality, while exposure to light at night can disrupt circadian rhythms and interfere with sleep.

The central circadian clock is also responsible for synchronizing many peripheral clocks throughout the body [47]. However, recent research has shown that peripheral clocks also play an essential role in regulating various physiological functions [48, 49] and helps to fine-tune the overall circadian rhythm. Peripheral clocks are located in various tissues and organs, including the liver, pancreas, adipose tissue, heart, and lungs [47, 50]. These peripheral clocks are also capable of generating a circadian rhythm, which can be influenced by the central clock in the SCN by sending feedback signals, as well as by environmental cues such as food intake and physical activity [51].

The peripheral clocks help to regulate local processes in each tissue or organ, such as neural, hormonal, and metabolic signals, gene expression, and cell proliferation, thus ensuring that these processes are synchronized with the overall circadian rhythm [52]. For instance, the liver clock regulates glucose and lipid metabolism [53], while the adipose tissue clock [54] regulates lipid storage and release. The skeletal muscle clock regulates energy metabolism, muscle regeneration, and protein synthesis. Disruptions to peripheral clocks due to irregular meal timing or changes in the timing of physical activity can lead to metabolic disturbances and other health problems.

Peripheral clocks also play a crucial role in regulating the immune system. The immune system contains a variety of immune cells that are under the control of the circadian clock, and the timing of immune cell migration, cytokine release [55], and other immune functions are regulated by the peripheral clocks [56]. Therefore, understanding the importance of central and peripheral clocks and how they function is essential for maintaining a healthy circadian rhythm and preventing various diseases.

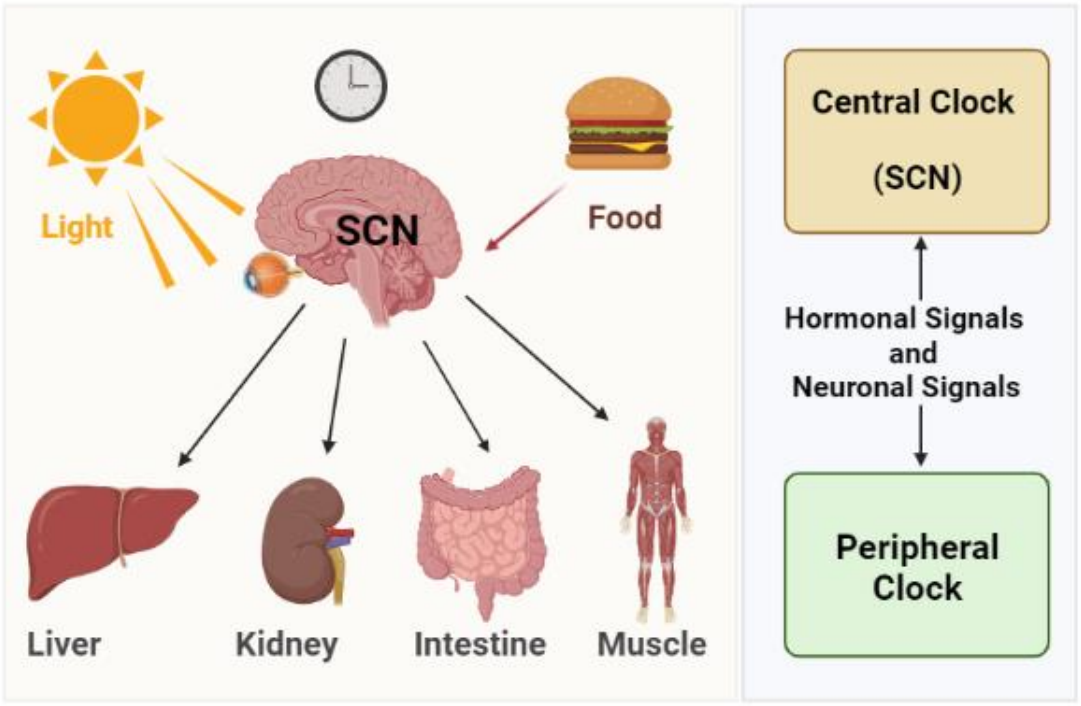

Figure 2. 2: Schematic representation of the synchronization of the central clock (SCN) and peripheral clocks by environmental factors. This figure was adapted from [50, 51] and created with BioRender: Scientific Image and Illustration Software, BioRender.com.

2.5. Molecular Components of Circadian Clock

Research into circadian rhythm has a long history, and many studies have explored its underlying mechanisms, its effects on health, and potential therapeutic interventions. Circadian rhythms are controlled by a network of genes. A key breakthrough in the understanding of the circadian clock came in the 1970s when behavioral geneticists discovered a *period* (*per*) gene in *Drosophila melanogaster* [57]. Through searching mutant fruit flies for clock genes, Konopka and Benzer discovered the *period* gene. Three mutants, one with a shorter period of 19 hours, one with a longer period of 28 hours, which were different from the normal period of 24 hours, and one with an arrhythmic phenotype with no periodicity, showed abnormal circadian rhythm. These three mutations were all located in the *period* gene on the single allele of the X chromosome.

A decade after this discovery, developed DNA sequencing technologies allowed the isolation and characterization of the *period* gene by Rosbash, Hall, and Young [58-61], which this study earned them the 2017 Nobel Prize in Physiology or Medicine. Further research on *Drosophila melanogaster* showed that both mRNA of *period* and PERIOD protein oscillates in the brain of *Drosophila melanogaster* within 24 hours [62, 63].

In 1994, another important core clock gene was identified by Takahashi and his group, named *Clock* "the Circadian Locomotor Output Cycles Kaput" in *Mus musculus* [64]. The group screened mutant mice, and the *Clock* gene was characterized by a period-lengthening mutation which caused loss of rhythm in homozygote mice under constant darkness [65, 66]. The amino acid sequence of CLOCK showed that it contains PAS-A, PAS-B, basic-helix-loop-helix (bHLH), and C-terminal domains. Later CLOCK protein was determined as a transcription factor and a member of the basic-helix-loop-helix (bHLH)-PAS domain family [67].

Hogenesch discovered the BMAL1 protein (Brain and Muscle Aryl Hydrocarbon Receptor Nuclear Translocator (ARNT)-Like Protein 1) as one of the circadian clock components in 1998 [68, 69]. Further studies reported that $Bmal1^{-/-}$ mice were arrhythmic under constant darkness, indicating the role of BMAL1 protein in the central clock mechanism [70].

Cryptochromes, photolyase-like flavoproteins, have been long known as a blue light photoreceptor in plants and a circadian clock protein in fruit flies [71-73], while they were identified in humans by Aziz Sancar and his group in 1996 [74, 75]. In addition to other core clock proteins, the Cryptochrome protein may be the photoreceptor responsible for regulating the biological clock by transmitting the light information to the central clock [76-78]. $Cry1^{-/-}$ knockout mice showed a shorter circadian rhythm, while $Cry2^{-/-}$ knockout mice had a longer circadian rhythm compared to the wild-type controls. When both *Cry* were double knock-out ($Cry1^{-/-}$, $Cry2^{-/-}$), mice exhibited a complete loss of rhythm under constant darkness [79-81].

The mammalian circadian clock is a complex system of cellular and molecular processes that regulate daily rhythms in behavior and physiology. Although the components of the internal clock differ between organisms, the fundamental of the working principle is based on positive and negative feedback loops at the molecular level. The clock genes and proteins interact with various signaling pathways and feedback mechanisms to create robust and stable rhythms [82, 83].

The circadian core clock proteins, BMAL1, CLOCK, PERIOD, and CRYPTOCHROME, interact in complex transcription-translation feedback loops (TTFL) that control the expression of the other clock genes and create a cyclic pattern of gene expression [19, 84-86]. The positive arm of the feedback loop is driven by the transcriptional activators CLOCK and BMAL1, which bind to specific sequences of E-box or E'-box elements in the DNA and promote the expression of genes involved in circadian rhythm regulation, including PER and CRY [87]. Once translated, PER and CRY proteins form a complex that inhibits the activity of CLOCK and BMAL1, thereby creating a negative feedback loop that slows down the rate of gene expression and resets the clock [88, 89]. Understanding these rhythms and clocks is crucial for maintaining overall health and preventing various diseases [90].

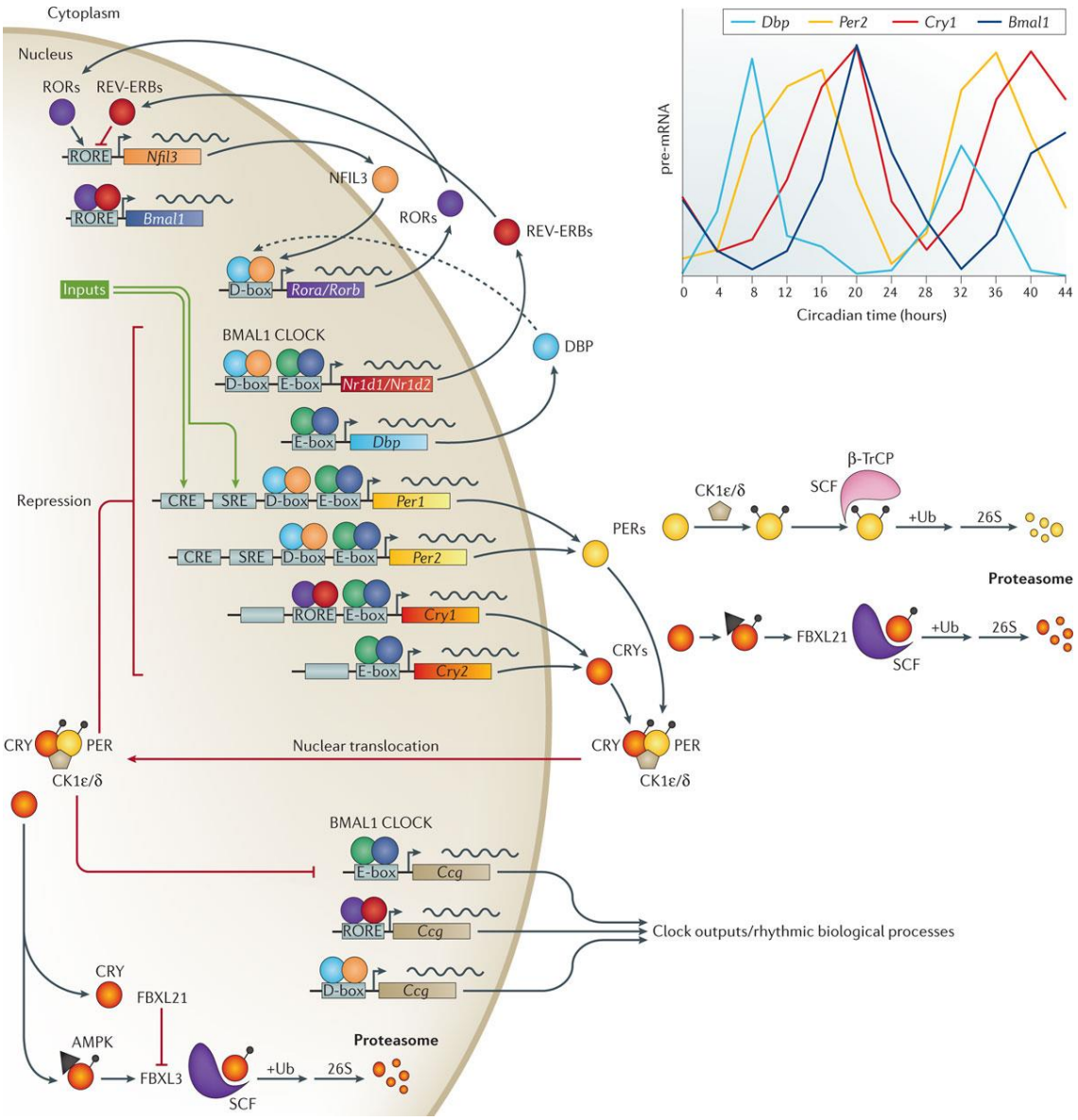

Figure 2. 3: The circadian gene network in mammals. At the core, CLOCK and BMAL1 activate the *Per1*, *Per2*, *Cry1*, and *Cry2* genes, which interact and repress their own transcription [91]. These interlocked transcriptional feedback loops represent the major transcriptional regulators of the cycling genes. *Permission to reuse this figure was given in Appendix E.

2.6. Stability of Cryptochrome in Mammalian Circadian Clock

Cryptochrome is a photolyase-like protein that was first identified as a circadian clock protein in fruit flies; it plays an important role in the mammalian circadian clock, where it is involved in the negative feedback loop that regulates the timing of the circadian rhythm [92, 93]. In mammals, there are two types of Cryptochrome proteins, CRY1 and CRY2, which are expressed in different tissues but most abundantly in the inner retina and play distinct roles in the circadian clock [94]. For example, CRY1 has been shown to regulate the expression of genes involved in DNA damage response and repair, while CRY2 has been implicated in the regulation of cell proliferation and differentiation [95-98].

At the molecular level, CRY1 and CRY2 repress the CLOCK:BMAL1 mediated transcription, and this repression activity of CRYs, strengthened their role in the negative arm of the circadian clock mechanism [99, 100]. The activity and stability of Cryptochrome are critical for its function in the circadian clock and other biological processes such as DNA repair, apoptosis, and development. It is regulated by a variety of factors, including protein-protein interactions, translocations, and post-translational modifications [101-104]. One of the key mechanisms involved in the regulation of Cryptochrome stability is the ubiquitin-proteasome pathway, which targets proteins with polyubiquitination for degradation by the proteasomes. The E3 ubiquitin ligases, FBXL3 and FBXL21, target the CRY proteins for degradation, which helps to maintain the stability of the negative feedback loop that drives the circadian rhythm [105-108].

Cryptochrome binds to PER proteins in the cytoplasm and then translocate back to the nucleus, where they suppress the activity of BMAL1:CLOCK and, subsequently, their own expression. PER2 binds to CRY on the CC-helix region and competes with the FBXL3 ligase binding site [109]. The ubiquitination by FBXL3 cannot occur while the CRY:PER2 complex is formed. In turn, the stability of the CRY increases. The competition between PER2 and FBXL3 plays a critical role in the degradation rate of CRY [110-112].

Additionally, post-translational modifications such as phosphorylation, acetylation, and sumoylation have been implicated in the regulation of Cryptochrome stability and function [113]. Cryptochrome1 phosphorylate by adenosine monophosphate-activated protein kinase (AMPK) [114], and Cryptochrome2 phosphorylate by glycogen synthase kinase 3β (GSK-3β) [115]. As a result, the binding affinity of FBXL3 is reduced when CRY is phosphorylated.

Disruptions to the stability of Cryptochrome can have various negative effects on health and well-being, and this highlights the importance of understanding the molecular mechanisms involved in its regulation. For example, mutations in the *CRY1* gene that disrupt the stability of CRY proteins have been linked to familial advanced sleep phase syndrome, a disorder characterized by an abnormally early sleep-wake cycle, also other health problems, including cancer, diabetes, and neurodegenerative diseases. Understanding the function of Cryptochrome proteins is important for understanding the molecular basis of circadian rhythm regulation and for developing new treatments for circadian rhythm disorders.

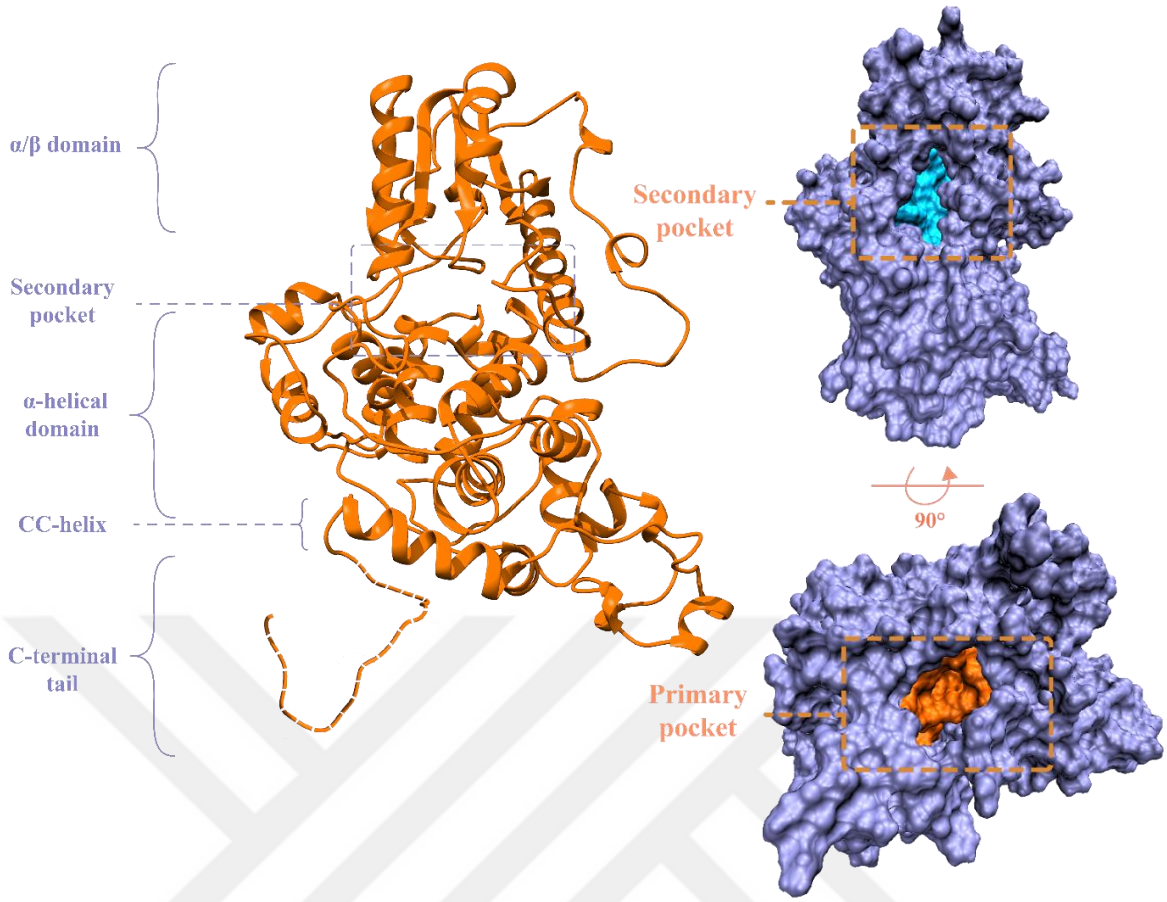

Figure 2. 4: Structure of mCRY1. 3D ribbon structure of mCRY1 and Functionally important CRY1 pockets colored to show domains, primary pocket (orange) where photolyases bound FAD (FAD binding pocket) and secondary cofactor pocket (cyan) [86]. *Permission to reuse this figure was given in Appendix E.

2.7. Glucose Metabolism Regulated by Circadian Clock

Glucose metabolism and circadian clock are tightly linked. The circadian clock is an internal biological clock that regulates many physiological activities, including glucose metabolism [116]. The circadian clock controls the expression of genes involved in glucose metabolism, such as those encoding for enzymes in glycolysis, gluconeogenesis, and glycogen metabolism. For instance, the gene expression of glucokinase [117], one of the key enzymes in glucose metabolism which converts glucose into glucose-6 phosphate, is regulated by the circadian clock. In turn, glucose metabolism can also affect the circadian clock.

Glucose is a key source of energy for the body, and its availability can influence the activity of physiological processes. Gluconeogenesis is a metabolic pathway that converts non-carbohydrate sources such as amino acids and fatty acids into glucose, which is then released into the bloodstream to provide energy to cells throughout the body [118]. The gluconeogenesis pathway is regulated by a variety of factors, including hormones such as glucagon [119], insulin [120], adiponectin [121], leptin [122], and the circadian clock.

Leptin is a hormone that plays an important role in obesity by binding to certain receptors in the hypothalamus to suppress appetite and increase metabolic rate. Leptin expression and secretion are completely under the control of the circadian rhythm, and in humans, it has the maximum effect during the sleep phase [123]. In recent studies, it was found that leptin production and activity were not affected by feeding time changes or adrenalectomy. However, the removal of the SCN abolished the circadian timing of leptin production [124]. Melatonin secretion is also under the control of SCN, and glucose homeostasis is affected by this rhythmic gene expression of the melatonin hormone [125].

Cryptochrome interacts with several enzymes involved in the gluconeogenesis pathway, such as phosphoenolpyruvate carboxykinase (PEPCK) and glucose-6-phosphatase (G6Pase), which plays an important role in glucose homeostasis and energy metabolism [126]. PEPCK and G6Pase are critical enzymes in the gluconeogenesis pathway, as they catalyze the conversion of pyruvate and glucose-6-phosphate into glucose [127].

Cryptochrome and the gluconeogenesis pathway appear to be bidirectional, with Cryptochrome influencing the activity of enzymes in the pathway and the gluconeogenesis pathway affecting the expression of Cryptochrome [128]. Cryptochrome is regulated by gluconeogenic signals such as cyclic adenosine monophosphate (cAMP) and glucagon, which are known to activate the gluconeogenesis pathway. At hunger state releasing the glucagon to the bloodstream stimulates the cAMP/CREB signaling through G-protein coupled receptors. The glucagon-mediated cAMP accumulation is inhibited by high levels of Cryptochrome in the morning, while inhibitory impact becomes less pronounced by decreased Cryptochrome levels at night [129].

In addition to its role in the gluconeogenesis pathway, Cryptochrome has been implicated in a variety of other metabolic processes, including lipid metabolism and insulin signaling. Lipid metabolism is regulated by interacting with peroxisome proliferator-activated receptors (PPARs), a family of transcription factors involved in lipid

metabolism [130]. Knock-out *Cry1* mice were more resistant to gaining weight on a high-fat diet and had less fat storage compared to wild-type controls [131]. Double Knock-out *Cry* mice, on the other hand, were more prone to develop tissue-specific hyperinsulinemia and insulin resistance [132].

The bidirectional interaction between Cryptochrome and the gluconeogenesis pathway highlights the complexity of the mammalian circadian clock and its role in regulating metabolism and energy homeostasis. The identification of new targets for the treatment of metabolic disorders such as insulin resistance, diabetes, and obesity may be facilitated by a better understanding of the interaction between Cryptochrome and the gluconeogenesis pathway.

2.8. Circadian Rhythm and Metabolic Diseases

Disruption of the circadian rhythm has been associated with various health issues, including increased risk of metabolic disorders such as obesity and diabetes, cardiovascular diseases, infertility, sleep disorders, mood disorders, mental health problems such as depression and anxiety, and cancer [90, 133].

Circadian rhythm sleep disorders (CRSDs) are a group of sleep disorders that occur due to disruptions in the body's internal clock. This impairment can be caused by a variety of factors, including genetic predisposition, environmental factors such as exposure to bright light at night or shift work, and medical conditions such as sleep apnea or depression. CRSDs can lead to difficulties falling asleep, staying asleep, or waking up at the appropriate time, causing significant disruptions to a person's daily life. There are several types of CRSDs, including delayed sleep-wake phase disorder (DSWPD), advanced sleep-wake phase disorder (ASWPD), irregular sleep-wake rhythm disorder (ISWRD), and non-24-hour sleep-wake rhythm disorder (N24SWD) [134, 135].

DSWPD is characterized by a delayed sleep onset time, making it difficult for individuals to fall asleep at a normal time, resulting in a delayed wake-up time. This disorder is commonly observed in adolescents and young adults [136, 137]. ASWPD is characterized by an early sleep onset time, resulting in early waking times. Individuals with ASWPD may fall asleep early in the evening but wake up very early in the morning, causing

significant daytime sleepiness. ISWRD is characterized by a highly irregular sleep-wake pattern. Individuals with this disorder may sleep in multiple episodes throughout the day and night, making it difficult for them to maintain a regular sleep schedule.

N24SWD is characterized by a sleep-wake cycle that is longer than 24 hours. Individuals with this disorder may experience periods of insomnia or excessive sleepiness at different times of the day and night, making it difficult for them to maintain a regular sleep schedule [138]. Treatment for CRSDs varies depending on the specific disorder and its underlying causes, and some options may include light therapy, melatonin supplements, behavioral therapy, or medications such as stimulants or sedatives [139]. These sleep disorders can have a significant impact on a person's daily life. Understanding the causes and treatments for CRSDs is important for improving sleep quality and overall health.

Circadian rhythm and obesity are intricately linked, and disruptions to the body's natural internal clock can lead to weight gain and an increased risk of obesity-related health issues. One of the main ways that circadian rhythm disruption leads to obesity is through changes in the hormones that regulate appetite, glucose homeostasis, and metabolism. The hormone leptin is produced by fat cells and helps regulate appetite and metabolism by signaling to the brain that the body has had enough food. Disruptions to the circadian rhythm can lead to decreased leptin production and an increase in the hunger hormone ghrelin, causing individuals to feel hungry even when they have consumed enough calories. This can lead to overeating and weight gain over time [140].

In addition to changes in hormone levels, circadian rhythm disruptions can also affect the body's metabolic rate. The body's natural metabolic rate fluctuates throughout the day, with the highest metabolic rate occurring in the morning and the lowest at night [141]. Disruptions to the circadian rhythm can lead to a decrease in the body's metabolic rate, causing the body to burn fewer calories and leading to weight gain over time [142]. Frequent traveling across time zones is also a factor that can disrupt the body's natural internal clock because of causing jetlag [143]. To mitigate the negative effects of circadian rhythm disruption on obesity, lifestyle changes such as establishing a regular sleep schedule, avoiding exposure to artificial light at night, and limiting late-night eating can be helpful. In addition, maintaining a healthy diet and regular exercise routine can also help regulate hormones and promote healthy metabolism [144].

Diabetes Mellitus is a lifelong chronic disease that develops when the pancreas cannot produce enough insulin hormone, or the produced insulin hormone cannot be used effectively throughout the body. The insulin hormone regulates blood glucose levels by facilitating cellular uptake and using it as a primary energy source. Type 2 Diabetes (T2D), a chronic condition characterized by high blood glucose levels, results from the body's ineffective usage of insulin hormone [145].

Individuals who have irregular sleep patterns have a higher risk of developing type 2 diabetes than those with regular sleep patterns. This is because disruptions to the circadian rhythm can affect the body's ability to regulate response to glucose, leading to an increased risk of insulin resistance, a condition in which the cells become less responsive to insulin, causing an increase in blood glucose levels and type 2 diabetes [146]. In addition to disruptions to the circadian rhythm, genetic factors can also play a role in the development of type 2 diabetes [147]. Several genes involved in the regulation of the circadian rhythm have been linked to an increased risk of developing the condition.

Cancer is a disease characterized by abnormal growth and spread of cells in the body. Impaired circadian rhythm can increase the risk of several types of cancer, such as breast, prostate, and colorectal cancer. This is because the circadian rhythm plays a critical role in regulating the immune system and cellular repair mechanisms, both of which are essential for preventing the development of cancer [148]. Disruptions to the circadian rhythm can affect the body's response to environmental factors that contribute to the development of cancer, such as exposure to toxins and radiation, as well as cancer treatment outcomes.

Cancer treatment protocols may be adjusted to consider the patient's circadian rhythm, with treatments scheduled at times when the patient's immune system and cellular repair mechanisms are most active. Studies have shown that the timing of chemotherapy and radiation therapy can have a significant impact on treatment efficacy and patient outcomes. For example, administering chemotherapy at a time when the patient's circadian rhythm is most active can improve treatment outcomes and reduce the risk of side effects [149]. Awareness of the impact of circadian rhythm disruptions on cancer risk and treatment outcomes can help individuals take steps to maintain a healthy lifestyle and improve their overall health and well-being.

2.9. Small Molecules: A Modifiers in Circadian Clock

Numerous studies in recent years have concentrated on the identification of small molecules that interact with target proteins to treat metabolic diseases. Small molecules are organic compounds with low molecular weight, typically less than 900 daltons, and this serves them the benefit of passing through the cell membrane easily. These molecules can interact with the specific proteins and enzymes in the circadian clock network, modulating their activity and altering the timing and amplitude of clock gene expression [150]. In addition to their use as research tools, small molecules that modify the circadian clock have potential therapeutic applications [151, 152]. Small molecules that target the circadian clock have been identified through high-throughput screening, target-based screening, and rational design approaches, and their effects on the circadian clock have been characterized using cell-based assays, animal models, and human studies [153].

One class of small molecules that modify the circadian clock is the agonists and antagonists of the nuclear receptors REV-ERBs and RORs [154]. REV-ERBs and RORs are transcription factors that play a critical role in regulating the expression of clock genes, including the core clock genes PER and CRY. Small molecules that activate REV-ERBs or inhibit RORs can alter the circadian rhythm of gene expression and physiological processes, including sleep and metabolism. For example, the REV-ERB agonist SR9009 [155] has been shown to shorten the circadian period of mice, improve glucose tolerance, and reduce liver fat accumulation in mouse models of metabolic disorders, while the ROR antagonist SR1078 [156] has been shown to lengthen the circadian period and alter sleep patterns.

Another class of small molecules that modify the circadian clock is the inhibitors of casein kinase 1 (CK1) and glycogen synthase kinase 3 (GSK3). CK1 and GSK3 are kinases that phosphorylate and destabilize clock proteins, including PER and CRY. Small molecules that inhibit CK1 and GSK3 can stabilize clock proteins, leading to changes in the timing and amplitude of clock gene expression. The CK1 inhibitor PF-670462 [157] has been shown to lengthen the circadian period of mice and human cells, improve sleep quality and reduce symptoms of depression in human studies, while the GSK3 inhibitor CHIR99021 [158] has been shown to shorten the circadian period and enhance light-induced phase shifting.

Small molecules have also been used to modulate the activity of other components of the circadian clock network, including the transcriptional activators CLOCK and BMAL1, the nuclear receptor PPARα, and the histone deacetylase SIRT1. Small molecules that target these proteins can alter the amplitude and phase of clock gene expression, as well as other physiological processes, including lipid metabolism and aging. A CLOCK-binding small molecule named CLK8, recently discovered by the Kavakli group, disrupts the interaction between CLOCK and BMAL1, interferes with the nuclear translocation of CLOCK both in vitro and in vivo, and enhances circadian rhythm amplitude [159]. Findings suggest that CLK8 can be used as a tool for further investigation into CLOCK's function in controlling the amplitude of circadian rhythms as well as a potential therapeutic candidate for the treatment of diseases characterized by dampened circadian rhythms, including aging.

The development of strategies to enhance the stability of Cryptochrome and other clock proteins has the potential to lead to new treatments for circadian rhythm disorders and other metabolic diseases. By using the unbiased cell-based circadian phenotypic screening, a small molecule, KL001, was identified that specifically interacts with Cryptochrome. KL001 increased the stability of Cryptochrome by preventing FBXL3-mediated ubiquitin-dependent proteasomal degradation and lengthened the circadian period [160, 161]. Furthermore, Cryptochrome stabilizer small molecule inhibited the glucagon-mediated gluconeogenesis in primary hepatocytes. KL001 and its derivatives provide a tool to study the regulation of CRY-dependent physiology and circadian clock-based therapeutics [162].

The functional domains of Cryptochromes contribute to their diverse functions and interactions. The highly fluctuated C-terminal extension, also known as the C-C helix, and photolyase homology region (PHR) are two functionally essential domains that are found in CRYs [163]. The PHR domain is a conserved domain found in Cryptochromes and contains the α-helical domain in the primary pocket, where is the flavin adenine dinucleotide (FAD) binding site, and α/β domain in the secondary pocket [164]. On the other hand, the extended C-terminal region is crucial for the interaction of other proteins like CBS and PER2 that contribute to the localization and function of Cryptochromes [165, 166].

Another small molecule M47, Cryptochrome1 stabilizer, was identified via a structure-based small molecule design approach by the Kavakli group. The molecule enhanced the stability of CRY1 both in vitro and in vivo and increased the circadian period length. Furthermore, repetitive administration of M47 increased the median lifespan of $p53^{-/-}$ mice. Collectively results suggest that M47 can be a promising small molecule for the treatment of cancer caused by the p53 mutation [167].

Small molecules that modulate the circadian clock have potential applications in both basic research and therapeutic development and could offer a new approach to treating a variety of diseases, including metabolic disorders, neurological disorders, and cancer, by restoring normal circadian rhythms and improving physiological function. Studies have shown that the timing of drug administration can affect drug metabolism and efficacy, as peripheral clocks regulate the expression of drug-metabolizing enzymes and transporters [168]. This finding suggests that the timing of drug administration could be optimized based on the circadian rhythm of the target tissue. Chronotherapy, which involves timing medications or other treatments to match the body's circadian rhythms, has been shown to be effective in treating a range of conditions, including hypertension, asthma, and cancer [169, 170].

Additionally, approaches such as gene therapy and genome editing have been proposed as potential strategies for restoring the stability and function of Cryptochrome and other clock proteins in patients with circadian rhythm disorders. Some individuals have genetic variations that affect the functioning of the biological clock, leading to differences in sleep-wake cycles, hormone secretion, and other circadian processes. These variations have been linked to increased risk of conditions such as obesity, diabetes, and depression. Overall, research into circadian rhythm has provided valuable insights into the fundamental processes that govern our physiology and behavior. Further studies are needed to fully understand the complex mechanisms involved and to develop effective interventions to manage circadian disruptions and related health problems.

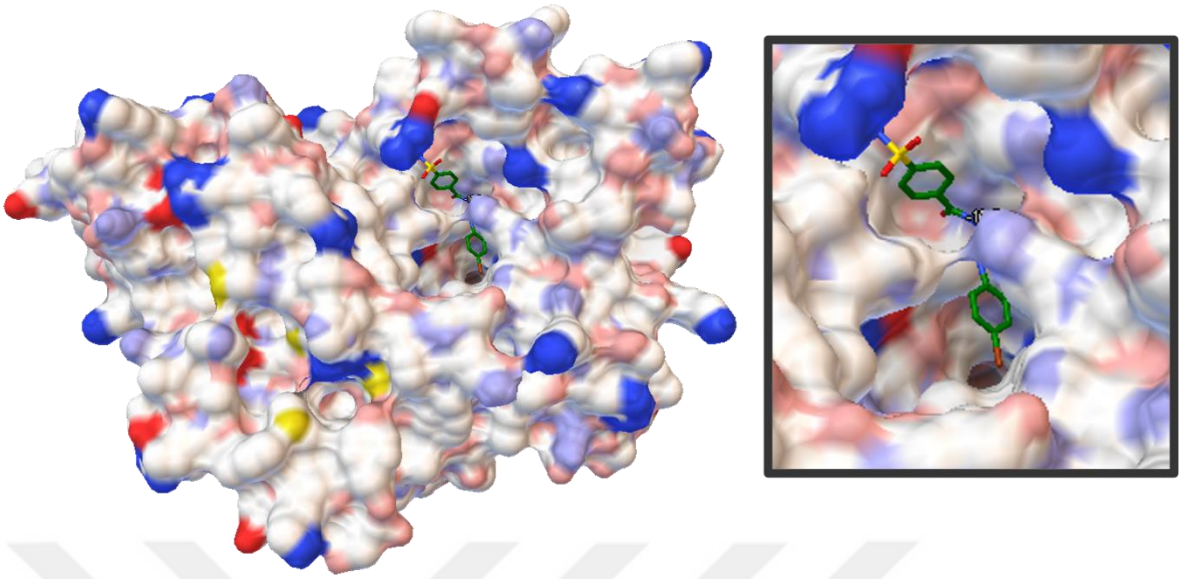

Figure 2. 5: CRY1 structure and FAD binding site in primary pocket targeted for docking simulation shown in surface, a small molecule docked into cavity shown in the sticks.

Chapter 3

MATERIALS AND METHODS

3.1. Molecular Dynamics and Docking Simulation

Wild type structure for mouse CRY1 generated via homology modeling by using RaptorX web server. Protein sequence retrieved from NCBI database with NP_031797.1 accession number. Amino acids between 3-491 are used to model the PHR domain for CRY1 to complete missing residues. Cry1 PHR model simulated for 300 nanoseconds by using NAMD2 software [171]. The molecular dynamics simulations were performed by using a CHARMM-36m force field [172]. The Langevin thermostat and barostat were used to control the temperature and pressure, respectively. Periodic boundary conditions and Particle Mesh Ewald (PME) were used for full electrostatic interactions with a 12 Å cutoff. After minimization, the system gradually heated to 310 °K. During equilibration, harmonic constraints, 3 kcal*mol-1*A-2, on CA atoms were gradually removed. Equilibration and production runs are performed under the constant number of atoms, pressure, and temperature (NPT). Trajectory subjected to clustering analysis based on root mean square deviation (RMSD) values in UCSF Chimera [173]. Cluster representatives of the most populated cluster were used as representative structures in docking studies.

Around 2 million small molecules from Ambinter Library with non-characterized functions were docked to the primary, FAD-binding pocket of mCRY1 structure via the AutoDock Vina program to identify novel molecules that control CRYs stability [174]. The library of small molecules was initially filtered according to Lipinski's rule of 5 (molecules should have less than 5 H-bond donors, less than 10 H-bond acceptors, less than 500 Da molecular weight, an octanol-water partition coefficient log P, smaller than 5). Docked conformation with the lowest binding energy to mCRY1 was additionally simulated for 20 nanoseconds. PyMol software was used to visualize the protein structure [175]. RMSD, RMSF, and H-Bond/Interaction calculations were performed by using the Visual Molecular Dynamics (VMD) software. The molecular mechanics energies combined with generalized Born and surface area continuum solvation (MM/GBSA)

method used to calculate the free binding energy (ΔG) and energy decomposition analysis (EDA) taking advantage of MMGBSA.py script implemented in AmberTools software [176]. The best candidate molecules with binding energies smaller than -8.5 kcal/mol were selected for further experimental studies. In-silico screening of the study was performed by Seref Gul, Ph.D., and Onur Ozcan in Kavakli Laboratory.

3.2. Cell Culture

HEK293T, U2OS, NIH3T3 cell lines were maintained in filtered complete Dulbecco's modified Eagle's Medium (DMEM, Gibco) supplemented with 10% heat-inactivated fetal bovine serum (FBS, Gibco), 100 µg/mL streptomycin and 100 µg/mL penicillin (Gibco). The cell cultures were grown in an 85% humidified incubator at 37°C with 5% CO2. To subculture the cells when they reached 80% confluency, the cultured medium was removed, and the attached cells were washed with 5 mL PBS (137 mM NaCl, 2.7 mM KCl, 10 mM Na2HPO4, 1.8 mM KH2PO4, pH 7.4). Then the cells were detached in 1 mL Trypsin/EDTA (0.25%:0.02%, PAN Biotech) by incubating at 37°C for a few minutes, then resuspended with 4 mL fresh complete medium. Finally, in a new sterile 10 cm plate (NEST Biotechnology), 1 mL of the resuspended cells were seeded with 9 mL fresh complete medium.

3.3. Cytotoxicity Assay

MTT (3-(4,5-dimethylthiazol-2-yl)-2,5-diphenyltetrazolium bromide, AppliChem) cytotoxicity assay was performed to determine the non-toxic doses of small molecules [177]. Human osteosarcoma U2OS cells were seeded in triplicates to a transparent 96-well plate at a density of 4×10^3 cells per well. After 48 hours of incubation, small molecules that dissolved in dimethyl sulfoxide (DMSO) were added to cells at appropriate concentrations in 10 uL DMEM. The same volume of DMSO was used as a positive control in the experiment since the small molecules were dissolved in it, and the 5% DMSO was used as a negative control since known to be toxic to cells. 48 hours later than molecule treatment, the cultured medium was removed and 80 µL DMEM mixed with 20 µL MTT solution (1 mg/mL) was added to each well. The cells were incubated

for 3.5 - 4 hours in a humidified incubator at 37°C with 5% CO2. Then, the MTT solution was removed, and the formazan salts were dissolved in a 1:1 mixture of DMSO and 100% ethanol. The absorbance values (A) were measured at 600nm and 690nm by using Synergy H1 Microplate Reader (Bio-Tek Instruments). The % cell viability was calculated using equation 3.1.

$$\%\ Cell\ Viability\ = \frac{(\mathrm{A600nm} - \mathrm{A690nm})\mathrm{molecule}}{(\mathrm{A600nm} - \mathrm{A690nm})\mathrm{DMSO}} \times 100 \qquad (3.1)$$

3.4. LUC Protein Degradation Assay

HEK293T cells transiently transfected with either 40 ng pcDNA-*Cry1-Luc* (C-terminally luciferase-fused, CRY1-LUC), 40 ng pcDNA-*Cry2-Luc* (C-terminally luciferase-fused, CRY2-LUC) or 4 ng pcDNA-*Luc* plasmids mixed with empty pCMV-Sport6 plasmid for total 300 ng/well in 50 uL serum-free DMEM. HEK293T cells were reverse transfected at a density of 4×10^4 cells per well on 96-well opaque white flat bottom plates (Corning Costar) by using 6 μL polyethyleneimine (PEI, Polysciences, 23966-1) transfection reagent. After 24 hours of post-transfection, small molecules were added to cells at appropriate concentrations. Another 24 hours after small molecule treatment, 10 mM HEPES-NaOH (pH 7.2) and 1 mM luciferin was supplemented to the medium. 2 hours later, to inhibit the protein synthesis, cycloheximide (CHX, Sigma, 66819) was added with a final concentration of 30 μg/mL [178]. The plate was sealed with thermal film and placed in Synergy H1 Microplate Reader (Bio-Tek) and the luminescence was measured for 24 hours every 10 minutes. The half-life of the protein was calculated by fitting the data to one phase exponential decay curve by using GraphPad Prism 9 software. Dose-response curves were obtained from GraphPad Prism 9 sigmoidal curve fitting used to calculate EC50 (half maximal effective concentration) and R^2 (coefficient of determination) values.

3.5. Lentivirus Production

80% confluent, low passage numbered HEK293T cells in 10 cm plate with 5 mL of growth medium were transfected with 10 μg pLV6-*Bmal1-Luc* plasmid, 9 μg pCMV-*ΔR8.2dvpr* packaging vector and 1 μg pCMV-*VSVG* envelope vector via 20 μL of PEI (Polysciences, 23966-1) transfection reagent in 400 μL of DMEM. After 16 hours post-transfection, 3 mL of fresh complete medium was added, and the cells were incubated for 24 hours. The next day, the cultured medium was replaced with 8 mL of fresh complete medium. As lentiviral particles were released into the cultured medium, they were harvested by collecting the medium at 72-hour and 96-hour post-transfection. The virus containing medium was filtered through a 0.45 μm filter and the solution was aliquoted as 750-1000 μL of lentiviral particle and stored at -80°C.

3.6. Bioluminescence Assay

In initial screening to determine the effects of small molecules on the circadian rhythm the cell-based circadian assay was performed by U2OS *Bmal1*-d*Luc* stable cell line. Cells were seeded on an opaque white 96-well plate at a density of 40 x 10^3 cells per well and cultured overnight in 10% complete medium. The next day cells were reset with dexamethasone (DXM, Sigma, D-4902) at 0.1μM final concentration for 2 hours then medium was replaced with the bioluminescence recording medium that contains the 10 mg/mL DMEM powder (Sigma, D-2902), 0.35 mg/mL sodium bi-carbonate (Sigma S5761), 3.5 mg/mL D(+) glucose powder (Sigma G7021), 10 mM HEPES buffer (pH 7.2, Gibco, 15140-122), 100 μg/ml Pen/Strep (Gibco) and 5% FBS. Luciferin with the 0.1mM final concentration and small molecules were added subsequently to the recording medium at the appropriate concentration. Plates were sealed with thermal clear film to maintain the homeostasis of the cells. The bioluminescence recordings were recorded at 32°C for every 30 minutes for 7-days using the 96-well plate reader Synergy H1 (BioTek). The period, amplitude and phase were calculated to define the circadian rhythm parameters by the BioDare2 software [179].

To investigate the effect of candidate molecules on the circadian period extensively, the higher-resolution LumiCycle32 luminometer was used. Human U2OS *Bmal1*-d*Luc* and mouse NIH3T3 *Bmal1*-d*Luc* stable cells were seeded on 35-mm plates at a density of

40×10^5 cells/plate to monitor the circadian rhythm. After 24 hours, a fresh medium containing 0.1 μM dexamethasone was added to synchronize the circadian rhythm. 2 hours later, the medium was replaced with the bioluminescence recording medium supplemented with freshly added 0.1 mM luciferin and the small molecules at the appropriate doses. Plates were sealed with silicone grease to prevent the gas exchange from evaporation and then placed in a LumiCycle32 luminometer (Actimetrics). The bioluminescence records were measured every 10 minutes at 37°C for 7 days. The period, amplitude and phase data were analyzed with LumiCycle Analysis software (Actimetrics).

3.6.1 Viral Transduction Bioluminescence Assay

To determine the effect of the molecules in the absence of CRYs, U2OS *Cry1-/- /Cry2-/-* (U2OS CRYDKO) cells transduced with pLV6-*Bmal1-Luc* (luciferase reporter) were used. CRYDKO cells prepared by Gul et al. as described in [167]. To monitor the circadian rhythm of *Bmal1*, $1x10^5$ U2OS CRYDKO cells were seeded in 35 mm plates with 10 mL complete medium. The next day, the cultured medium was discarded and a mixture of thawed 750 μL of lentiviral particle solution, 1 μL of protamine sulfate (final concentration: 8 mg/ml, Sigma Aldrich) and 250 μL of DMEM was added to the cells. After 16 hour-incubation, virus-containing media was replaced with 1.5 mL of fresh complete medium. Viral transduction was repeated one more time. At 72-hour post-transfection, the cultured medium was replaced with 1 mL of DMEM containing 0.1 uM Dexamethasone to synchronize cells. 2 hours later, the cultured medium was replaced with 2 mL bioluminescence recording medium which contained freshly added 0.1 mM of luciferin, and the appropriate dose of small molecules. The plates were sealed with silicone grease and then placed in a LumiCycle32 luminometer (Actimetrics). The bioluminescence records were measured every 10 minutes at 37°C for 7 days. The period, amplitude and phase data were analyzed with LumiCycle Analysis software (Actimetrics).

3.7. SDS-PAGE and Western Blotting

Cell Culture sample preparation: U2OS cells were seeded on 35-mm plates with a density of 40×10^5 cells/plate and incubated at 37°C with 5% CO2. After 24 hours, small molecules were added at appropriate doses. The cells were incubated for another 24 hours and harvested with ice-cold PBS. Harvested cells were centrifuged at 3000 x g, 4°C for 7 minutes and the supernatant was removed. The cell pellet was lysed in 60 µL RIPA buffer (50 mM Tris-HCl pH 7.4, 150 mM NaCl, 0.5% NP-40, 0.5% SDS) with freshly added 1 mM phenylmethylsulfonyl fluoride (PMSF) and 1X Protease Inhibitor Cocktail (PIC, Thermo Scientific) for 20 minutes on ice. The lysed cells were centrifuged at 13,000 x g, 4°C for 15 minutes and the supernatants were collected. Total protein concentration was measured by Pierce Protein Assay (Thermo Scientific). The protein samples were mixed with 4X Laemmli Buffer (0.1% bromophenol blue, 8% SDS, 400 mM β-mercaptoethanol, 40% glycerol) and samples were boiled at 95°C for 10 minutes.

Mice liver sample preparation: Mice were sacrificed 4 hours after orally administered 40 mg/kg TW68 or control vehicle. Organs were immediately frozen in liquid nitrogen and then kept at -80°C for downstream analysis. Liver samples were homogenized with Dounce homogenizer with 500 µL RIPA buffer (50mM Tris, 150mM NaCl, 1% Triton-X, 0.1% SDS and Protease inhibitor cocktail, and additionally 8 mg/mL phosphatase inhibitor cocktail and 2mM Na2VO4 for phosphorylated samples). Samples were incubated for 10 minutes on ice and then centrifuged for 10 minutes at 13000 rpm at 4ºC. After determining and equalizing the protein amounts by using the Pierce 660 nm Protein assay (Thermo Scientific) via Biotek Synergy H1, lysates were mixed with a 4X Laemmli buffer (277.8mM Tris HCl pH: 6.8, 4.4% LDS, 44.4% (w/v) glycerol, 0.02% Bromophenol blue, 5% volume of beta-Mercaptoethanol) and boiled at 95ºC for 10 minutes.

Protein samples were used for SDS-PAGE and transferred to the PVDF membrane (Merck-Millipore). The membrane was blocked with 5% milk solution in 0.15%TBS-Tween for 1 hour and then incubated with the following antibodies: Anti-CRY1 (Bethyl, A302-614A), Anti-CRY2 (Bethyl. A302-615A), Anti-PER (Bethyl. A303-109A), Beta-Actin (Cell Signaling, 8H10D10), Phospho-Akt (Cell Signaling, 4060), Akt (Cell Signaling, 4691), HRP conjugated secondary mouse (Santa Cruz, SC-358920) or rabbit

(Cell Signaling, 7074) antibodies. ECL buffer system (Advansta Western Bright) was used to visualize HRP chemiluminescence via BioRad ChemiDoc Touch visualizer.

3.7.1. Pull-Down Assay

To perform pull-down assay HEK293T cells were transiently transfected with either 10 μg pcDNA-*His-Myc-Cry1* or 10 μg pcDNA-*His-Myc-Cry2* plasmids. The cells at 80% confluency were forward transfected with the appropriate plasmid using 30 μL PEI in 1 mL DMEM. 24 hours post-transfection cells were harvested in cold 1x PBS and 1:5 diluted pellets were lysed with 500 μL Lysis Buffer (50 mM Tris-HCl pH 7.4, 2 mM EDTA, 1 mM $MgCl_2$, 0.2% NP-40, 1 mM Na_3VO_4, 1 mM NaF, 1X PIC) and incubated on ice for 20 minutes. Then samples were centrifuged at 7.000 xg for 10 minutes at 4°C. The supernatant was mixed with 2X binding buffer (100 mM Tris-HCl pH 7.4, 300 mM NaCl, 0.2% NP-40, 2 mM Na_3VO_4, 2 mM NaF, 1X PIC) at 1:1 ratio. While 5% of the mixture was kept as input, the remaining part was divided equally into three and incubated by continuous mixing with either DMSO, or 10 μM biotinylated-TW68 (bTW68) with or without 150 μM free TW68 (competitor) at 4°C for 2 hours. Meanwhile, the NeutrAvidin Agarose resin (Thermo Scientific, 29201) was equilibrated (30 μL settled resin/sample) according to manufacturer's protocol. Lysates were supplemented with equilibrated resin and incubated overnight at 4°C with constant rotation. The next day, samples were centrifuged at 2500 xg for 1 minute and then supernatants were discarded. The resin of each sample was washed 3 times with 1X binding buffer for 5 minutes with constant rotation at 4°C. Subsequently, resin of each sample was boiled with 30 uL, 4x Laemmli buffer for 10 minutes at 95°C for SDS-PAGE analysis.

3.7.2. Ubiquitination Assay

HEK293T cells were transiently forward transfected at a density of 5×10^5 cells per well on 6-well plate with 1200 ng of pcDNA-*His-Myc-Cry1*, 300 ng pBIND-*Fbxl3*, and 200 ng of p*hUb-Ha* via PEI in 100 uL DMEM. Cells were treated with DMSO or TW68 after 28 hours of transfection. After 42 hours of post-transfection cells were treated with 10 mM MG132 [180] to block proteasomal degradation or equal volume of DMSO to

negative control in 100 uL DMEM. 48 hours after transfection, cells were harvested with cold 1x PBS. Pellet was lysed with RIPA buffer (50 mM Tris, 150 mM NaCl, 1% Triton-X, 0.1% SDS) and mixed with equilibrated Myc resin (EZview Red Anti-c-Myc Affinity Gel, Sigma-Aldrich, E6654) according to the manufacturer's instruction and agitated for 2 hours at 4°C. After washing three times with RIPA buffer, proteins were eluted with 4X Laemmli buffer and boiled for 10 minutes at 95°C. Ubiquitination and expression levels of CRY1 was detected by Western blotting with anti-HA (Santa Cruz Biotechnology, sc7392) and anti-Myc (Abcam, ab18185) antibodies, respectively. Anti-Gal4(DBD) (Santa Cruz, sc-577) was used to detect Gal4-FBXL3 levels in the input.

3.8. RNA Isolation and cDNA Preparation

To investigate the effect of small molecules on expression levels of circadian genes, U2OS cells and mice liver samples were harvested as described in Section 3.7. The total RNA isolation from the samples was performed by the NucleoSpin RNA kit (Macherey-Nagel) following the DNase treatment. RNA samples were eluted with 50 µL DNase RNase free water. Using NanoDrop 2000 (Thermo Scientific) the concentration and purity of RNA samples were measured. The integrity of the eluted RNA was confirmed by 0.8% agarose gel electrophoresis which was prepared using DEPC (diethylpyrocarbonate) treated water. For cDNA synthesis, a mixture of 500 ng of RNA, 2 µL of oligo(dT) 23, 1 µL of 10 mM dNTP mix was completed up to 10 µL with DNase RNase free water. The mixture was incubated at 65°C for 5 minutes and consecutively placed on ice (+4°C). Then for the extension of cDNA, 2 µL from 10X M-MuLV buffer (New England Biolabs), 1 µL from M-MuLV Reverse Transcriptase (200 U/µL), 0.2 µL from RNase Inhibitor (40 U/µl) and 6.8 µL DNase RNase free water were mixed. The samples were kept at 42°C for 1 hour for extension reaction and then at 65°C for 20 minutes for inactivation of the enzyme. Produced cDNA samples were diluted 1:5 with DNase and RNase free water for storage at -20°C.

3.9. Real Time – quantitative Polymerase Chain Reaction (RT-qPCR)

Real time – quantitative PCR method was used for detecting the effect of small molecules on expression levels of core clock genes and gluconeogenic genes. Primer sequences are listed in Appendix C. The reference gene used for cell samples was ribosomal protein, large, P0 (*Rplp0*) and for liver samples was Cyclophilin-b. The reaction mixture consisted of 8 μL SYBR Green (Bioline), 8 μL DNase free water, 1 μL primer mixture (forward and reverse primers: 10 pmol each), and 3 μL cDNA obtained as described in Section 3.8. After 4 minutes of polymerase activation at 95°C, the cycling protocol is 8 seconds at 95°C (denaturation), 10 seconds at 60°C (annealing), 20 seconds at 72°C (elongation) using CFX Connect Real-Time PCR detection system (Bio-Rad). The product of qPCR was also analyzed by melt curve (Tm) and quantification cycle (Cq mean) values.

3.10. In Vivo Characterization

Male and female C57BL/6J mice, 8-12 weeks old, weighed 18-25 g were used in the in vivo studies with TW68. Mice were obtained from Koç University Animal Research Facility (KUARF) and experiments were conducted in accordance with the guidelines approved for animal experimental procedures by the Koç University Animal Research Local Ethics Committee (HADYEK No: 2017/08).

3.10.1. Animals and their synchronization

Mice were housed in polystyrene cages of up to four animals in a room equipped with temperature control (21 ± 2°C) and humidity (55 ± 5%). Mice were housed under 12 h of light (L) in alternation with 12 h of darkness (D) (LD 12:12) prior to any intervention and the same lighting regimen continued to the end of the experiment. Water and food were provided ad libitum throughout the experiments. These ambient conditions are described in Zeitgeber time (ZT), where ZT0 corresponds to lights on and ZT12 to lights off. TW68 or control vehicle was administered intraperitoneally and orally to mice at the same time every day at ZT3 (three hours after light onset). Animals were euthanized by cervical

dislocation. For animal welfare, animals were monitored on a daily basis and examined for following indications: body temperature, body weight changes, clinical signs, water and food consumption, and behavior. For ethical concerns, animals were sacrificed after observing excessive reduced locomotor activity (inability to access food and water), excess weight loss (>20% of body weight), dyspnea, and excessive hypothermia (<32°C).

3.10.2. Preparation of TW68 formulation

TW68 was dissolved in 2.5% DMSO and 15% Cremophor EL and then diluted with 82.5% isotonic sodium chloride solution (Control Vehicle = DMSO:Cremophor EL:0.9% NaCl; 2.5:15:82.5, v/v/v) on each study day to prepare freshly, prior to intraperitoneal or oral injection. In the oral administration formulation, distilled water (dH2O) was used instead of isotonic sodium chloride solution then performed by ball-point gavage needle accordingly. Solvents were reagent grade, and all other commercially available reagents were used as received unless otherwise stated.

3.10.3. Single Dose Toxicity Study

The dose levels to be used in the single dose toxicity study were selected according to the OECD Guidelines (Guidelines for the testing of chemicals, 2002). Male (n=2-3) and female (n=2-3) C57BL/6J mice were used at each dose level. Mice were treated with 50 and 300 mg/kg single doses of TW68 intraperitoneally, with one dose being used per group. Control mice (n=2 for both sexes) were only treated with the control vehicle (DMSO:Cremophor EL:0.9% NaCl; 2.5:15:82.5, v/v/v, i.p.). Careful observations of mice including body weight changes, body temperature, behavioral and clinical abnormality, and mortality were performed for 14 days, and a gross necropsy of all animals was carried out at the end of the experiment. Body weight was measured every day as an index of general toxicity. TW68-induced body weight change was expressed relative to body weight on the initial treatment day. The body temperatures of the mice were recorded by the rectal homeothermic monitor (Harvard Apparatus, US) for 5 days following the TW68 injection. Temperature measurements were performed at the same time each day. After the observation period, mice were exposed to isoflurane anesthesia

and blood was collected by cardiac puncture. Mice were immediately sacrificed by cervical dislocation after blood collection. Hematological parameters were analyzed in blood samples.

3.10.4. Maximum Tolerated Dose Toxicity Study

The single dose toxicity data were used to assist in the selection of the doses in this repeated dose toxicity study. C57BL/6J mice (n=6 per group) were treated with 50, 75 or 150 mg/kg doses of TW68 intraperitoneally for 5 days. Control mice (n=4) were only treated with control vehicle (DMSO:Cremophor EL:0.9% NaCl; 2.5:15:82.5, v/v/v, i.p.). Throughout the study, animals were monitored for mortality, clinical signs, body weight changes, body temperature, food and water consumption, behavior assessment and gross findings at the terminal necropsy. Body weights and body temperatures of mice were measured every day as an index of toxicity. Within 48 hours after the last dose of TW68 administration, blood was collected from mice by cardiac puncture under isoflurane anesthesia. The liver, spleen, and kidneys were removed and fixed in 10% formalin solution for histological examinations.

3.10.5. Subacute Toxicity Study

According to the results of the 5-day maximum tolerated dose determination study and histology results, the TW68 dose was determined as 20 mg/kg for the next 28-day subacute toxicity study. In this study, C57BL/6J mice (n=10) were treated with a 20 mg/kg dose of TW68 orally for 28 days. Control mice (n=5) were only treated with the control vehicle. Following this, the previously mentioned procedure (5-day maximum tolerated dose determination study) has been conducted in the same way.

3.10.6. Pharmacokinetic Studies

C57BL/6J female mice (n=4 per each time point) were treated with a 75 mg/kg single dose of TW68 intraperitoneally and orally. Blood samples were collected at 0.5, 1, 2, 4, 8, 24 and 48 hours after administration of TW68 by cardiac puncture under isoflurane anesthesia. Plasma was obtained by centrifugation from heparinized tubes and stored at -80°C until analysis. Liver, kidney, and ileum tissues were quickly removed and stored at -80°C for further processing. For assessment of the tissue exposure of TW68, levels in these tissues were determined according to maximum concentrations of the molecule in plasma.

3.10.7. Determination of TW68 Levels in Plasma and Tissues

Liquid chromatography coupled to tandem mass spectrometry (LC-MS/MS) was used to obtain high mass accuracy data of the analytes in plasma and tissue samples for the determination of TW68 and Internal standard (IS) dihydro capsaicin. The instrument was operated in full scan mode and ion source parameters were optimized for the type of analytes. The optimized conditions of the electrospray ionization (ESI) source were as follows: mass scanning range: 100-900 m/z, gas temperature, 320°C; gas flow, 10 L/min; capillary voltage, 3,80 kV. For the separation of the analytes, a conventional reversed-phase LC separation on C18-bonded silica (150 x 3 mm, 5 μm; Troyasil) was used, with distilled water (A, % 0.1 Formic acid) and Methanol (B, % 0.1 Formic acid) as mobile phase. TW68 was extracted from plasma samples by using liquid-liquid extraction with Acetonitrile Ethanol and Methanol. For tissue samples, a two-step lyophilization protocol followed by the extraction method specified for plasma was used. 5 μL of the sample was injected into the LC-MS/MS system. Thermo HPLC system (UltiMate 3000) and Q-Exactive Orbitrap Mass Spectrometer (Thermo Scientific, USA) were used in the analyses.

3.10.8. Pharmacokinetic Analysis

Peak plasma concentration (C_{max}) and time to reach peak plasma concentration (t_{max}) values were directly obtained from the TW68 plasma and tissue concentration-time curve. The area under the plasma and tissue concentration-time curve from 0 to 24h ($AUC_{0\text{-}24h}$) was calculated by the trapezoidal method. The elimination rate constant (kel) was calculated from the last four points of the TW68 plasma and tissue concentration-time plot, and the slope of this line was equal to (kel). To calculate the $AUC_{24h\text{-}\infty}$ value C24sa/kel formula was used. Terminal elimination half-life ($t_{1/2}$) was calculated by ln-linear approximation of terminal points of the data. $t_{1/2}$ and kel were interconverted with the following formula: $t_{1/2} = ln_2$ / kel. Other pharmacokinetic parameters of TW68 were calculated by the non-compartmental method.

3.10.9. Analysis of Antidiabetic Effects in Type 2 Diabetes Models

B6.Cg-Lep^{ob}/J transgenic mice from Jackson Laboratory (Strain #:000632) were used for the determination of the antidiabetic effect of TW68 in the genetic background of obesity. Female and male Lep^{ob} transgenic mice, 8-12 weeks old, weighed over 35 g were used. After 4-h fasting, the plasma glucose levels were determined before and after oral administration of 40 mg/kg TW68 molecule, 30 mg/kg pioglitazone, or control vehicle via glucometer (Accu-check, Performa Nano, Roche, Switzerland) over 4 days (n=3). Day-1 (before the TW68 administration) and Day-7 (after the TW68 administration for 5 days) plasma samples were taken from the tail vein and stored at -80°C until determined the insulin, glucagon, and ACTH values.

3.10.10. Fat-Induced Diet and Obesity

6 weeks old C57BL6/J wild type mice were randomly assigned to high-fat diet feeding group for fat-induced obesity. Mice were fed ad libitum with a diet containing 60% kcal fat (Formula #: D12492, Research Diet, USA) until the body mass increased over 35 g and plasma glucose levels above 190-200 mg/dL. For the determination of the antidiabetic

effect of TW68 on fat-induced obese mice, after a 4-h fasting the plasma glucose levels were determined before and after oral administration of 40 mg/kg TW68 molecule, 30 mg/kg pioglitazone, or control vehicle via glucometer (Accu-check, Performa Nano, Roche, Switzerland) over 4 days (n=3). Day-1 (before the TW68 administration) and Day-7 (after the TW68 administration for 5 days) plasma samples were taken from the tail vein and stored at -80°C until determine the insulin, glucagon, and ACTH values.

3.10.11. ELISA Analysis

Plasma samples taken from the mice tail vein on Day-1 and Day-7 were processed for ELISA analysis by using mouse glucagon (Catalog No: E-EL-M0555), insulin (E-EL-M1382) and ACTH (E-EL-M0079) kits (Elabscience Biotechnology, USA) according to manufacturer's protocol.

3.11. Statistical Analysis

All data were expressed as means ± standard error of the means (SEM) for each studied variable. Statistical analyses were performed using GraphPad Prism 9 software (GraphPad Software, California, USA). The statistical significance of differences between groups was validated with either of these: Student’s t-test and one- or two-way analysis of variance (ANOVA), following Dunnett's multiple comparisons, Tukey or Bonferroni post hoc tests to compare each dose with the control separately in a pair-wise manner. The type of significant test used in each experiment and their significance (p-value) was indicated in the figure legends.

Chapter 4

RESULTS

4.1. In-silico Screening

The stability of CRYs is important to regulate the timing of the mammalian circadian clock, and it is controlled by the interaction of the E3 ligases, FBXL3/21, through their primary pocket in PHR [105, 109]. We utilized a structure-based drug design approach to find novel small molecules that regulate CRY stability by targeting the FBXL3 binding site to dock the small molecules **(Figure 4.1)**. Around 2 million small molecule libraries with non-characterized functions were screened through molecular docking in silico. Root mean square deviation (RMSD) of backbone atoms (C, N, Cα), root mean square fluctuation (RMSF) of residues, and interacted H-bonds were analyzed during the simulation to monitor the convergence **(Figure 4.2)**. The top 90 candidate molecules with the lowest binding energies to CRY1 were selected for further experimental studies.

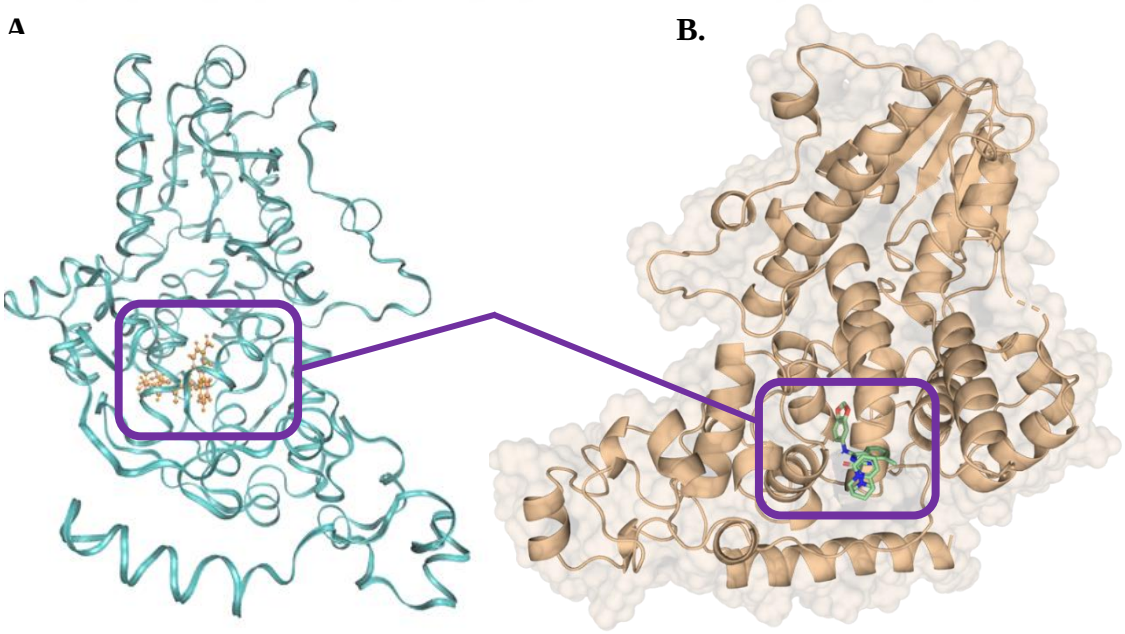

Figure 4. 1: Small molecules docked to the PHR domain of mCRY1. A. CP53 and **B.** TW68 were selected as representative small molecules. The purple box indicates the PHR domain of mCRY1. The best pose was captured via Autodock4 and PyMOL.

A.

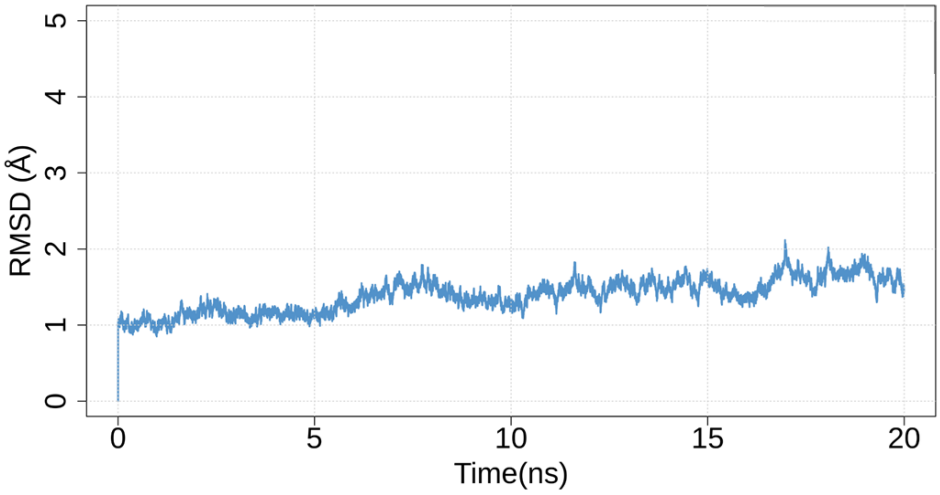

B.

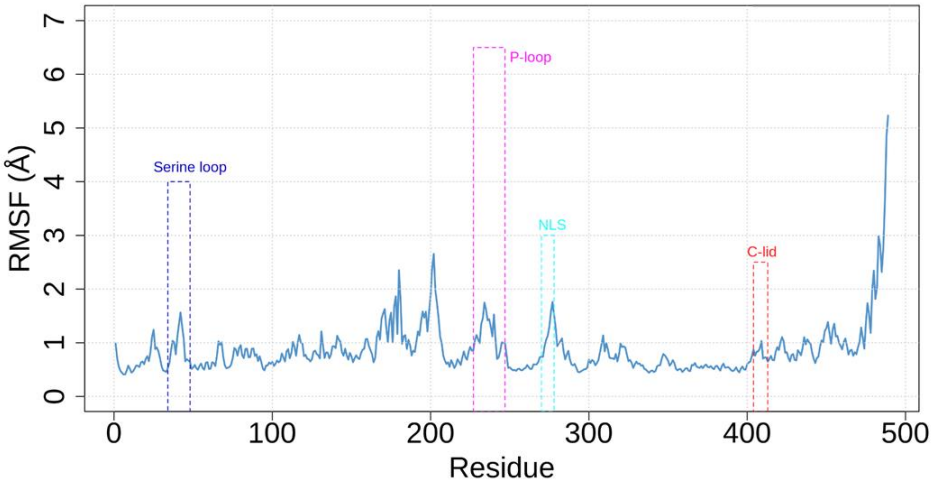

C.

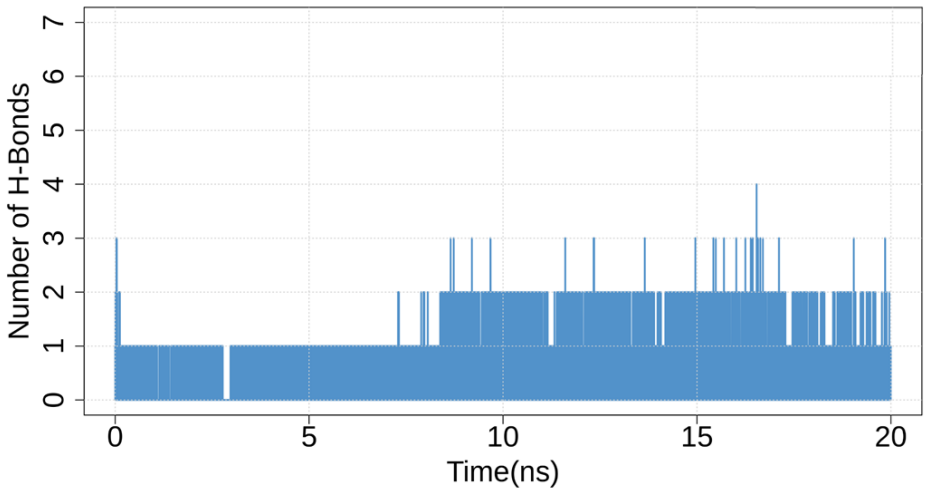

Figure 4. 2: Simulation results are shown in A. RMSD values of CRY1 simulation (20ns), **B.** RMSF values of backbone atoms (N-Cα-C) for each amino acid residue and **C.** Interacted H-bonds. The calculations were performed using the Visual Molecular Dynamics (VMD) software.

4.2. Determining the Cytotoxicity of Small Molecules

The small molecules were purchased from Ambinter and subjected to cytotoxicity assay using U2OS cells at doses of 20 μM, 10 μM, and 2.5 μM to determine the non-toxic highest doses. Dimethyl sulfoxide (DMSO) was used as a positive control in the experiment since the small molecules were dissolved in it, and the 5% DMSO was used as a negative control. The results of the cell viability assay for small molecules are given in **Figure 4.3.** The 70 molecules with a cell viability of more than 90% were identified as non-toxic at the given doses and selected for further characterization. 20 molecules that yielded less than 90% cell viability were eliminated from the following in vitro experiments. The small molecules with their selected non-toxic highest doses are shown in **Table 4.1.**

Table 4. 1: The small molecules with their selected non-toxic doses

Molecule ID	Non-toxic Dose	Molecule ID	Non-toxic Dose	Molecule ID	Non-toxic Dose
CP1	20 μM	**CP31**	20 μM	**CP61**	Toxic
CP2	2.5 μM	**CP32**	10 μM	**CP62**	20 μM
CP3	Toxic	**CP33**	Toxic	**CP64**	Toxic
CP4	Toxic	**CP34**	10 μM	**CP65**	20 μM
CP5	20 μM	**CP35**	10 μM	**CP66**	20 μM
CP6	20 μM	**CP36**	Toxic	**CP67**	20 μM
CP7	Toxic	**CP37**	20 μM	**CP68**	20 μM
CP8	10 μM	**CP38**	20 μM	**CP69**	Toxic
CP9	20 μM	**CP39**	Toxic	**CP70**	20 μM
CP10	Toxic	**CP40**	20 μM	**CP71**	2.5 μM
CP11	20 μM	**CP41**	10 μM	**CP72**	20 μM
CP12	Toxic	**CP42**	20 μM	**CP73**	20 μM
CP13	2.5 μM	**CP43**	10 μM	**CP74**	20 μM
CP14	20 μM	**CP44**	10 μM	**CP75**	20 μM
CP15	20 μM	**CP45**	10 μM	**CP76**	20 μM
CP16	20 μM	**CP46**	2.5 μM	**CP77**	20 μM
CP17	20 μM	**CP47**	20 μM	**CP78**	20 μM
CP18	20 μM	**CP48**	Toxic	**CP79**	20 μM
CP19	20 μM	**CP49**	20 μM	**CP80**	Toxic
CP20	20 μM	**CP50**	20 μM	**CP81**	2.5 μM
CP21	20 μM	**CP51**	10 μM	**CP82**	2.5 μM
CP22	20 μM	**CP52**	10 μM	**CP83**	2.5 μM
CP23	20 μM	**CP53**	10 μM	**CP84**	20 μM
CP24	Toxic	**CP54**	10 μM	**CP85**	2.5 μM
CP25	10 μM	**CP55**	Toxic	**CP86**	20 μM
CP26	Toxic	**CP56**	20 μM	**CP87**	20 μM
CP27	Toxic	**CP57**	2.5 μM	**CP88**	Toxic
CP28	20 μM	**CP58**	Toxic	**CP89**	Toxic
CP29	20 μM	**CP59**	2.5 μM	**CP90**	20 μM
CP30	20 μM	**CP60**	2.5 μM	**TW68**	20 μM

A.

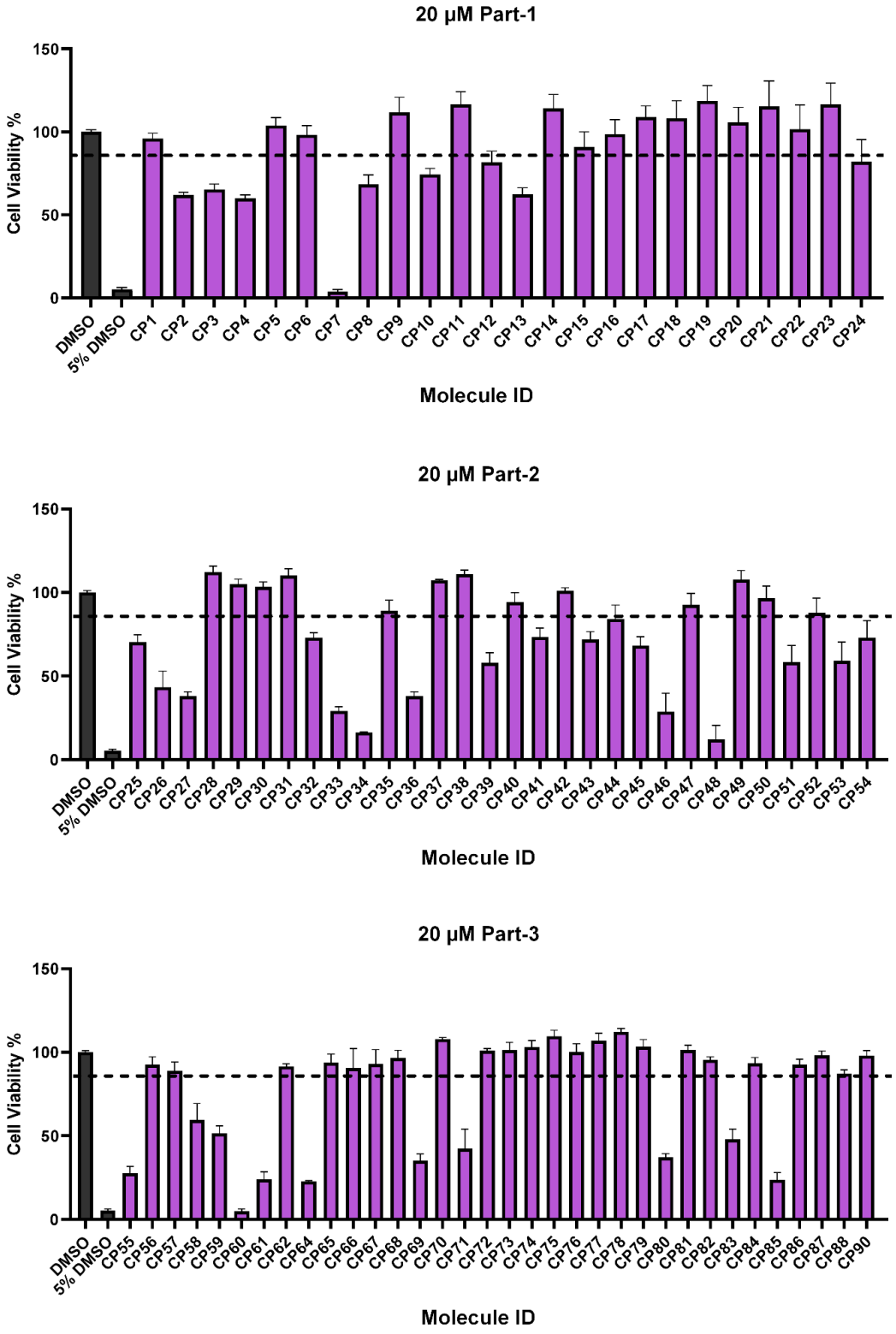
20 µM Part-1
Cell Viability %
150
100
50
0
DMSO
5% DMSO
CP1
CP2
CP3
CP4
CP5
CP6
CP7
CP8
CP9
CP10
CP11
CP12
CP13
CP14
CP15
CP16
CP17
CP18
CP19
CP20
CP21
CP22
CP23
CP24
Molecule ID
20 µM Part-2
Cell Viability %
150
100
50
0
DMSO
5% DMSO
CP25
CP26
CP27
CP28
CP29
CP30
CP31
CP32
CP33
CP34
CP35
CP36
CP37
CP38
CP39
CP40
CP41
CP42
CP43
CP44
CP45
CP46
CP47
CP48
CP49
CP50
CP51
CP52
CP53
CP54
Molecule ID
20 µM Part-3
Cell Viability %
150
100
50
0
DMSO
5% DMSO
CP55
CP56
CP57
CP58
CP59
CP60
CP61
CP62
CP64
CP65
CP66
CP67
CP68
CP69
CP70
CP71
CP72
CP73
CP74
CP75
CP76
CP77
CP78
CP79
CP80
CP81
CP82
CP83
CP84
CP85
CP86
CP87
CP88
CP90
Molecule ID

B.

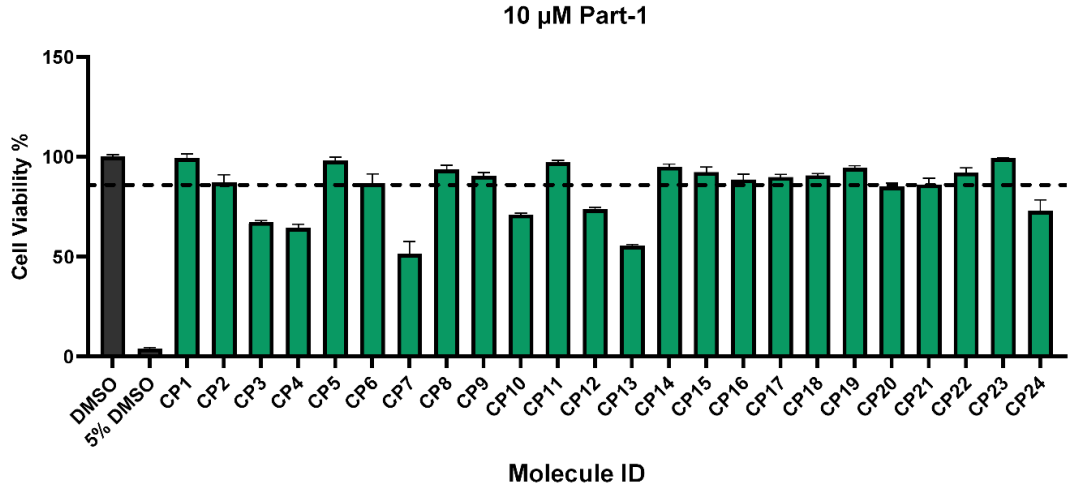
10 µM Part-1
Cell Viability %
150
100
50
0
DMSO
5% DMSO
CP1
CP2
CP3
CP4
CP5
CP6
CP7
CP8
CP9
CP10
CP11
CP12
CP13
CP14
CP15
CP16
CP17
CP18
CP19
CP20
CP21
CP22
CP23
CP24
Molecule ID

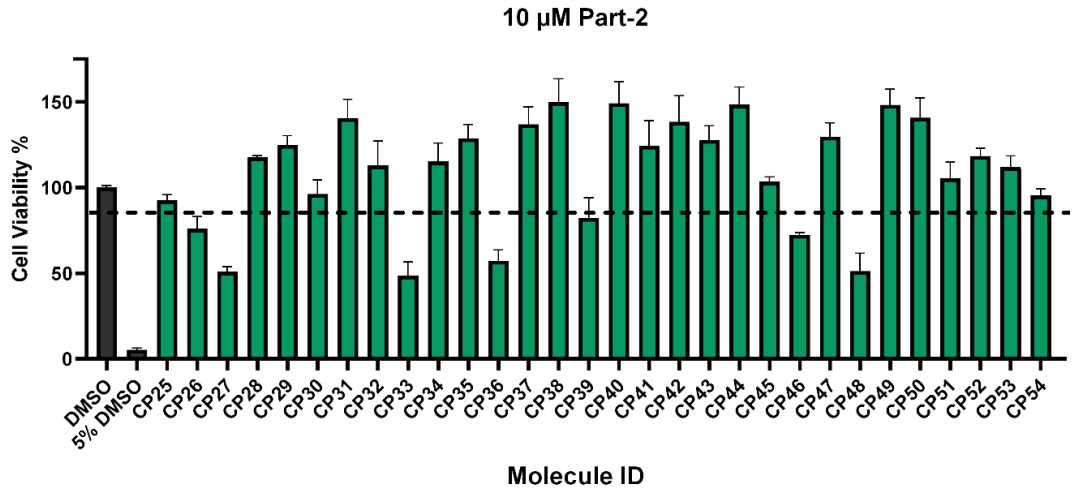
10 µM Part-2
Cell Viability %
150
100
50
0
DMSO
5% DMSO
CP25
CP26
CP27
CP28
CP29
CP30
CP31
CP32
CP33
CP34
CP35
CP36
CP37
CP38
CP39
CP40
CP41
CP42
CP43
CP44
CP45
CP46
CP47
CP48
CP49
CP50
CP51
CP52
CP53
CP54
Molecule ID

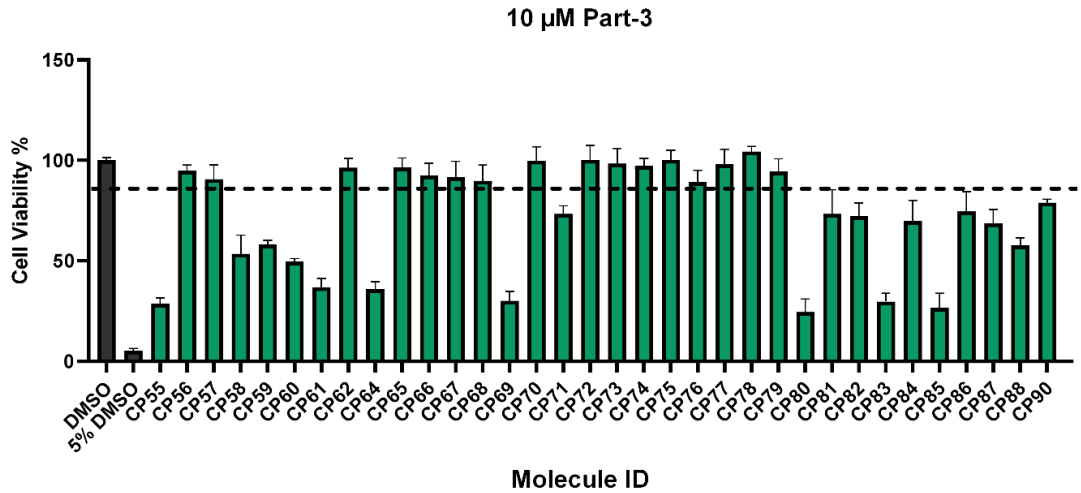
10 µM Part-3
Cell Viability %
150
100
50
0
DMSO
5% DMSO
CP55
CP56
CP57
CP58
CP59
CP60
CP61
CP62
CP64
CP65
CP66
CP67
CP68
CP69
CP70
CP71
CP72
CP73
CP74
CP75
CP76
CP77
CP78
CP79
CP80
CP81
CP82
CP83
CP84
CP85
CP86
CP87
CP88
CP90
Molecule ID

C.

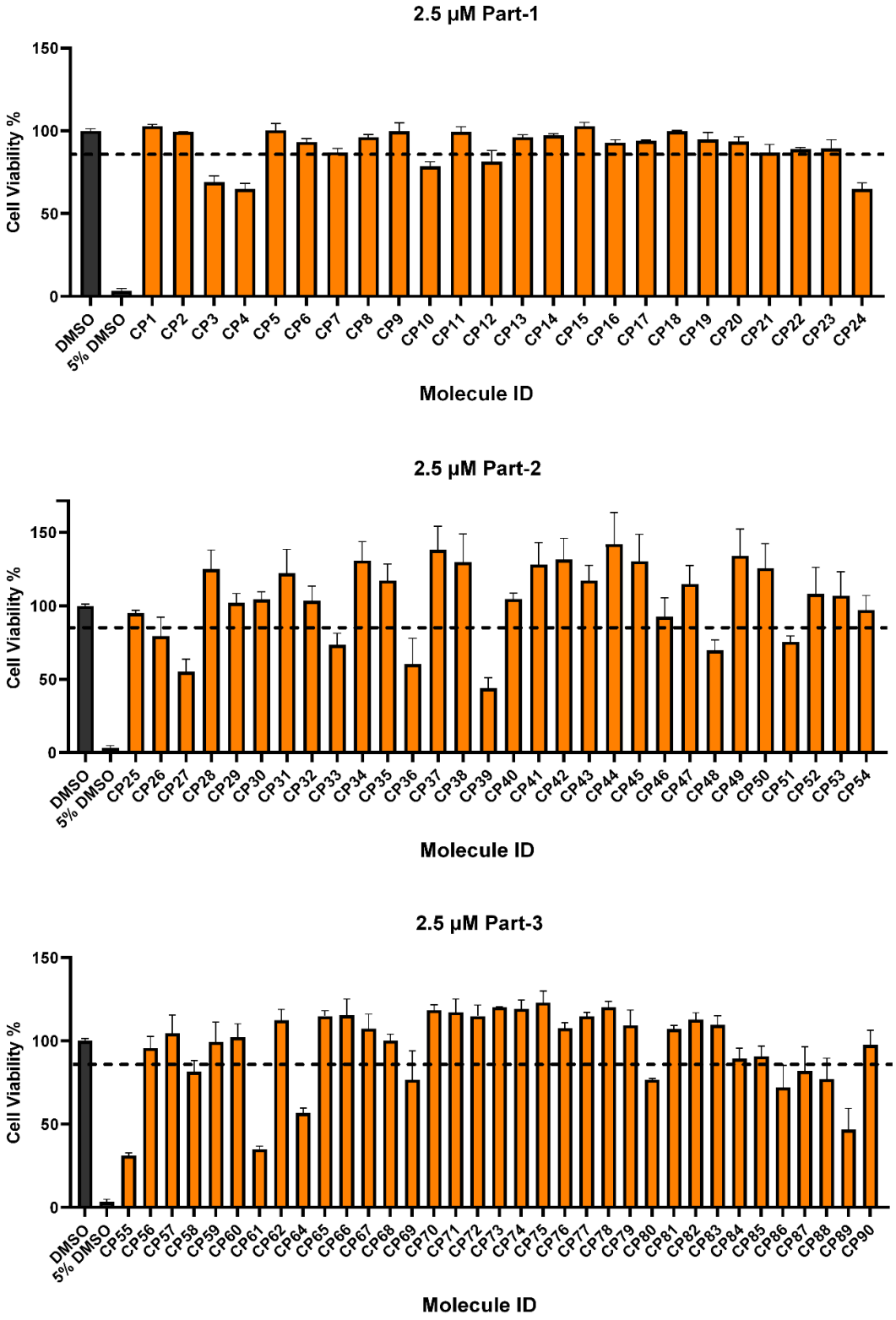

Figure 4. 3: Cell viability assay of U2OS cells treated with small molecules at doses of A. 20 µM, **B.** 10 µM, and **C.** 2.5 µM. The dashed black line indicates 90% cell viability. Data represent the mean ± SEM, n=3.

4.3. The Effect of Small Molecules on LUC Half-life

Several in vitro tools were used in this study based on the luciferase system. To eliminate the possibility that the small molecules might interfere with luciferase half-life or stability, I first tested the effect of non-toxic small molecules on luciferase enzymatic activity [178]. The HEK293T cells were transfected with a plasmid harboring the d*Luc* gene and then treated with selected small molecules at the non-toxic highest doses. After 24 hours of treatment with small molecules, protein synthesis was inhibited by cycloheximide, and real-time luciferase readings were recorded for 24 hours via Synergy H1 (BioTek) **(Figure 4.4)**. The 30 molecules that significantly affect the luciferase half-life were eliminated from further experiments.

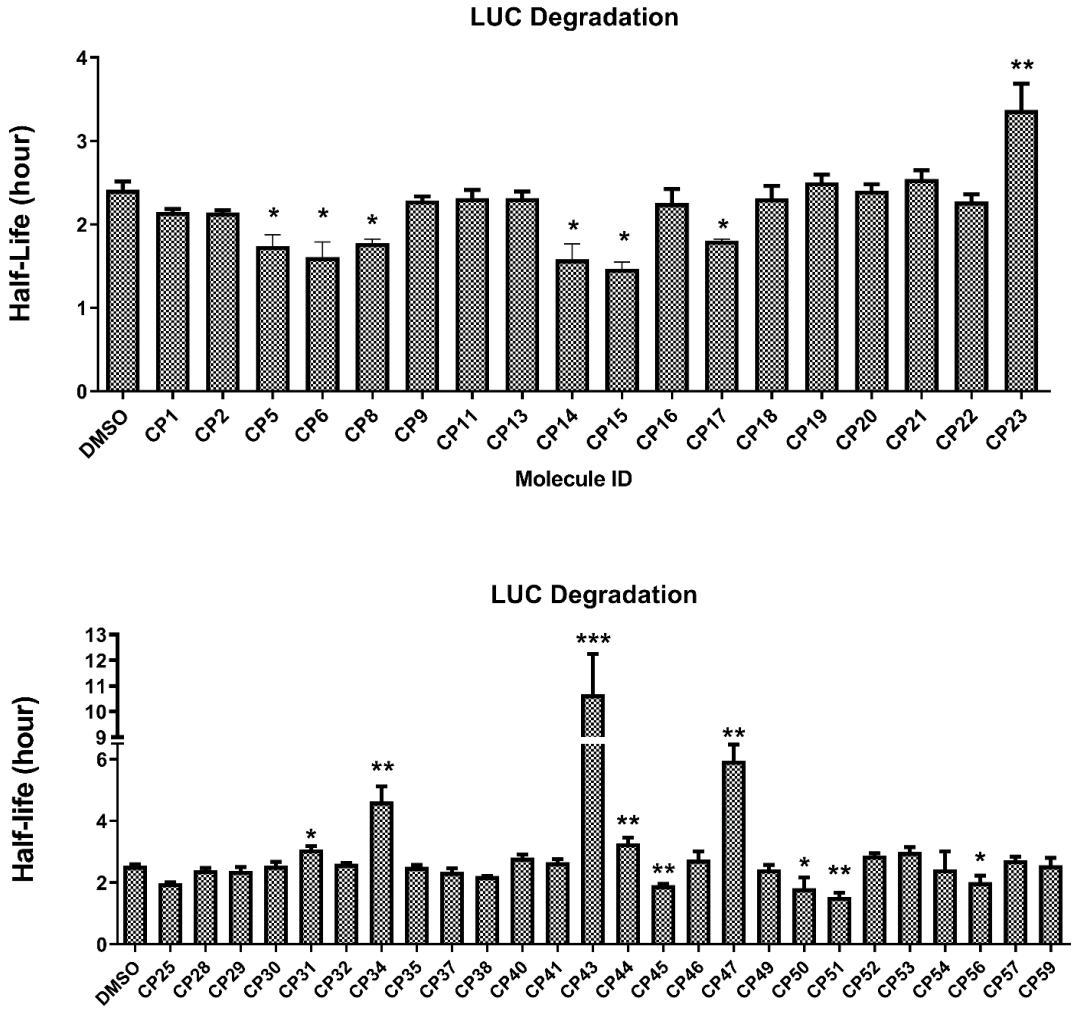

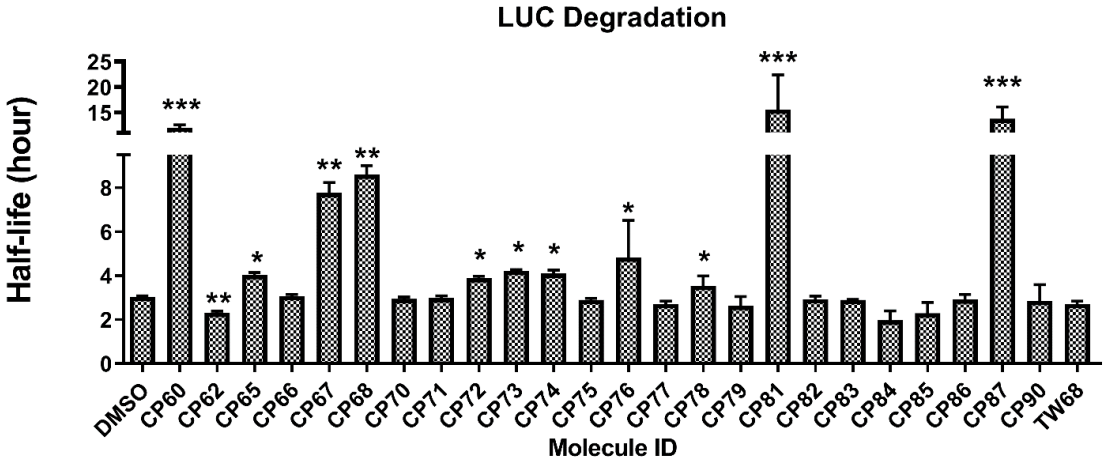

Figure 4. 4: Effect of small molecules on LUC half-life. Data are given as mean ± SEM, n=3. The half-life of each molecule was calculated via a one-phase exponential decay function in GraphPad Prism 9 software. Statistical analysis was performed by using Student's t-test versus DMSO control (*p<0.05, **p<0.01, ***p<0.001, all others are non-significant).

4.4 The Effect of Small Molecules on Circadian Rhythm

After the elimination of the molecules that affect LUC half-life then, the effect of small molecules on the circadian rhythm was determined using the U2OS-*Bmal1*-d*Luc* cell line. The 40 molecules were tested by circadian reporter assay and the bioluminescence recordings were monitored for 7 days by using the 96-well plate via Synergy H1 (BioTek). The period, amplitude and phase properties of the cells were calculated to detect the effect of the molecules on circadian rhythm by using the BioDare2 software [179].

The molecules were classified according to their phenotypical changes in the circadian period. The 8 molecules caused arrhythmic phenotypes, while 16 (inert) molecules didn't cause any changes in circadian rhythm phenotype. Additionally, 16 molecules significantly increased the circadian period length **(Figure 4.5).**

Since the reporter *Bmal1* promoter is under the control of the circadian clock, we hypothesized that these effector molecules might interfere with the CRYs stability or activity as previously reported [181, 182]. For this aim, 24 molecules that showed

promising effects on the circadian rhythm were further investigated on CRYs stability. The inert 16 molecules were eliminated from downstream experiments.

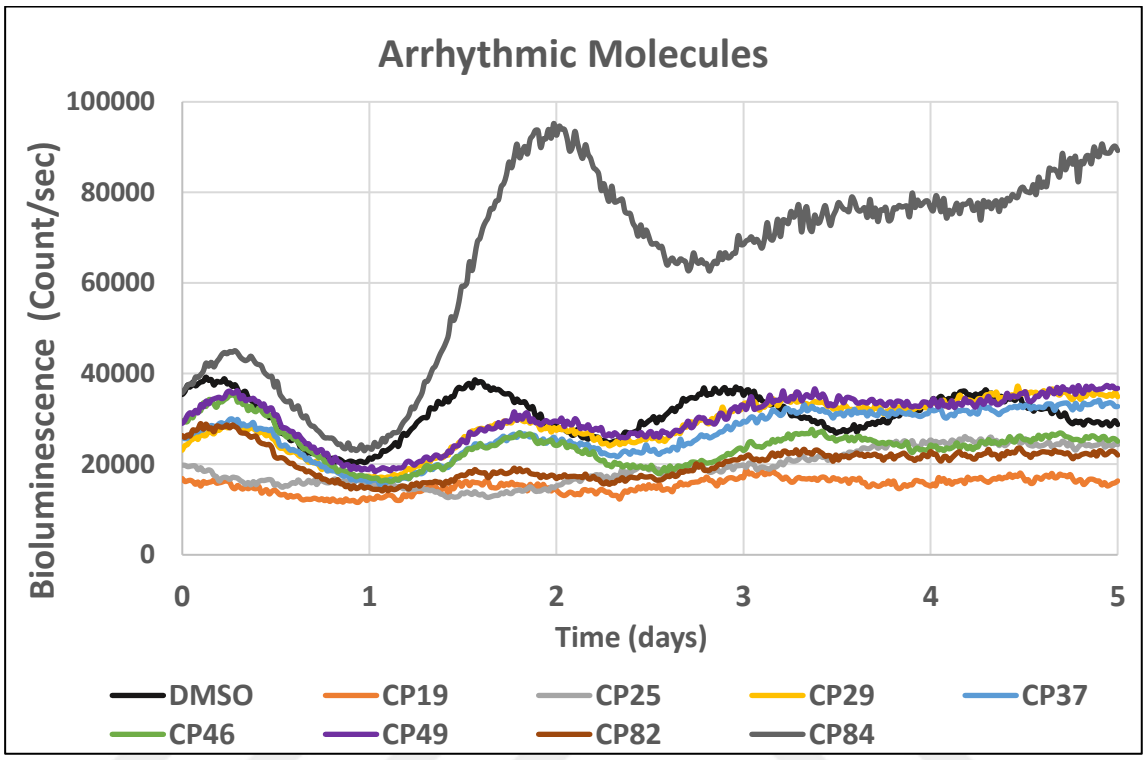

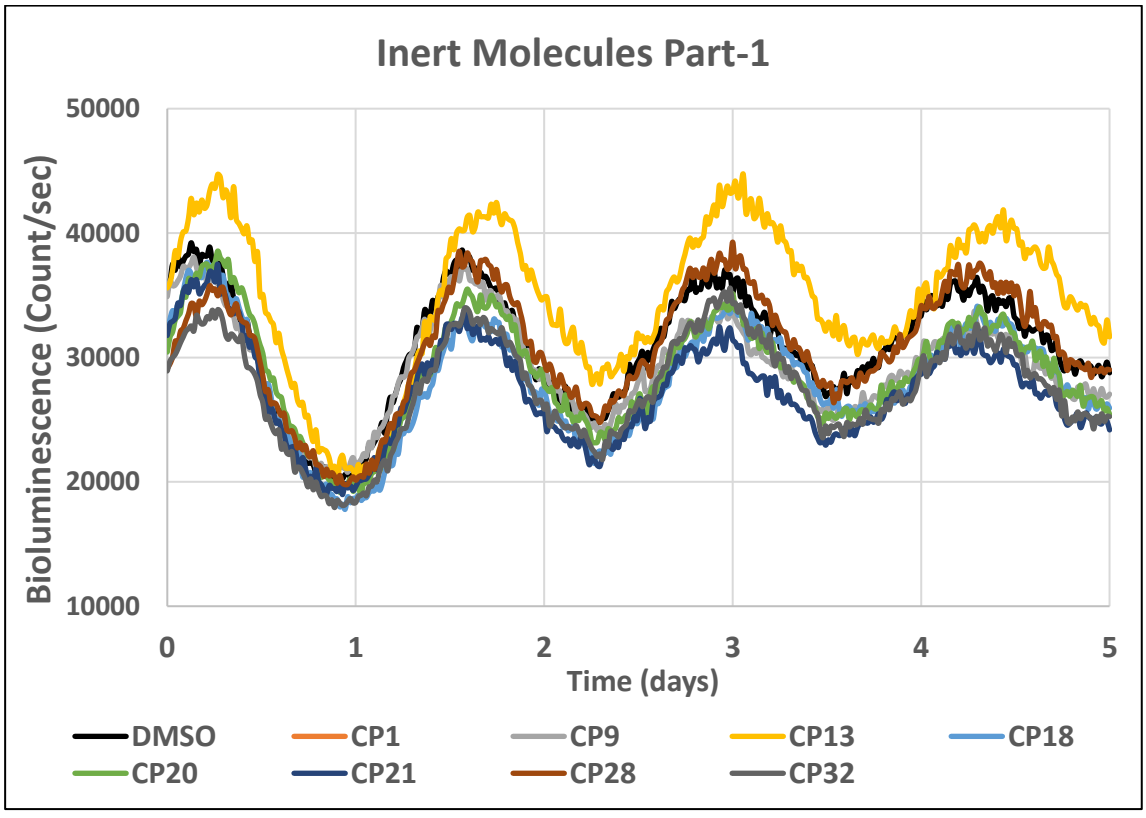

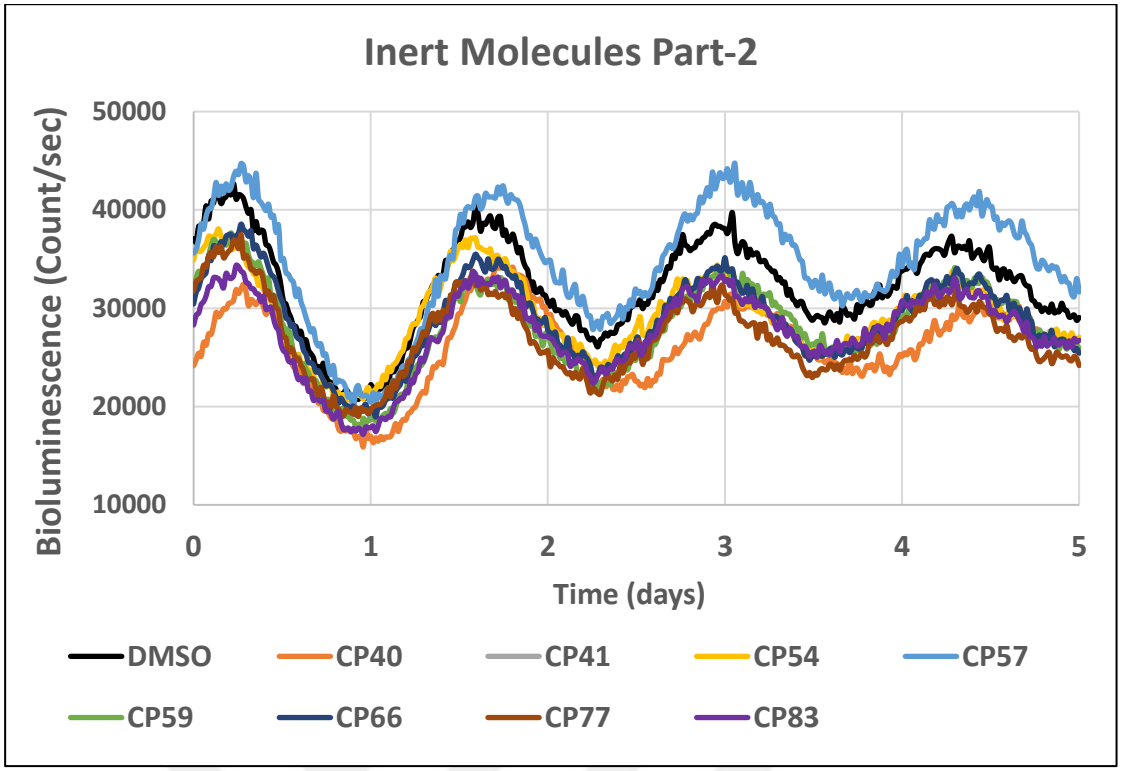
Inert Molecules Part-2
Bioluminescence (Count/sec)
50000
40000
30000
20000
10000
0
1
2
3
4
5
Time (days)
DMSO
CP40
CP41
CP54
CP57
CP59
CP66
CP77
CP83

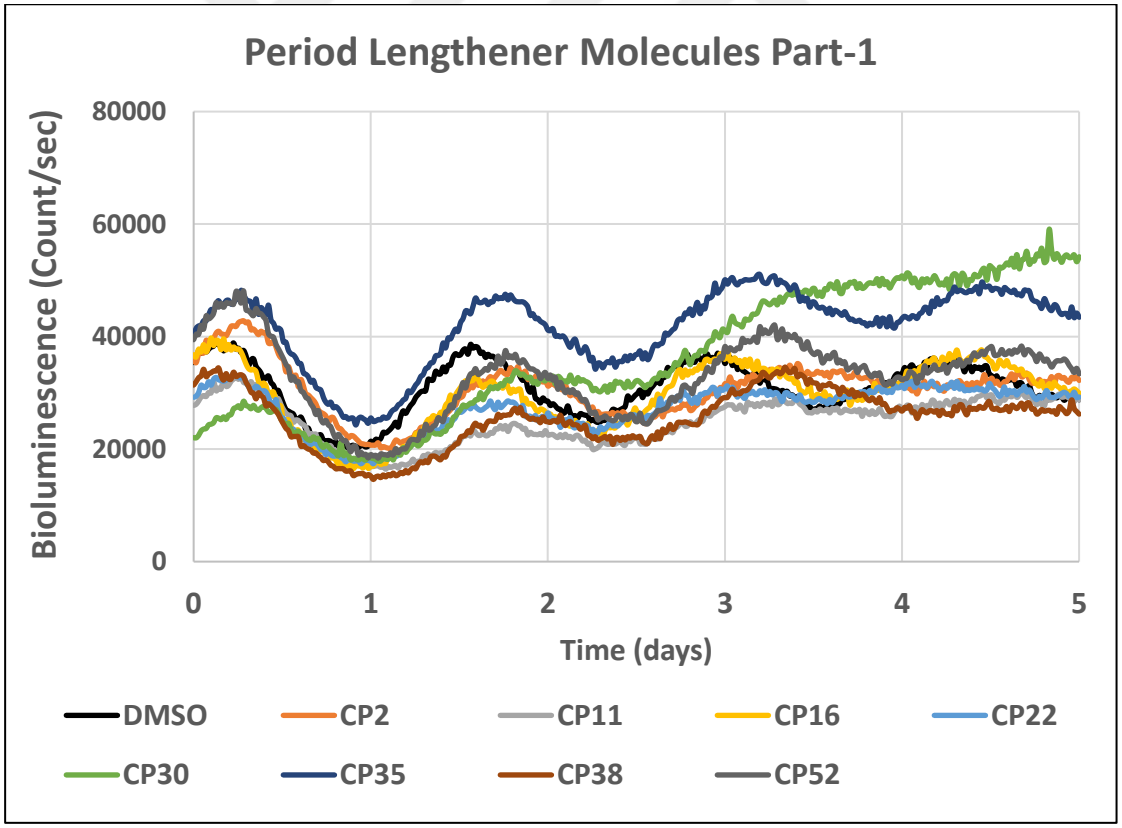
Period Lengthener Molecules Part-1
Bioluminescence (Count/sec)
80000
60000
40000
20000
0
0
1
2
3
4
5
Time (days)
DMSO
CP2
CP11
CP16
CP22
CP30
CP35
CP38
CP52

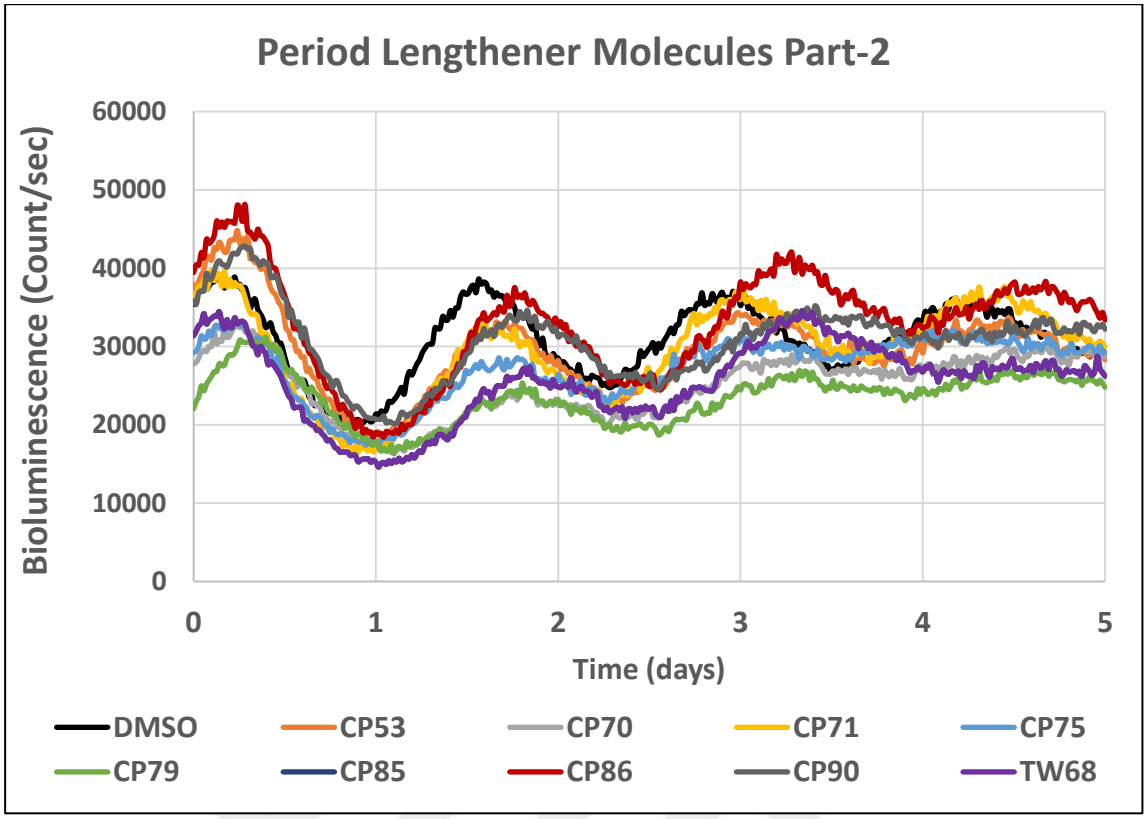

Figure 4. 5: The effect of the small molecules on circadian rhythm. The bioluminescence rhythm of U2OS *Bmal1*-d*Luc* cells was monitored for 7 days in the presence of molecules. DMSO control was drawn a black line in each graph, n=3.

4. 5 The Effect of Small Molecules on CRYs Half-life

To determine the effect of the molecules on the half-life of CRYs, I performed the LUC protein degradation assay to determine the effect of the 24 active small molecules on the half-life of CRY1 and CRY2 by measuring the one phase exponential decay rates of the LUC fused CRYs as previously described [183]. HEK293T cells were reverse transfected with either pcDNA-*Cry1-Luc* or pcDNA-*Cry2-Luc* plasmids, followed by small molecule treatment at non-toxic doses. Then protein synthesis was stopped by cycloheximide, and luciferase readings were recorded for 24 hours by Synergy H1 (BioTek).

Among these screening TW68 was found to increase the half-life of both CRY1 and CRY2, and 2 molecules CP79 and CP85 exclusively enhance the half-life of CRY2 significantly. While the 10 molecules **CP25**, CP30, **CP35**, CP38, **CP53**, CP71, CP75, CP85, CP86 and CP90 decreased the half-life of CRY1, and the 5 molecules **CP25**, **CP35**, CP46, CP49, **CP53** decreased the half-life of CRY2 significantly **(Figure 4.6)**. The small molecules which regulated both CRY1 and CRY2 stability, CP25, CP35, CP53 and TW68 were further investigated for their dose-dependent effects.

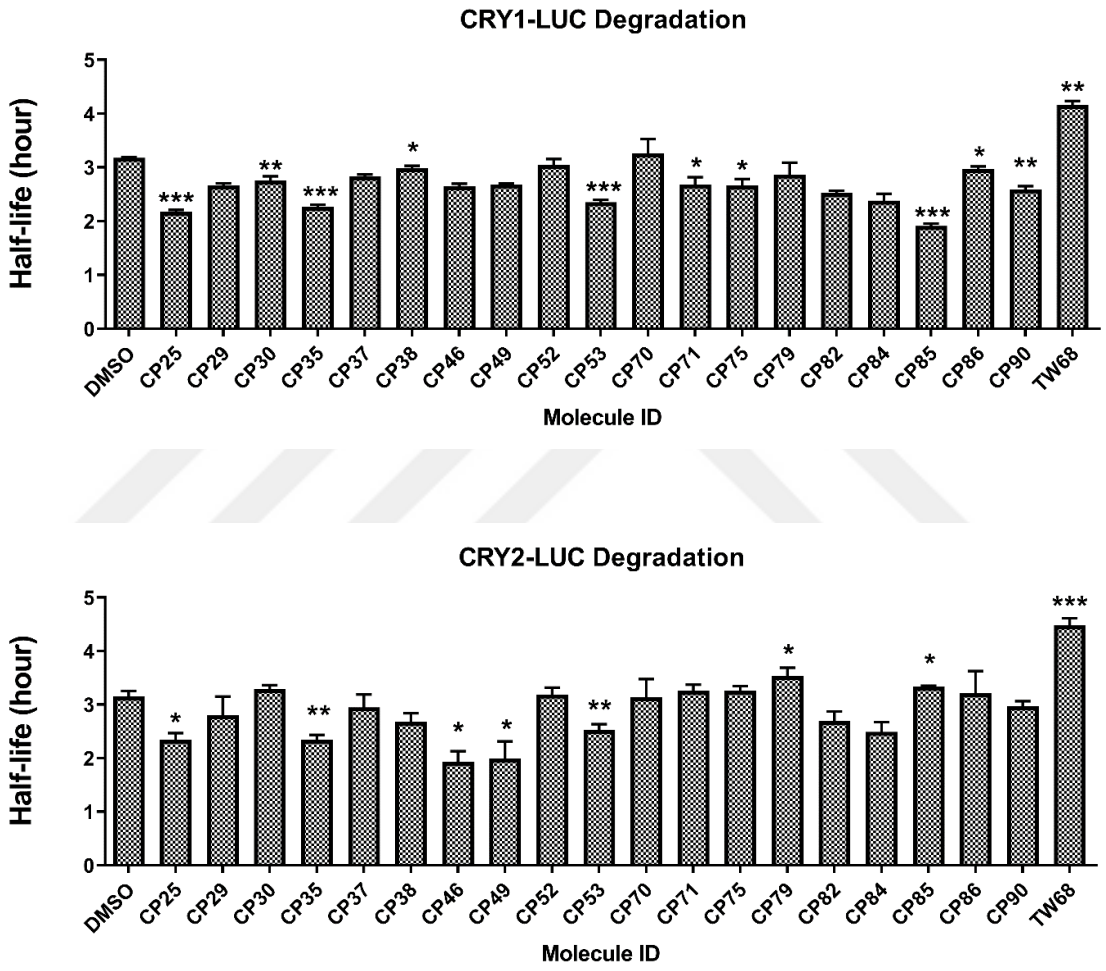

Figure 4. 6: Effect of small molecules on **A.** CRY1-LUC and **B.** CRY2-LUC half-life. Data represent the mean ± SEM, n= 3. The half-life of each molecule was calculated via a one-phase exponential decay function in GraphPad Prism 9 software. Statistical analysis was performed by using Student's t-test versus DMSO control (*p<0.05, **p<0.01, ***p<0.001, all others are non-significant).

Then CP25, CP35, CP53 and TW68 were tested in CRY1-LUC and CRY2-LUC degradation assay for dose-dependent effect. CP25 and CP35 had no dose-dependent activity on CRY1 and CRY2 half-life **(Figure 4.7)**. While CP53 caused a decrease in both CRY1-LUC and CRY2-LUC half-life dose-dependently, TW68 increased the half-life of CRY1-LUC and CRY2-LUC significantly in a dose-dependent manner **(Figure 4.8)**. In order to discover small molecules that modify both CRYs stability, from this point, we focused on the two active molecules, CP53 and TW68, that have dose-dependent effects on both CRY1 and CRY2, and also regulate the circadian rhythm.

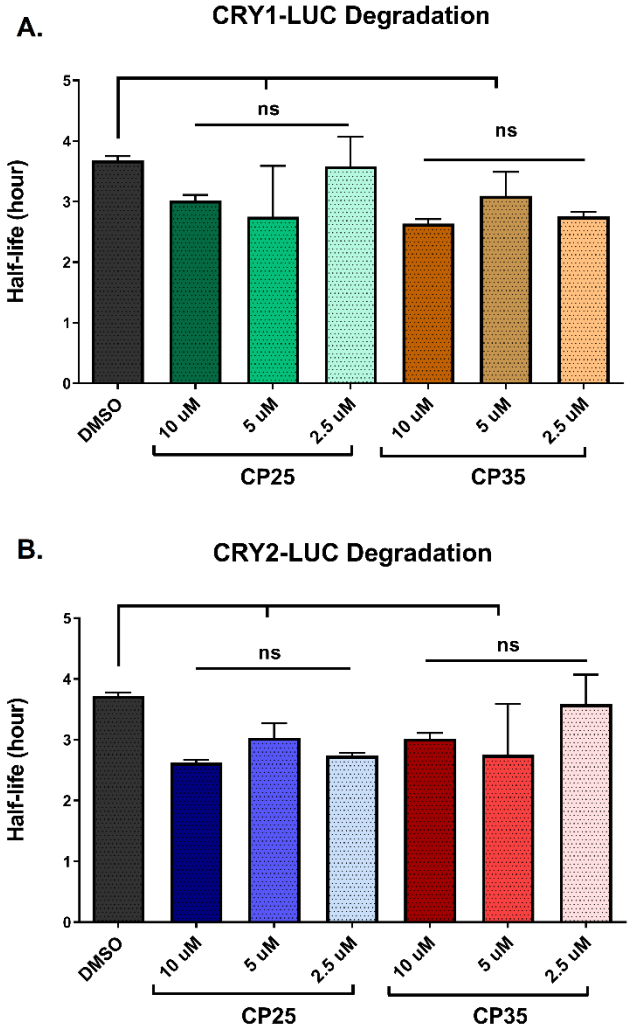

Figure 4. 7: Dose-dependent effects of CP25 and CP35 molecules on **A.** CRY1-LUC and **B.** CRY2-LUC half-life, respectively. Data are given as mean ± SEM, n= 3. The half-life of each molecule was calculated via a one-phase exponential decay function in GraphPad Prism 9 software. Statistical analysis performed by Ordinary one-way ANOVA with Dunnett's multiple comparisons test versus DMSO control (ns= non-significant).

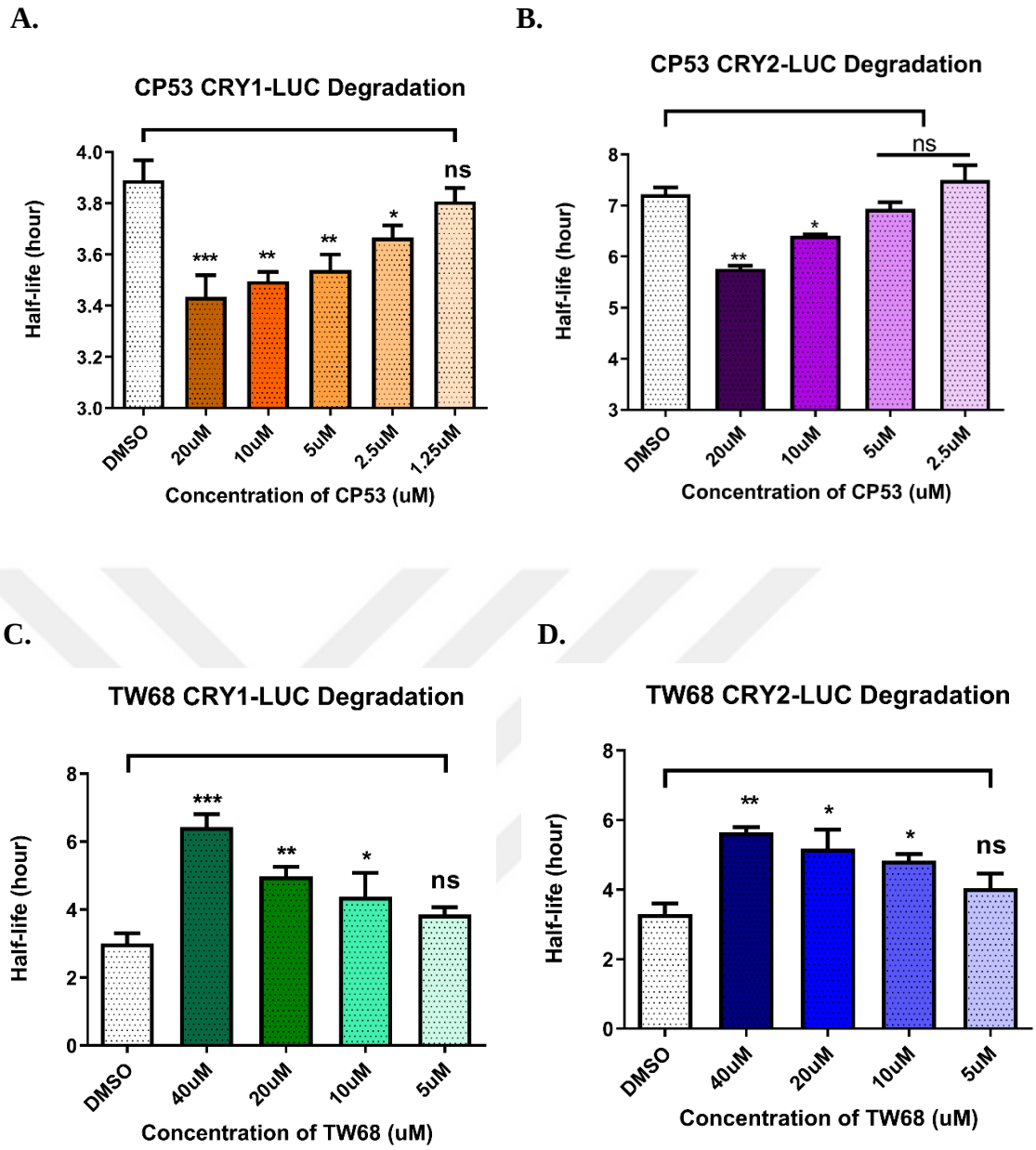

Figure 4. 8: The CP53 significantly decreased the **A.** CRY1-LUC and **B.** CRY2-LUC half-life dose-dependently. The TW68 significantly increased the **C.** CRY1-LUC and **D.** CRY2-LUC half-life dose-dependently. Data are given as mean ± SEM, n= 3. Half-life was calculated via one-phase exponential decay function in GraphPad Prism 9 software. Statistical analysis was performed by using Student's t-test versus DMSO control (*p<0.05, **p<0.01, ***p<0.001, ns= non-significant).

4.6 The Effect of CP53 and TW68 on Circadian Rhythm

Establishing a dose-response relationship is an important criterion in drug discovery studies. It typically involves a range of compound concentrations usually prepared by serial dilutions tested in an assay to assess the concentration or dose dependency. In vitro experiences, EC50 (half-maximal effective concentration) represents the concentration of a compound where 50% of its maximal effect is observed [184], and EC50 dose can be calculated by plotting dose-response curves [185]. Small molecules, CP53 and TW68 were tested at 0, 2.5, 5, 10, 20 and 40 µM for their effect on *Bmal1*-d*Luc* reporter assay. Dose-response curves plotted for CP53 and TW68 were given in **Figure 4.9**. The EC50 value for CP53 was calculated as ~5 µM, so in the following experiments 1.25 µM, 2.5 µM, 5 µM and 10 µM doses were used for CP53, and the EC50 value for TW68 was calculated as ~10 µM, so in the following experiments 10 µM, 20 µM, 40 µM doses were used for TW68.

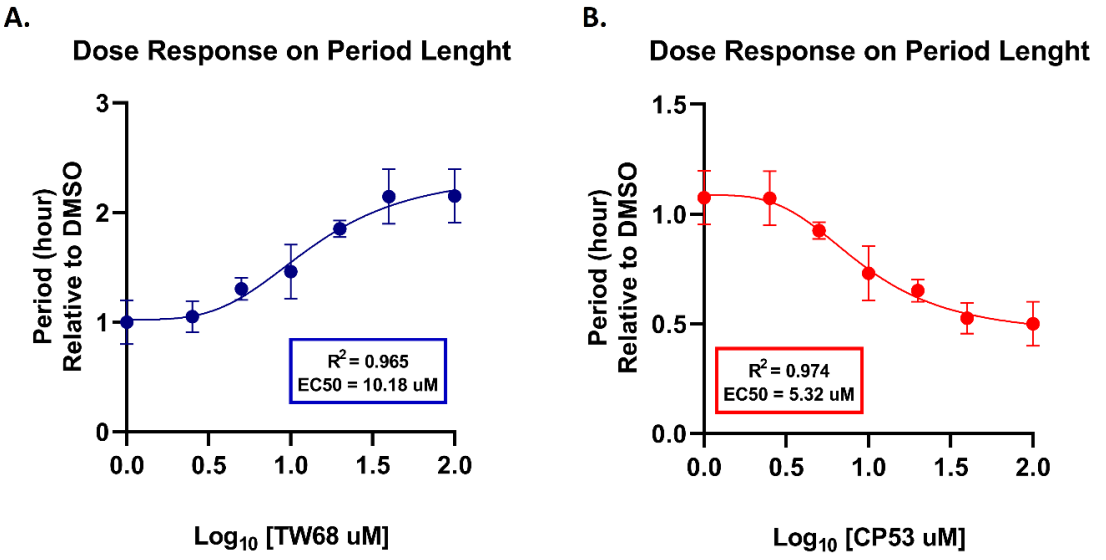

Figure 4. 9: Dose-response curves of **A.** TW68 and **B.** CP53 on U2OS *Bmal1*-d*Luc* cells. EC50, the half maximal effective concentration, and R^2 the coefficient of determination values calculated on the corresponding plot by the nonlinear regression function in GraphPad Prism 9. Data represent mean ± SEM, n=3.

To investigate the effect of CRY-regulator molecules CP53 and TW68 on the circadian period extensively, we tested the dose-dependent effect of these molecules on the circadian rhythm via cell-based reporter assay. Two different genetic backgrounds, human U2OS *Bmal1-dLuc* and mouse NIH3T3 *Bmal1*-d*Luc* stable cell lines were treated with different doses for each molecule, and their bioluminescence recordings were monitored for 7-days by using high-resolution LumiCyle32 luminometer (Actimetrics). The circadian rhythm parameters, period, and amplitude were obtained from the LumiCycle Analysis program and values were calculated from data fitted to 2nd order polynomial. CP53 treatment of U2OS *Bmal1*-d*Luc* cells significantly lengthened the period dose-dependently and reduced the amplitude, while the period increased in NIH3T3 *Bmal1*-d*Luc* cells **(Figure 4.10).**

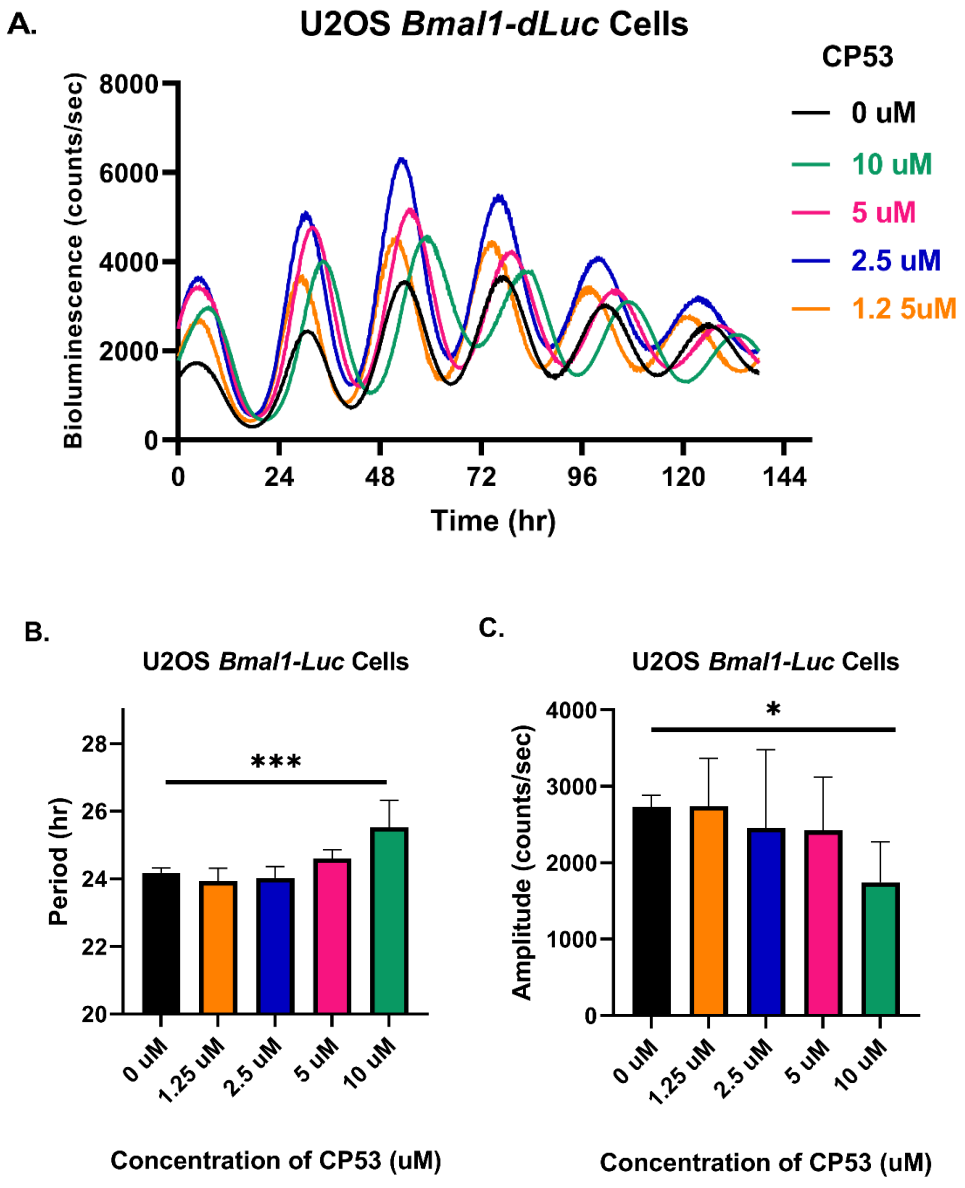

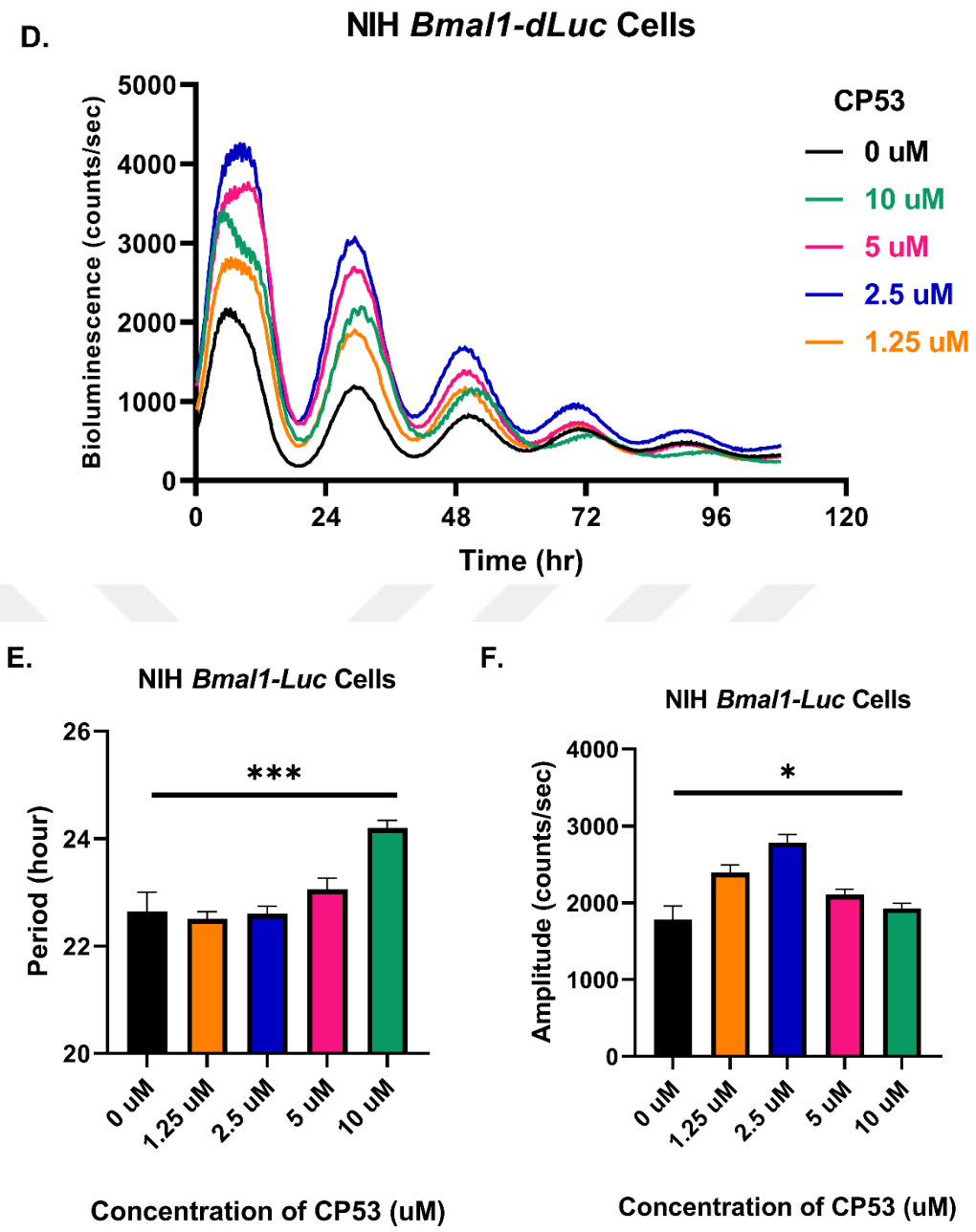

Figure 4. 10: Dose-dependent effect of CP53 on the Circadian Rhythm. Bioluminescence, period (hr) **(B, E)** and amplitude (counts/sec) **(C, F)** determined on **A.** U2OS Bmal1-d*Luc* cells and **D.** NIH Bmal1-d*Luc* cells. Data are given as mean ± SEM, n=3 with duplicates. Statistical analysis was performed by using one-way ANOVA with Dunnett's multiple comparisons test versus 0 uM control (*p<0.05, **p<0.01, ***p<0.001).

On the other hand, when U2OS *Bmal1*-d*Luc* cells were treated with TW68 the period increased significantly in a dose-dependent manner. Hence TW68 increased the period and amplitude dose-dependently in NIH *Bmal1*-d*Luc* cells as shown in **Figure 4.11**. These results suggested that CP53 and TW68 affect the circadian period and might regulate the stability and activity of CRYs.

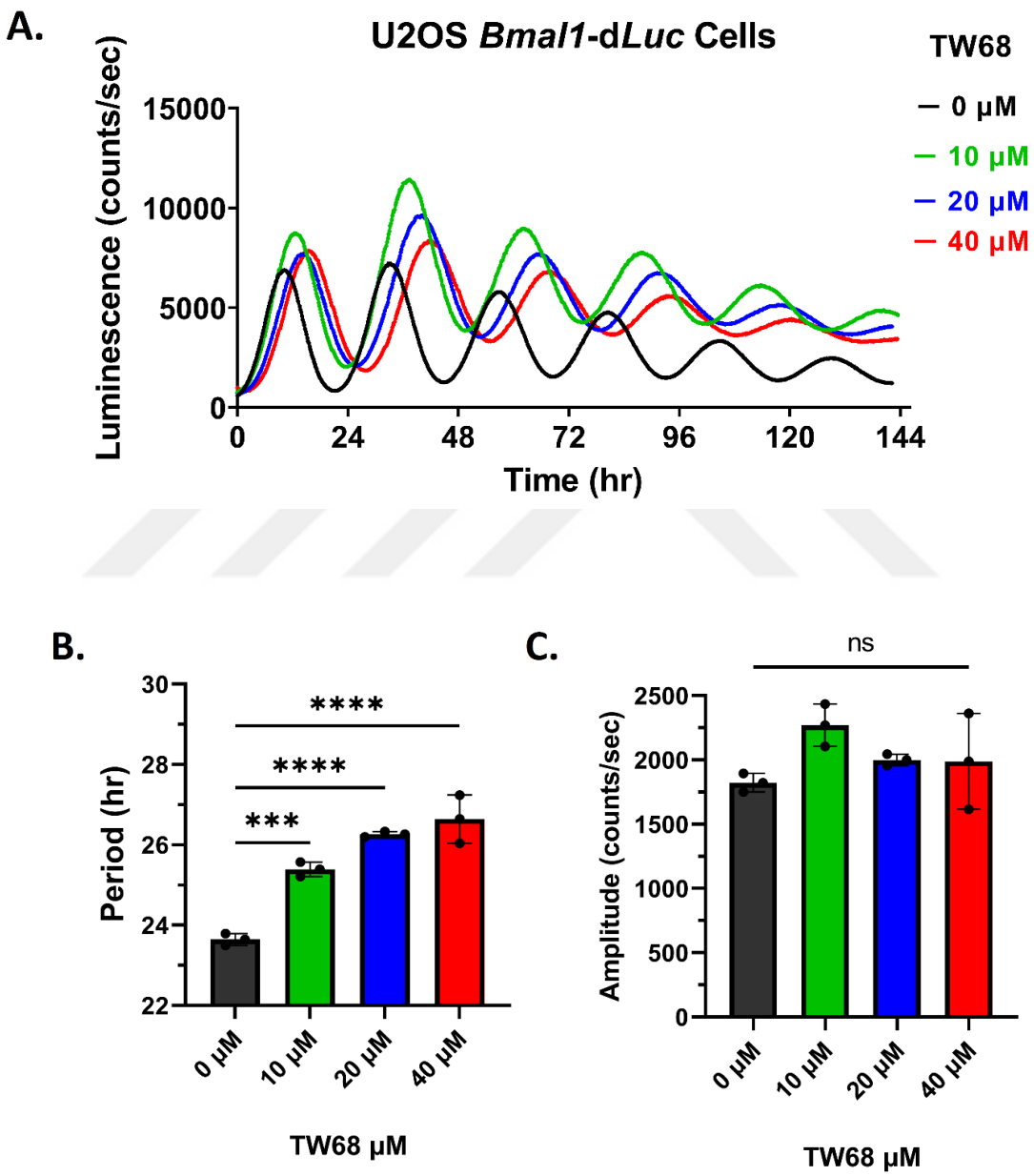

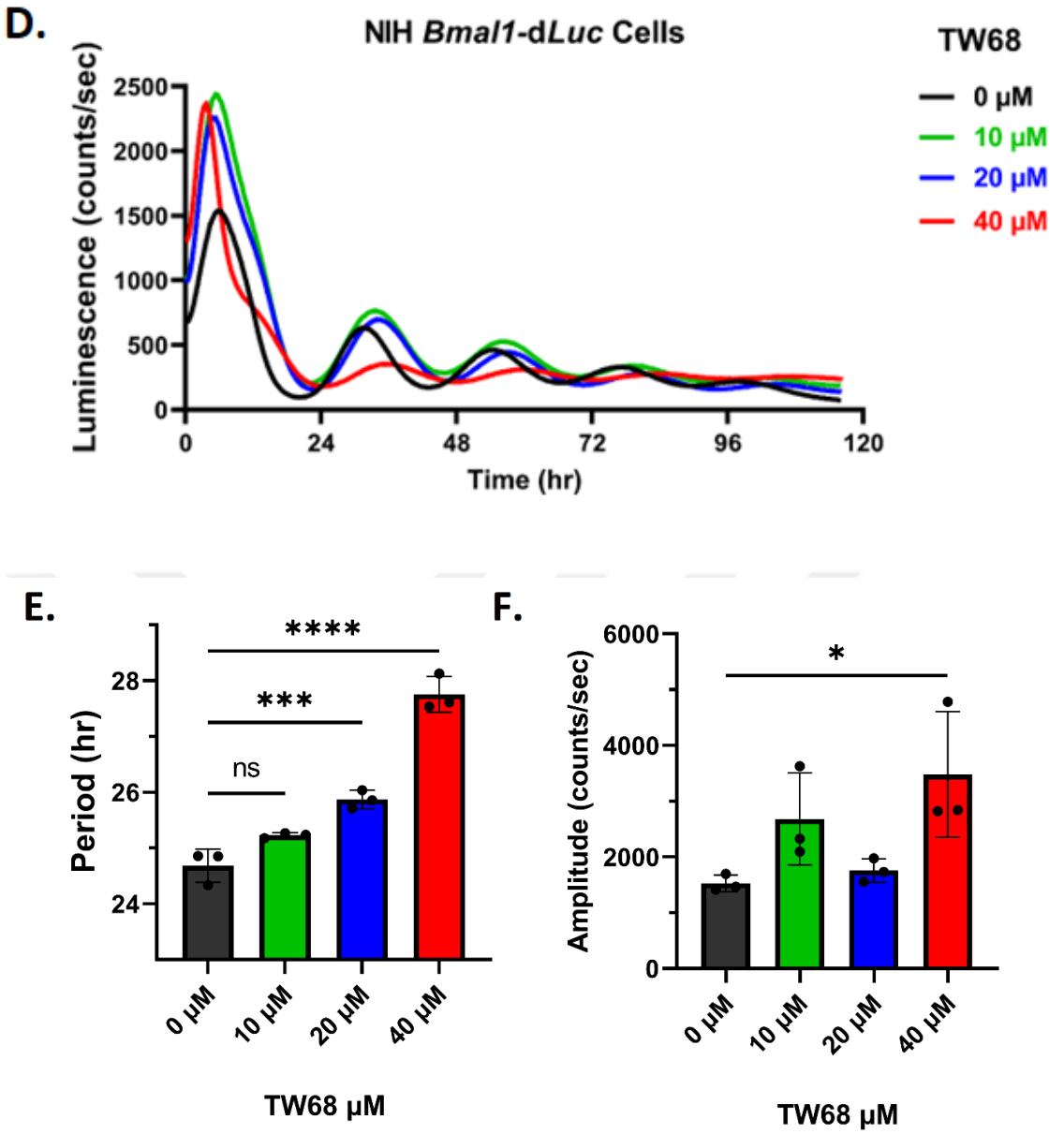

Figure 4. 11: Dose-dependent effect of TW68 on the circadian Rhythm. Bioluminescence, period (hr) **(B, E)** and amplitude (counts/sec) **(C, F)** determined on **A.** U2OS Bmal1-d*Luc* cells and **D.** NIH Bmal1-d*Luc* cells. Data are given as mean ± SEM, n=3 with duplicates. Statistical analysis was performed by using one-way ANOVA with Dunnett's multiple comparisons test versus 0 uM control (*p<0.05, **p<0.01, ***p<0.001).

4.7 The Effect of CP53 and TW68 on the Protein and mRNA Levels of Clock Genes

Small molecules that stabilize the CRYs are expected to cause an increase in the CRYs protein level [101]. This stabilization leads the CRY:PER complex to repress BMAL1:CLOCK transactivation strongly which causes a decrease in the expression of *Cry1/2*, *Per1/2*, and clock output genes, *Dbp*, and *Rev-erbα* [91]. On the contrary, when small molecules decrease the stability of CRYs, the loss of repression activity on BMAL1:CLOCK cause an increase in the expression of *Cry1*, *Cry2*, and clock output genes. In order to evaluate the effect of CP53 and TW68 on the endogenous protein and mRNA levels of circadian clock genes biochemical analyses were performed with the aid of Western blot and RT-qPCR. Unsynchronized U2OS cells were treated with small molecules either CP53 or TW68 and DMSO as a control. 24 hours after treatment whole cell lysate was subjected to Western blot analysis.

TW68 had significantly increased the protein level of both CRY1 and CRY2 as well as PER2 in a dose-dependent manner [186]. With a broader range of doses of TW68 and including other core clock proteins, the results were consistent with the previous studies. However, CLOCK and BMAL1 protein levels were not affected by the TW68 treatment **(Figure 4.12)**. The results suggested that TW68 stabilizes CRY1 and CRY2. This stability in CRYs, also stabilizes the PER2 due to forming of CRY:PER2 complex, and that leads to a decrease in the degradation rate of free PER2 in the cell [187].

A.

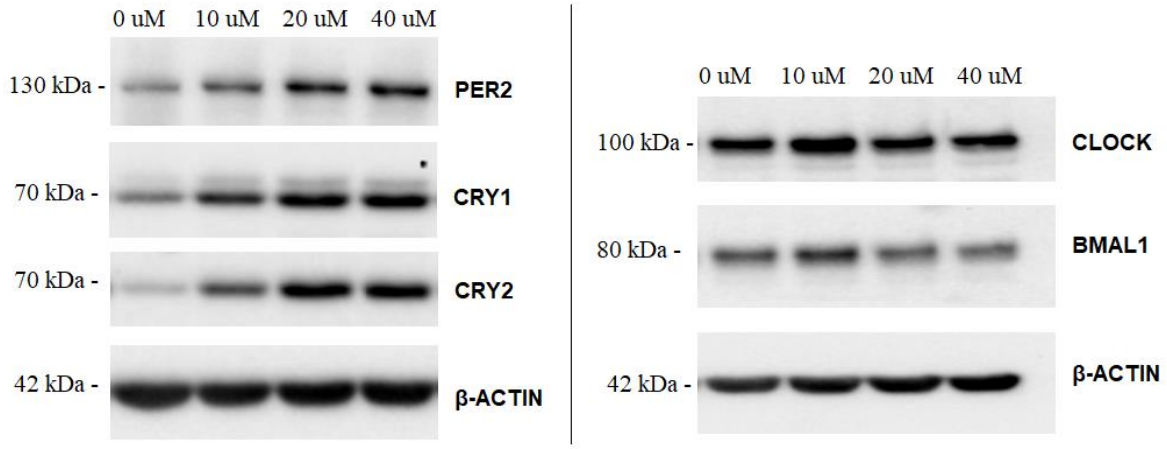

B.

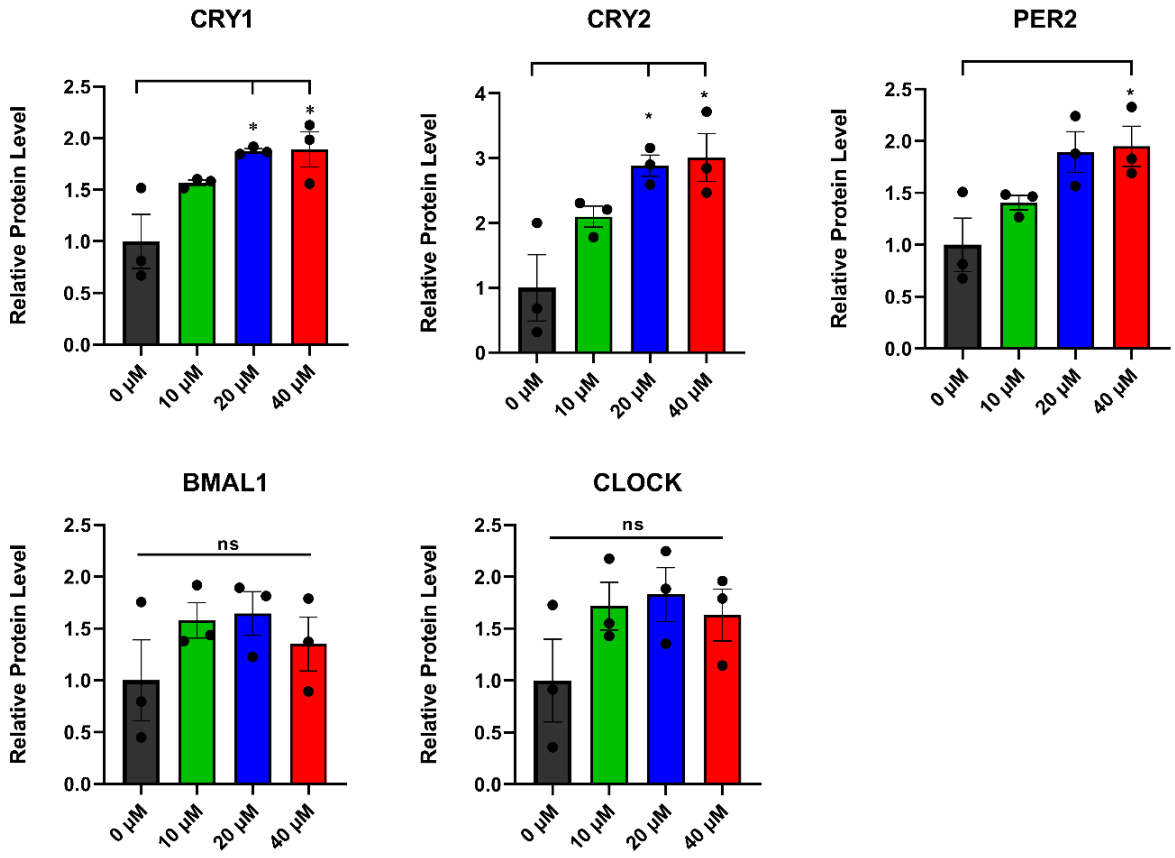

Figure 4. 12: Western blot analysis of unsynchronized U2OS cells treated with TW68. A. CRY1, CRY2, PER2, BMAL1 and CLOCK core clock proteins, and **B.** Protein levels that normalized with β-ACTIN, relative to 0 uM control. Data are given as mean ± SEM, n=3. Statistical analysis was performed using one-way ANOVA with Dunnett's multiple comparisons test (*$p<0.05$, ns = non-significant).

On the other hand, CP53 had no significant dose-dependent effect on CRY1 and CRY2 protein levels **(Figure A.3 in Appendix A).** The lack of dose dependent effect made me hypothesize that it could be because of the unsynchronization of the circadian rhythm in the cells. For this aim U2OS cells were synchronized with Dexamethasone (DXM) and treated with CP53. Cells were harvested between 24-44 hours after synchronization with 4-hour intervals. As a result, CP53 increased the level of CRY1 and CRY2, especially between 36-40 hours **(Figure 4.13).**

A.

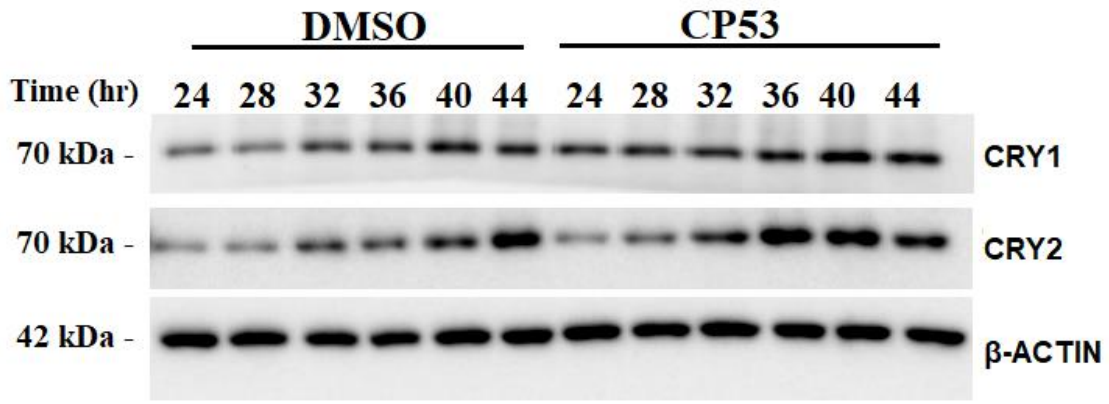

B.

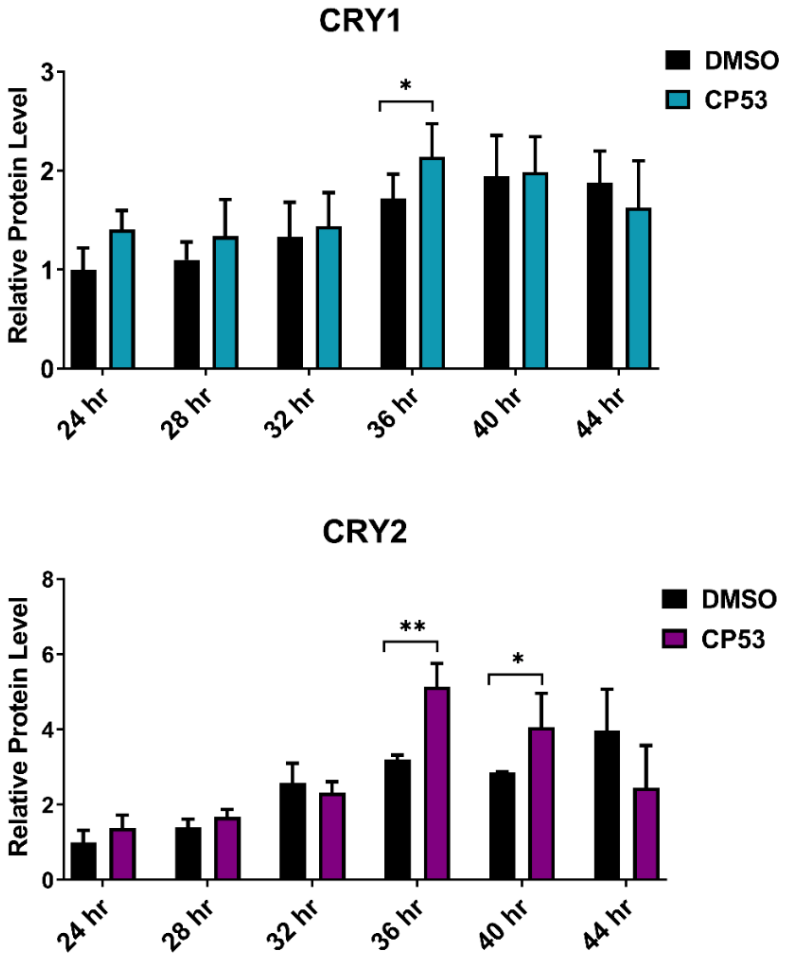

Figure 4. 13: Western blot analysis of synchronized U2OS cells treated with CP53. **A.** Time-dependent CRY1 and CRY2 proteins, and **B.** Protein levels that normalized with β-ACTIN, relative to DMSO (24 hr) control. Data are given as mean ± SEM, n=3. Statistical analysis was performed using a one-way ANOVA test (*p<0.05, **p<0.01, ns = non-significant).

Next, to assess the effect of the CP53 and TW68 on clock output genes U2OS cells that were treated with small molecules were subjected to determine the mRNA levels of clock genes by RT-qPCR (Reverse-Transcription-Quantitative Polymerase Chain Reaction) analysis. The mRNA levels were normalized with *RPLP0* gene expression as internal control since its expression level is independent of circadian gene expression [188].

Results showed that the *CRY1*, *CRY2*, *PER2*, *DBP* and *REV-ERBα* expression significantly decreased with TW68 treatment in a dose-dependent manner. Since CRY1 and CRY2 proteins stabilized by TW68, the reduction in the expression of E-box regulated clock output genes was expected. The excess amount of CRYs represses the BMAL1:CLOCK transactivation by strengthening the negative arm of the circadian clock feedback loop. On the other hand, *BMAL1* and *CLOCK* expression was not affected by the TW68 treatment **(Figure 4.14).**

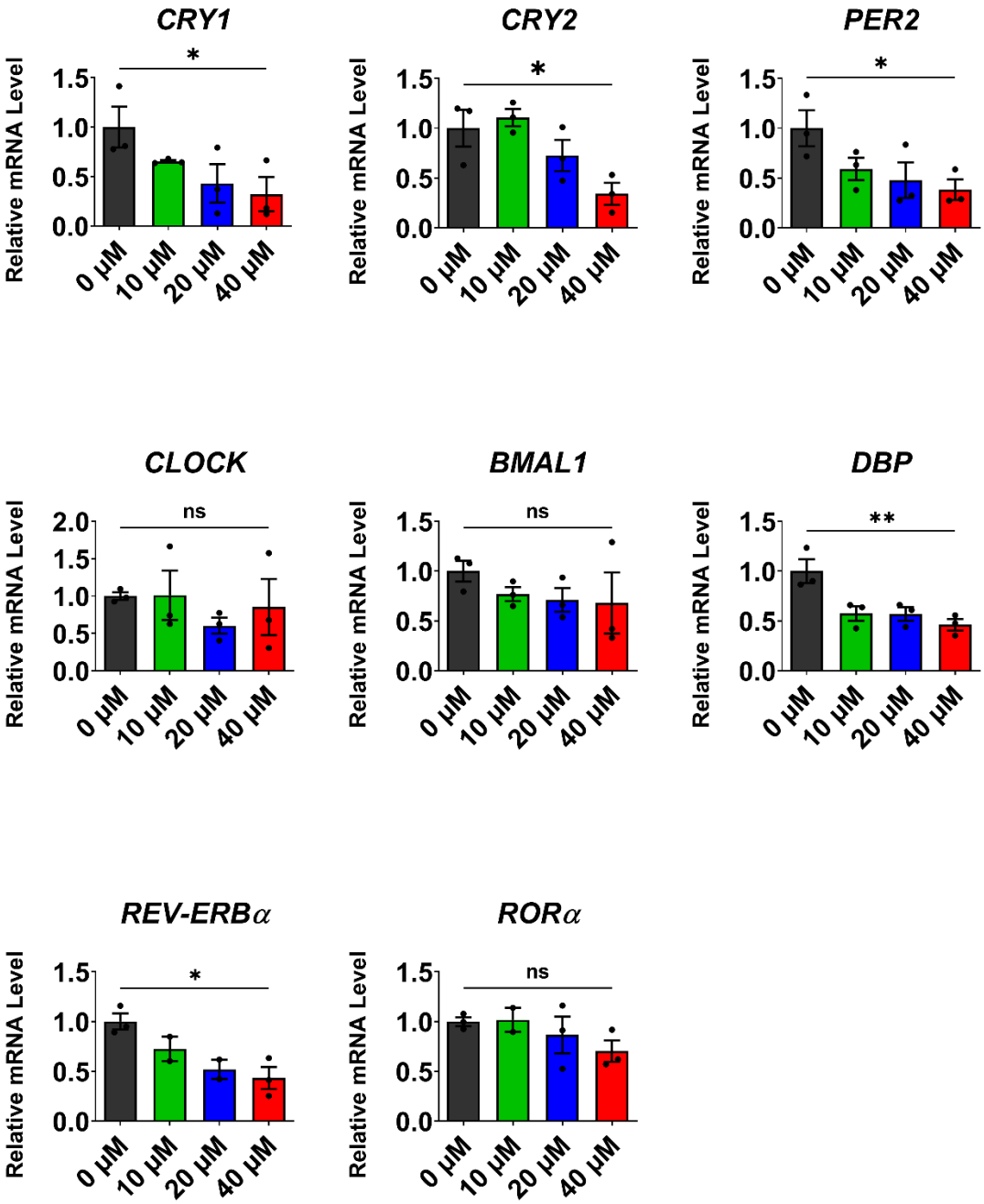

Figure 4. 14: RT-qPCR analysis of unsynchronized U2OS cells treated with TW68. mRNA levels of *CRY1*, *CRY2*, *PER2*, *DBP*, *REV-ERBα*, *RORα*, *CLOCK*, and *BMAL1* normalized with *RPLP0* and relative to 0 uM control. Data are given as mean ± SEM, n=3. Statistical analysis was performed using a one-way ANOVA test (*p<0.05, **p<0.01, ns: non-significant).

Results also showed that CP53 decreased *CRY1*, *CRY2* and *PER2* mRNA levels without changing the peak time, while there was no significant effect on clock output gene, *DBP* expression except at 44 hours after synchronization. Changing the peak time of *BMAL1* expression at 28 hours and 40 hours might happen because of the abundance of CRY1 and CRY2 protein levels at those time points, strongly repressing the BMAL1:CLOCK transactivation **(Figure 4.15).**

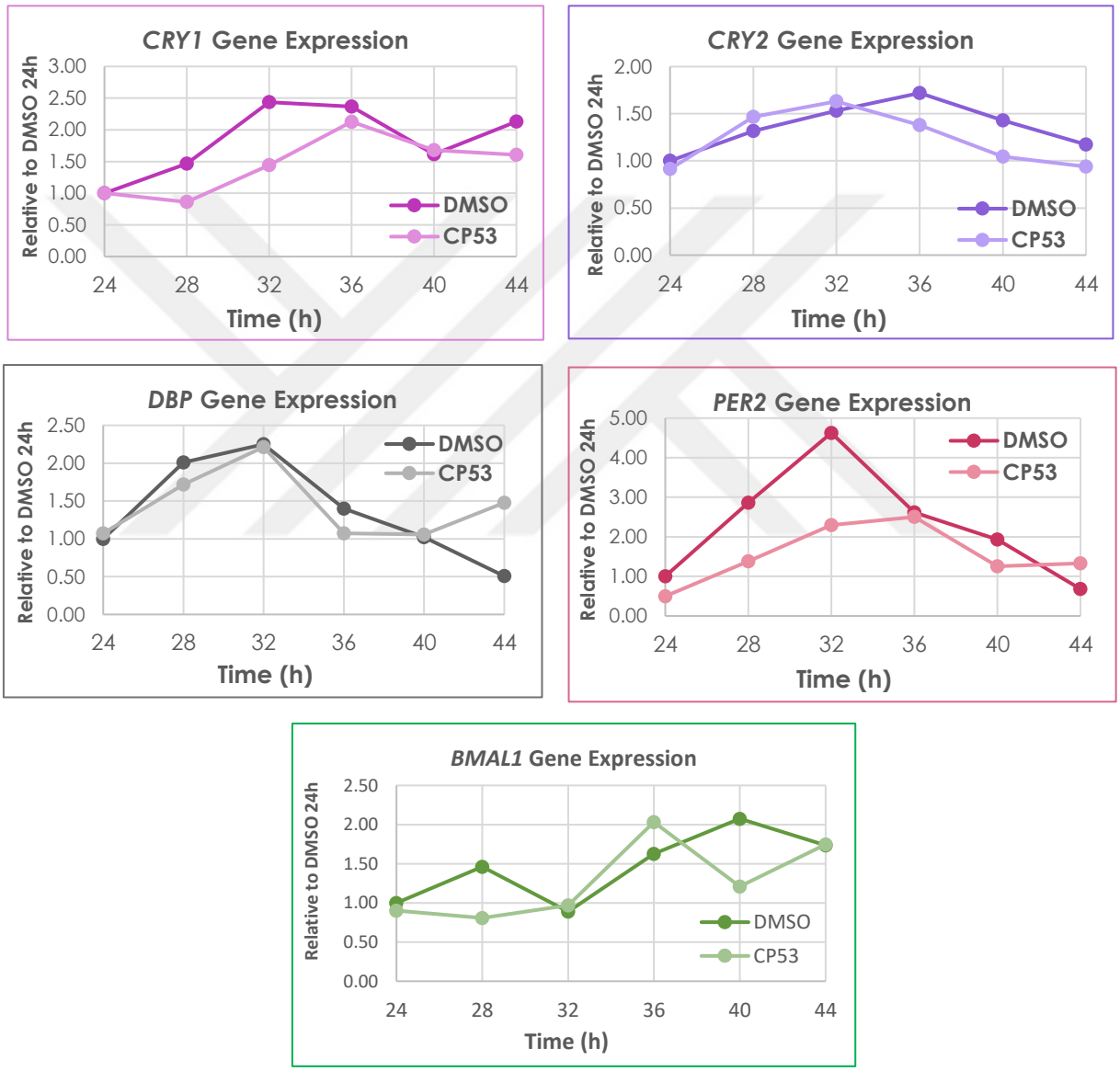

Figure 4. 15: RT-qPCR analysis of synchronized U2OS cells treated with CP53. mRNA levels of *CRY1*, *CRY2*, *PER2*, *DBP* and *BMAL1* normalized with *RPLP0* and relative to DMSO (24 h), n=2.

After screening the 90 molecules in vitro found that TW68 was a promising molecule to regulate the circadian clock mechanism through the CRY1 and CRY2 with good dose-response activity. Thus, we aimed to further characterize the CRY stabilizer molecule, TW68 on the circadian clock in vivo, and ex vivo through this thesis.

4.8 The Physical Interaction of TW68 to CRY

To understand the physical interaction between TW68 and CRY1/2 binding was tested with the help of a biotinylated molecule, b-TW68, that was synthesized commercially **(Figure 4.16).** To verify that b-TW68 binds to CRY1 and CRY2, pcDNA plasmids that contain His-Myc tagged *Cry1* and *Cry2* were transfected to HEK293T cells. The biotinylated small molecule was used to pull-down the CRY1-HIS-MYC and CRY2-HIS-MYC in the presence and absence of the competitor (free TW68) from total cell lysate. Eluted proteins were analyzed by Western blot probed by tag-specific antibodies.

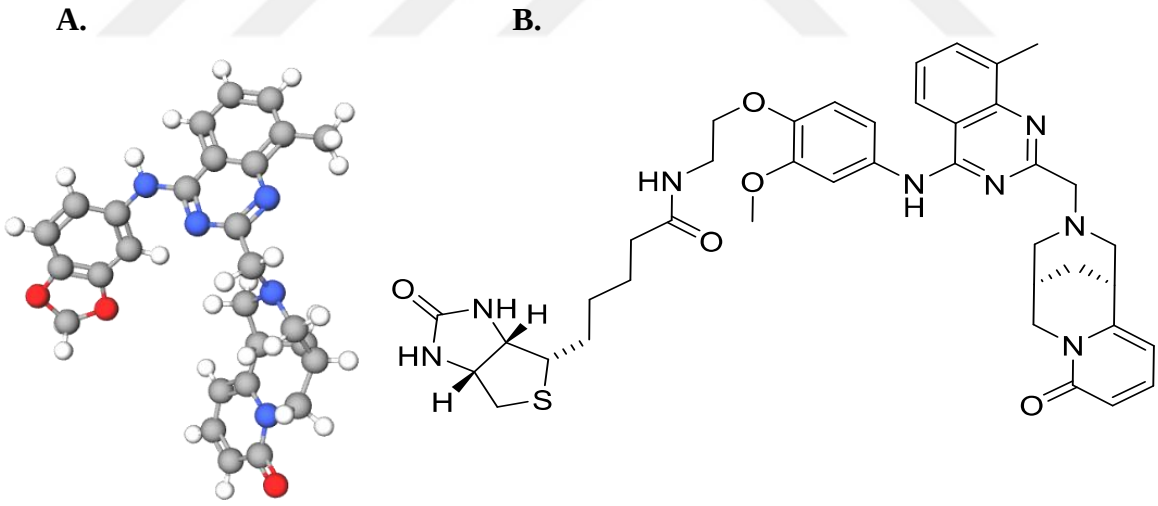

Figure 4. 16: The 3D Structure of **A.** TW68; **B.** Biotinylated-TW68 obtained from Ambinter Library, drawn in ball and stick model by MolView software.

Results showed that TW68 physically binds to CRY1 and CRY2 **(Figure 4.17)**. The binding of biotinylated small molecules to CRYs was diminished in the presence of the free competitors, which indicates the specific molecule-protein interaction.

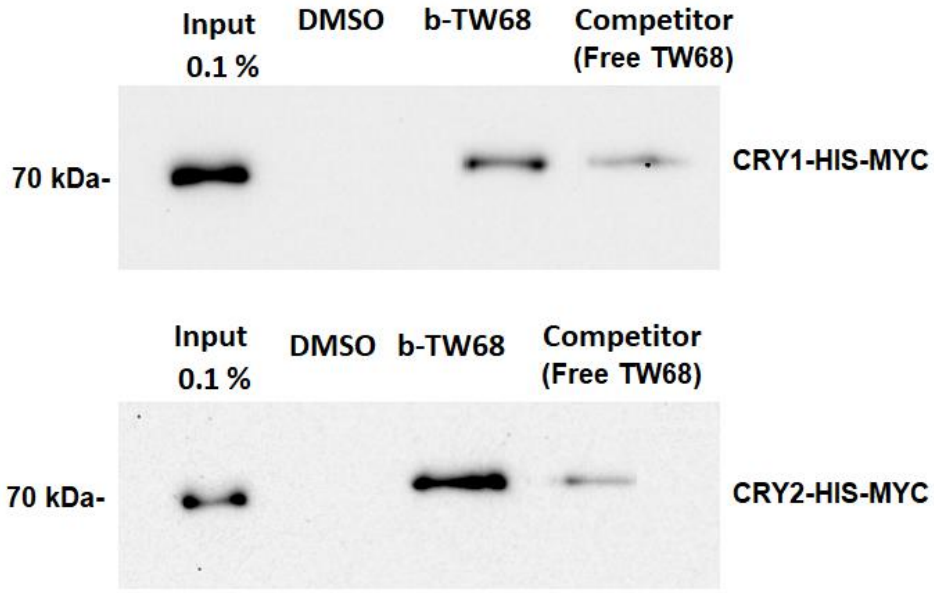

Figure 4. 17: Physical Interaction of TW68 with CRY1 and CRY2. Biotinylated TW68 was used to pull down CRY1 and CRY2 from HEK293T total cell lysate that transfected with pcDNA-*Cry1-His-Myc* and pcDNA-*Cry2-His-Myc*, (n=3).

4.9 Characterization of TW68

Previous crystal structure studies with one of the CRY stabilizer molecules, KL001, were shown that it binds to the PHR primary pocket of CRY1 [161]. According to computational studies, we found that the TW68 also binds to the primary pocket of CRY1 (PDB ID: 6KX7) and CRY2 (PDB ID: 6KX8) with the binding energies -9.7 kcal/mol, and -10.4 kcal/mol respectively **(Figure 4.18).**

Hence, I hypothesized that KL001 and TW68 should compete for the same binding site on CRYs PHR domain. Thus, a pull-down assay was performed for b-TW68 in the presence and absence of free KL001. The binding of b-TW68 was decreased in the presence of KL001 as expected because of the competing for binding CRYs primary pocket **(Figure 4.19).**

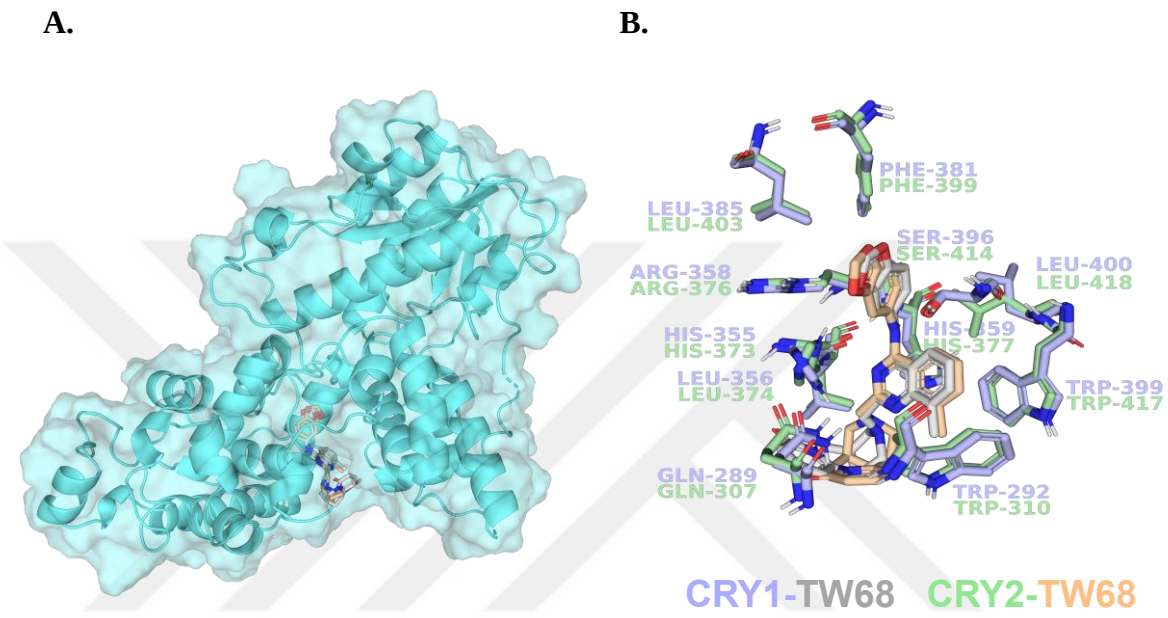

Figure 4. 18: Binding pose of TW68 on the equilibrated CRYs. A. TW68 docked into the primary pocket of mCRY1 PHR (PDB ID: 6KX7) and mCRY2 PHR domains (PDB ID: 6KX8) using Autodock Vina. The protein structure is shown in the surface, mCRY1 PHR domain is used as a representative. **B.** Common amino acid residues those Arg258 (Arg376 in CRY2), Ser396 (Ser 414 in CRY2), His355 (His373 in CRY2), and Trp399 (Trp417 in CRY2) in CRY1 are close contact with TW68. They were superimposed and presented as purple and green sticks, respectively.

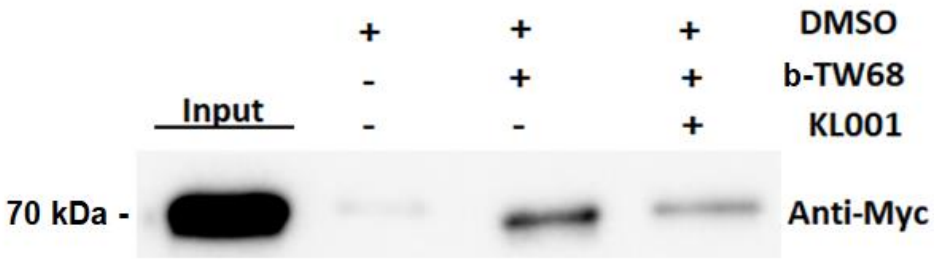

Figure 4. 19: KL001 and TW68 compete for binding to CRY. The binding of b-TW68 was reduced in the presence of KL001. Lysates of HEK293T cells which transfected with pcDNA-*Cry1-His-Myc* and pcDNA-*Cry2-His-Myc* plasmids were treated with solvent (DMSO), 10 μM b-TW68, and 150 μM KL001 (competitor), n=3.

Next, to investigate the off-target effect of TW68 b-TW68 used for the pull-down assay by the HEK293T cell lysate with and without the competitor (Free TW68). After elution of the protein extract, resins were subjected to the liquid chromatography-tandem mass spectrometry (LC-MS/MS) analysis [189]. The results are given in **Table 4.2.** The b-TW68 binds to CRY1, and its interaction is reduced when competitors are present. The other three identified proteins are in **Table 4.2.** were determined to be sticky proteins from the CRAPome Database [190].

Table 4. 2: Identification of TW68 binding proteins by using LC-MS/MS.

	Uniprot ID	DMSO			b-TW68			Competitor			CRAPome		
Gene Name		1st	2nd	3rd	1st	2nd	3rd	1st	2nd	3rd	Num of Expt. (found/total)	Ave SC	Max SC
Cryptochrome-1 OS=Homo sapiens GN=CRY1 PE=1 SV=1	Q16526	0	0	0	12	11	8	0	0	0	/716	0	
Exportin-1 OS=Homo sapiens GN=XPO1 PE=1 SV=1	O14980	0	0	0	8	10	6	0	0	2	237/716	3.8	52
Tubulin beta-4A chain OS=Homo sapiens GN=TUBB4A PE=1 SV=2	P04350	0	0	0	16	16	10	0	2	0	668/716	30.7	255
Tubulin alpha-1A chain OS=Homo sapiens GN=TUBA1A PE=1 SV=1	Q71U36	0	0	0	19	12	12	7	0	0	694/716	41.7	261

To show biotinylated TW68 is active and has an effect on the circadian rhythm, U2OS *Bmal1*-d*Luc* cells were treated with b-TW68 in dose-dependent manner. Results confirmed that b-TW68 also exhibits a similar phenotype on circadian rhythm as TW68 **(Figure 4.20).**

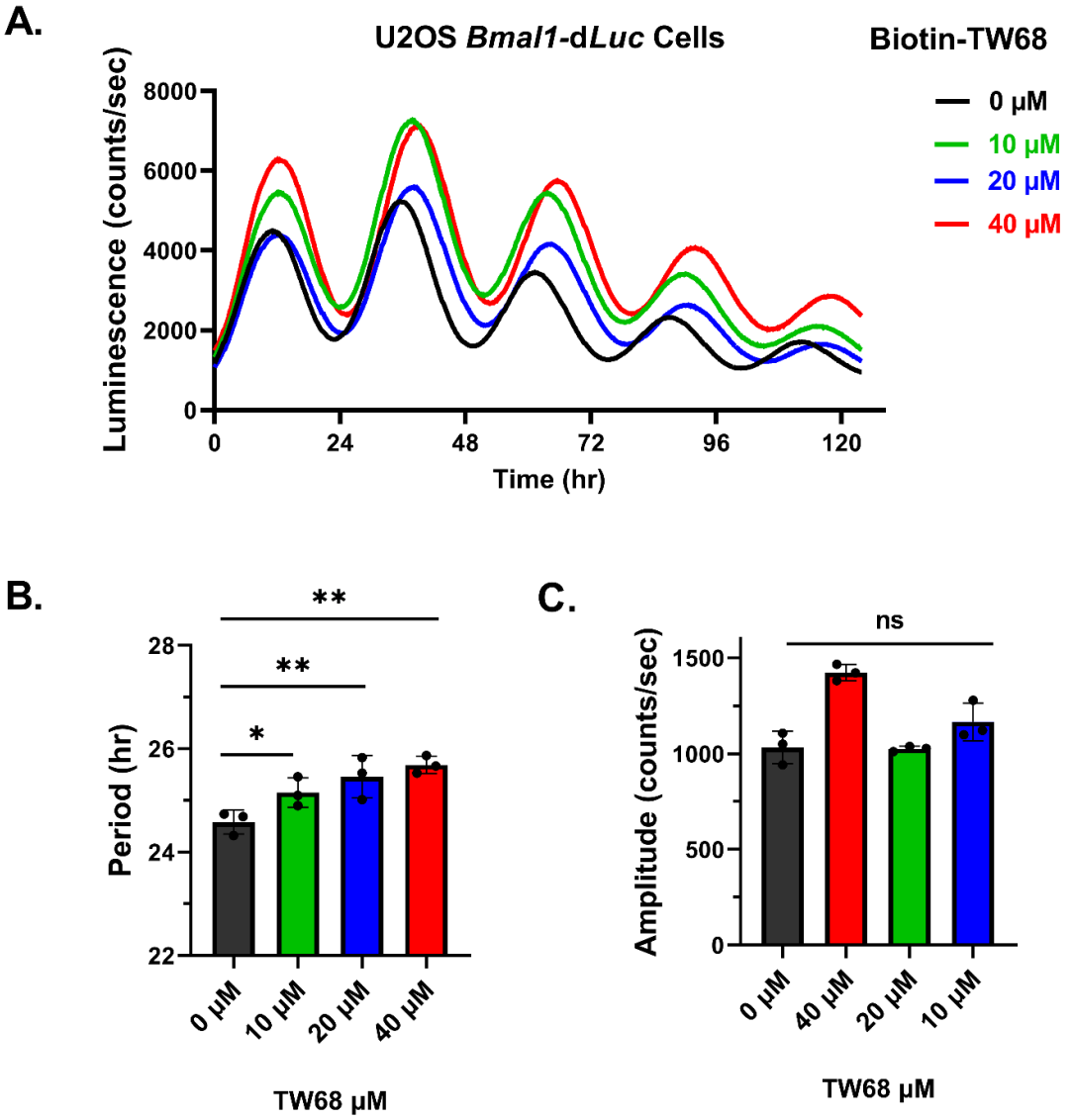

Figure 4. 20: Dose-dependent effect of b-TW68 on Circadian Rhythm. A. Bioluminescence **B.** period (hr) and **C.** amplitude (counts/sec) determined on U2OS *Bmal1*-d*Luc* cells. Data are given as mean ± SEM, n=3 with duplicates. Statistical analysis was performed by using one-way ANOVA with Dunnett's multiple comparisons test versus 0 uM control (*p<0.05, **p<0.01, ***p<0.001).

To eliminate the possibility that TW68 might alter the circadian rhythmicity through other proteins than CRYs, I tested the effect on the CRY1-CRY2 double knock out U2OS cells (*CRY* DKO U2OS) transduced with *Bmal1*-d*Luc* lentiviral particles. Results showed that TW68 had no dose-dependent effect on the circadian rhythm of the *CRY* DKO U2OS *Bmal1*-d*Luc* cells and thus suggested that the effect of TW68 was through CRYs **(Figure 4.21).**

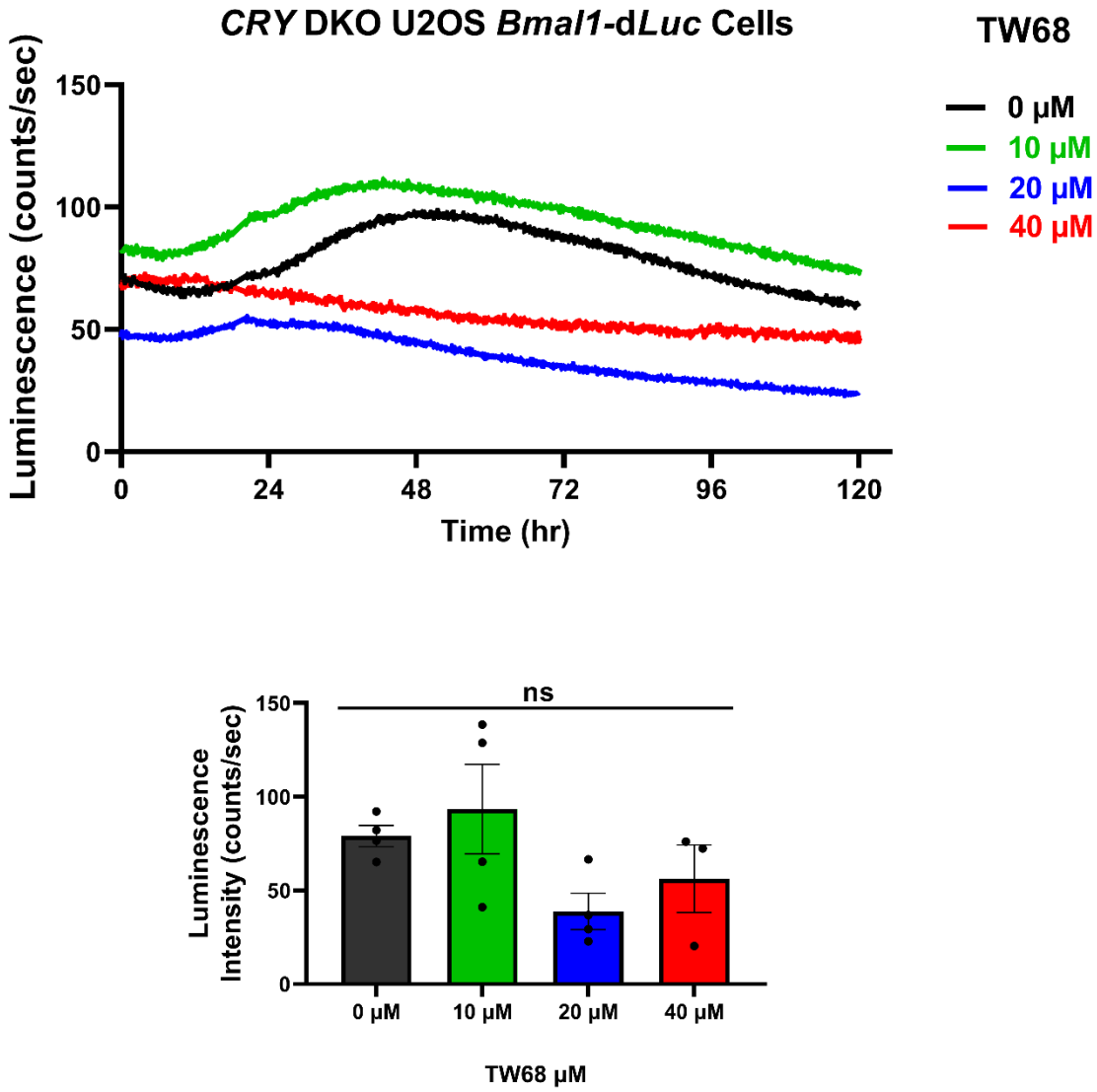

Figure 4. 21: Dose-dependent effect of TW68 on the circadian rhythm of *CRY* DKO U2OS cells transiently transduced with *Bmal1-Luc* reporter. Data represent the mean ± SEM, n=3 with duplicates. Statistical analysis was performed by using ordinary one-way ANOVA with the Brown-Forsythe test versus 0 uM control (ns=non-significant).

I hypothesized that TW68 increases the CRY half-life by binding to the PHR domain and decreases the ubiquitination by FBXL3 ligase [105-107]. To test this, HEK293T cells were transfected with pcDNA-*Cry1-His-Myc*, pBIND-*Fbxl3-Gal4*, and p*Ub-Ha* plasmids and then treated with TW68 or DMSO. After 42 hours of post-transfection, proteasomal degradation was inhibited by MG132 to determine the ubiquitination level of CRY1 [180]. Proteins were subjected to pull-down assay and ubiquitination levels were detected by Western blot. The ubiquitinated CRY1 protein levels revealed that the ubiquitination was decreased with the TW68 treatment compared to the DMSO control **(Figure 4.22)**.

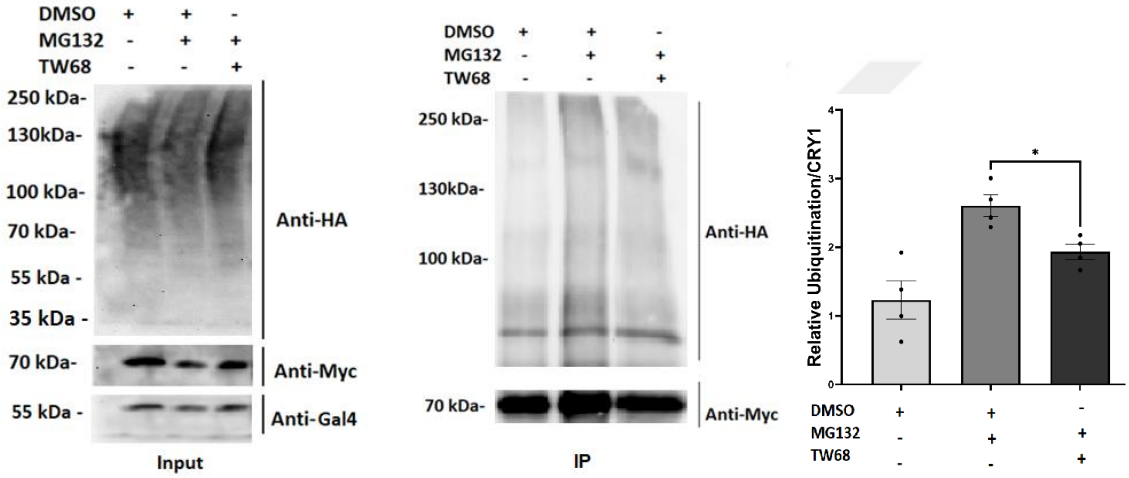

Figure 4. 22: The representative figure of the ubiquitination of CRY1 in the presence and absence of TW68. Data represent the mean ± SEM, n =4; *p<0.05 by DMSO control with unpaired t-test with two-tailed.

After several elimination steps found that TW68 physically interacted with both CRYs, increased the CRY1- LUC and CRY2-LUC half-life, and showed a good dose-response effect on the circadian rhythm. To investigate the pharmacological properties of TW68 in vivo, it has been subjected to mice studies.

4.10 Toxicity Studies of TW68 in Mice

To determine the toxicity of the TW68 in vivo, I performed single dose toxicity (SDT) study by using C57BL/6J mice. TW68 was administered intraperitoneally (i.p.) to mice in both sexes at doses of 50 mg/kg and 300 mg/kg. Parameters of food and water consumption, behavior assessment, body weight and temperature changes, physiological signs, mortality, and gross findings at terminal necropsy were used to evaluate the toxicity of the TW68. The animals treated with 300 mg/kg of the TW68 exhibited severe hypothermia, hunched posture, and reduced locomotor activity. Thus, the 300 mg/kg dose was considered a lethal dose and decided to sacrifice the animals for ethical reasons. Conversely, animals treated with 50 mg/kg of the TW68 did not exhibit any abnormal physiological signs as compared to the control animals that were treated with the vehicle. All these results suggested that a single dose of 50 mg/kg TW68 was well tolerated. The body weight changes for 14 days and body temperatures for 5 days were observed, and data are shown in **Figure 4.23.**

A.

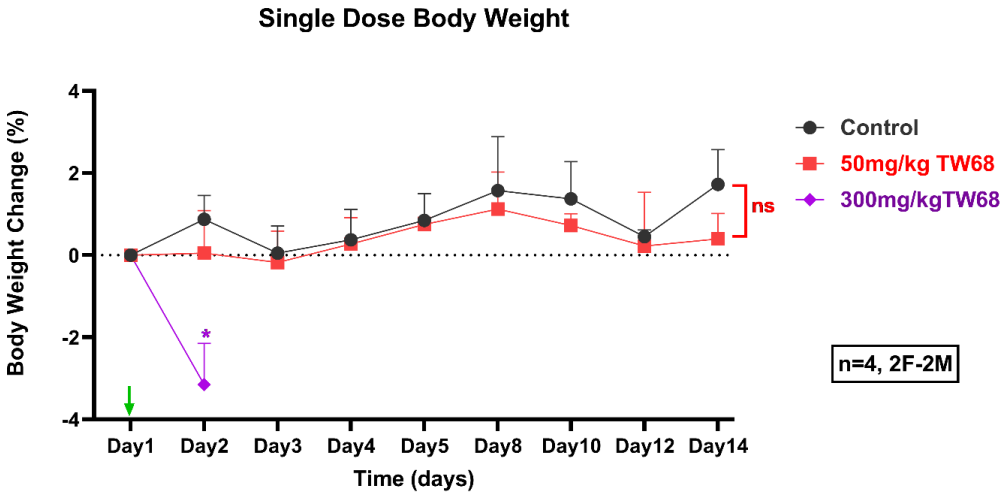

B.

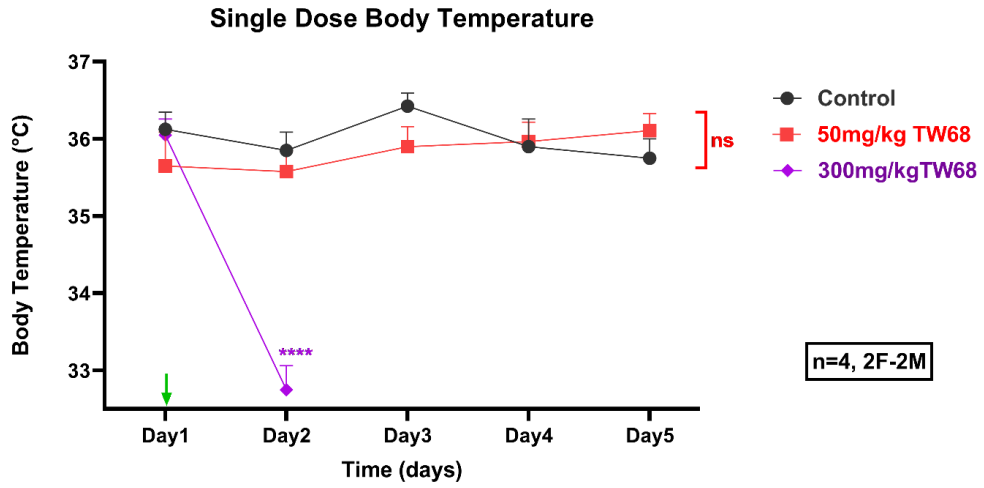

Figure 4. 23: Single Dose Toxicity of TW68 in mice. A. Body weight changes (%) in C57BL/6J mice treated with single intraperitoneal doses of 50 mg/kg, 300 mg/kg TW68 or Control vehicle during a 14-day observation period. **B.** Body temperatures in C57BL/6J mice treated with single intraperitoneal doses of 50 mg/kg, 300 mg/kg TW68 or Control vehicle during a 5-day observation period. Body weight changes (%) and Body temperatures (°C) were expressed as mean ± SEM. "↓" indicates the treatment days of TW68. *p<0.05, **p<0.01, ***p<0.001, **** p<0.0001 (Two-way ANOVA with Bonferroni post hoc test).

Then, the maximum tolerated dose (MTD) of TW68 was determined by using 50, 75, or 150 mg/kg with repeated intraperitoneal injections for 5 days. No adverse effect was observed in the animals that were treated with 50 and 75 mg/kg of the TW68. Three animals were dead at the end of the 2nd and 3rd day of treatment with 150 mg/kg of the TW68 (with a 66% mortality rate). The body weight and temperature changes were observed in animals when treated with either 50, 75, 150 mg/kg or control vehicle for 5 days. Among the doses, animals treated with 150 mg/kg had severe hypothermia and significant body weight loss as compared to the control vehicle. The dose of 75 mg/kg TW68 caused mild hypothermia. Animals showed no significant body weight and body temperature changes at 50 mg/kg of the TW68 compared to the control animals **(Figure 4.24).**

A.

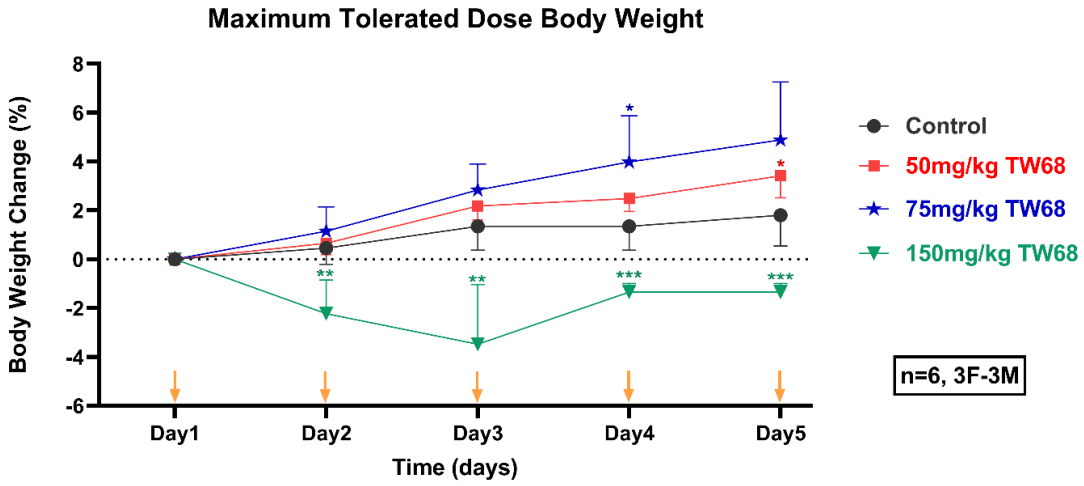

B.

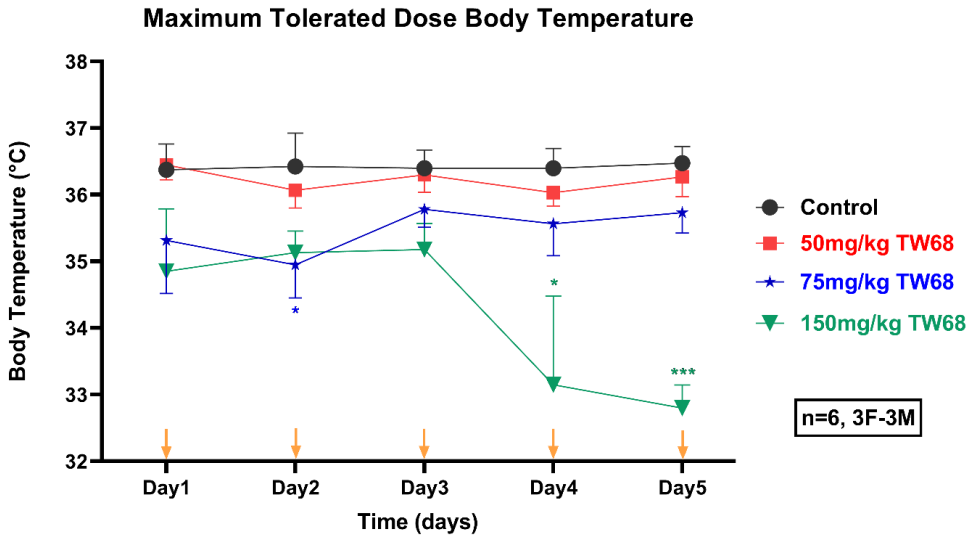

Figure 4. 24: Maximum tolerated dose of TW68 in mice. A. Body weight changes (%) in C57BL/6J mice treated with intraperitoneal doses of 50 mg/kg, 75 mg/kg, 150 mg/kg TW68 or Control vehicle for 5 days. **B.** Body temperatures in C57BL/6J mice treated with intraperitoneal doses of 50 mg/kg, 75 mg/kg, 150 mg/kg TW68 or Control vehicle for 5 days. Body weight changes (%) and Body temperatures (°C) were expressed as mean ± SEM. "↓" indicates the treatment days of TW68. *p<0.05, **p<0.01, ***p<0.001, **** p<0.0001 (Two-way ANOVA with Bonferroni post hoc test).

At the end of the 5 days injection, the thorax of the mice was opened under isoflurane anesthesia, and 0.6-1 ml of blood was taken from the heart to examine the hematological parameters and results shown in **Table 4.3.** To determine whether the molecule exhibits hepatotoxicity, and nephrotoxicity, liver and kidney samples were isolated and histopathological examinations were performed**.**

The morphology of the liver cells and the epithelial structures of the liver capillaries were normal in the control vehicle. At the dose of 50 mg/kg TW68, while hepatocyte morphology was normal, minor endothelial cell degeneration was observed in the capillary epithelial cells. At higher doses, 75 and 150 mg/kg of TW68 intra-tissue bleeding, sinusoid damage, swollen hepatocytes, vasodilation, and necrosis were observed **(Figure 4.25)**.

Table 4. 3: Hematological Parameters of Maximum Tolerated Dose (MTD) toxicity.

	WBC 10^3/uL	**LYM%**	**MID%**	**GRAN %**	**LYM 10^3/uL**	**MID 10^3/uL**
Control vehicle	4.93	79.05	6.13	14.83	3.95	0.25
50 mg/kg TW68	4.45	74.10	6.12	19.78	3.25	0.27
75 mg/kg TW68	4.40	74.10	6.30	19.72	3.72	0.33
150 mg/kg TW68	3.17	83.77	5.07	11.17	2.67	0.17
Reference	2,1-19,5	55-97	0,1-5	11355	2-14,1	0,1-98
	RBC 10^6/uL	**HGB g/dL**	**HCT%**	**MCV fL**	**MCH pg**	**MCHC g/dL**
Control vehicle	7.20	14.85	37.18	51.70	20.55	39.88
50 mg/kg TW68	7.15	14.53	37.12	51.75	20.22	39.02
75 mg/kg TW68	7.20	14.85	37.03	52.22	20.38	38.78
150 mg/kg TW68	6.59	13.13	35.27	52.23	19.97	37.47
Reference	5,3-10	14-18	35-52	50-62	16-23	31-40
	RDW-CV%	**PLT 10^3/uL**	**MPV fL**	**PDW%**	**PCT%**	**P-LCR %**
Control vehicle	14.20	388.75	10.90	8.28	0.42	24.33
50 mg/kg TW68	14.00	359.33	10.70	8.38	0.38	23.70
75 mg/kg TW68	14.70	496.67	10.90	8.48	0.52	23.47
150 mg/kg TW68	14.40	393.33	8.90	9.03	0.34	13.73
Reference	0,1-99,9	500-1370	0,1-30	0,1-30	0,01-9,99	0,1-99,9

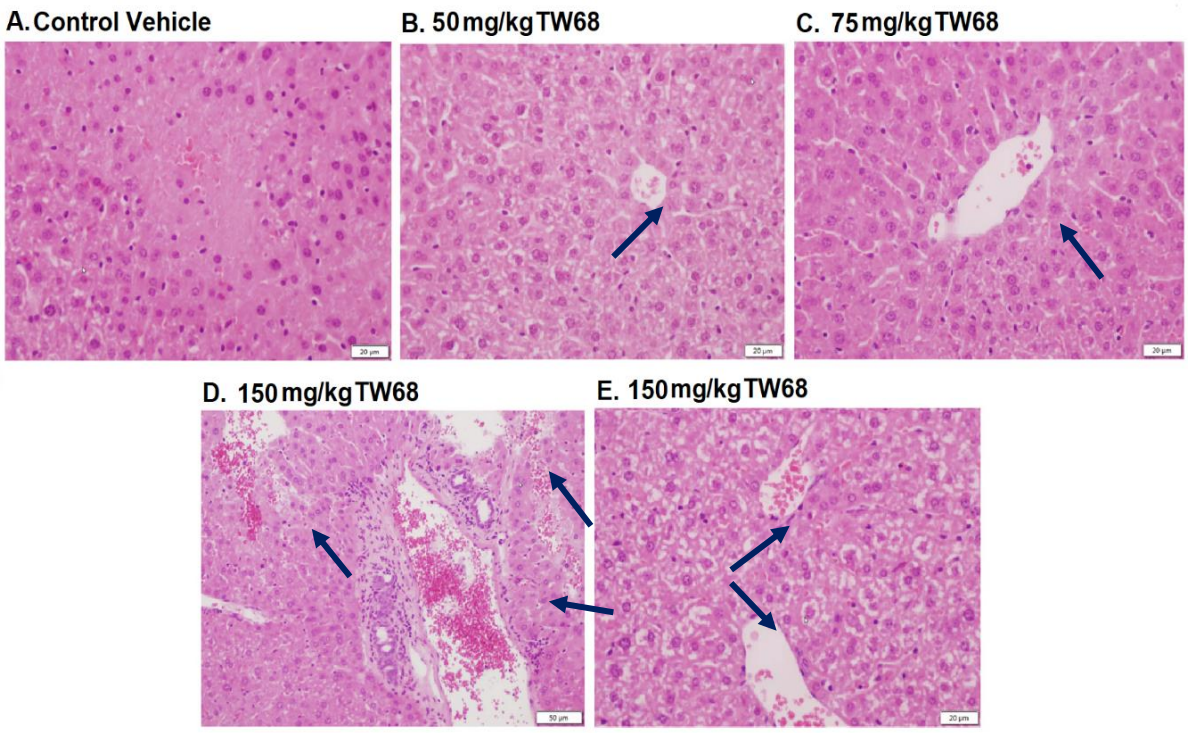

Figure 4. 25: Histopathology Results of Liver Tissue. Mice were euthanized end of the Maximum Tolerated Dose (MTD) toxicity, and a histopathological examination was performed on liver samples. The arrows on the figure indicate the morphological degenerations in the liver capillary epithelial tissue.

A healthy glomerular extracellular matrix and open Bowman's capsule were clearly observed in the control vehicle and 50 mg/kg TW68 administered kidney tissue. As the doses of TW68 increased, the Bowman capsule began to close. Also damaged proximal tubules and lumens, increased glomerular extracellular matrix, and nephrosis were observed **(Figure 4.26).** All these results suggested that repeated doses of 50 mg/kg or below were well-tolerated by mice.

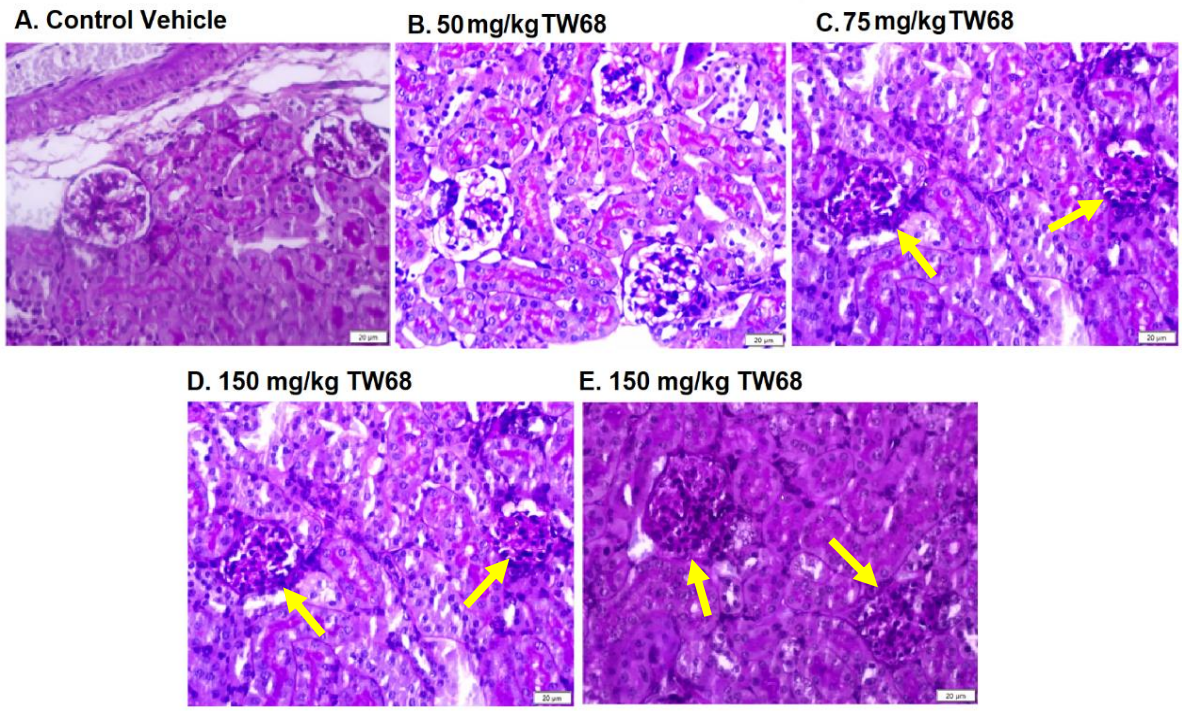

Figure 4. 26: Histopathology Results of Kidney Tissue. Mice were euthanized end of the Maximum Tolerated Dose (MTD) toxicity, and a histopathological examination was performed on kidney samples. The arrows on the figure indicate the morphological degenerations in the glomerular extracellular matrix epithelial tissue.

Hereby, decided to perform a subacute toxicity test at the dose of 20 mg/kg of TW68 on mice by administering it for 28 days. No physiological symptoms or mortality were observed in these animals. The body weight and temperature changes were comparable with control animals that were treated with a control vehicle for 28 days **(Figure 4.27).**

A.

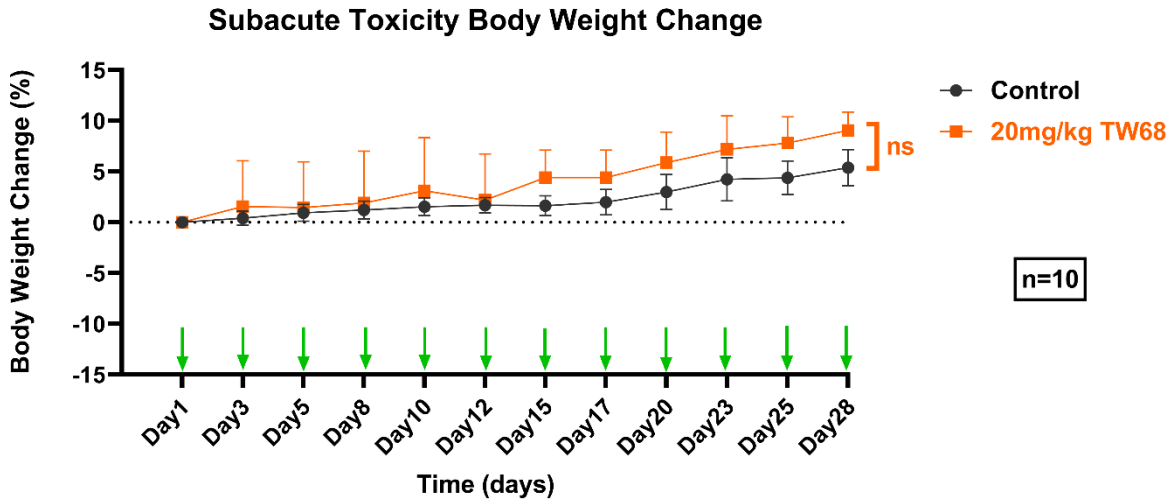

B.

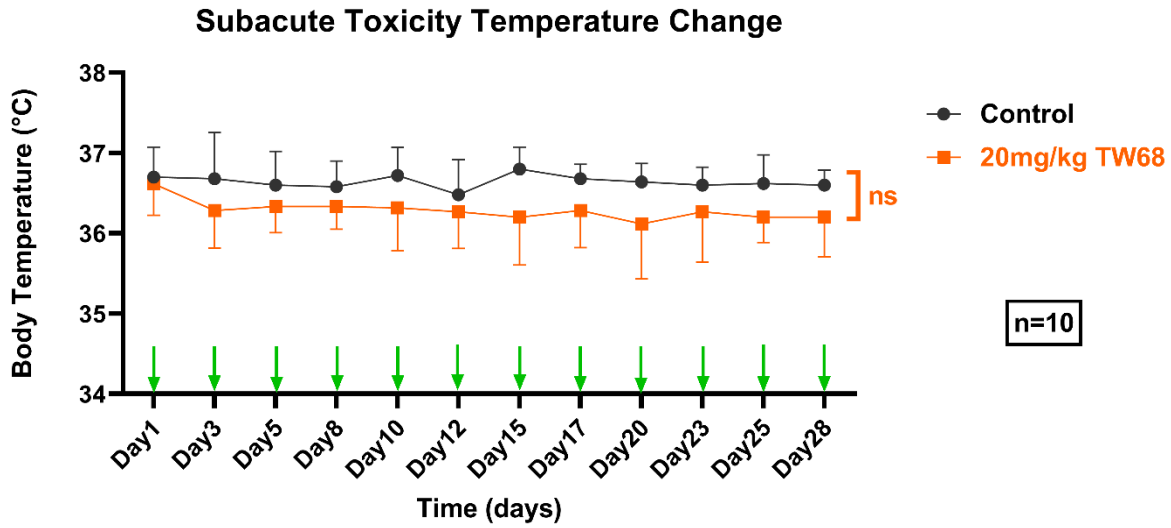

Figure 4. 27: Subacute Toxicity of TW68 in mice. A. Body weight changes (%) in C57BL/6J mice treated with an intraperitoneal dose of 20 mg/kg TW68 or Control vehicle for 28 days. **B.** Body temperatures in C57BL/6J mice treated with intraperitoneal dose of 20 mg/kg TW68 or Control vehicle for 28 days. Body weight changes (%) and Body temperatures (°C) were expressed as mean ± SEM. "↓" indicates the treatment days of TW68. ns=non-significant, control vs. 20 mg/kg TW68 (Two-way ANOVA with Bonferroni post hoc test).

4.11 Pharmacokinetic Profile of TW68 in Plasma and Tissues

To determine the pharmacokinetic profile, absorption and bioavailability in plasma and tissue, 75 mg/kg of TW68 was administered to mice in both intraperitoneal (i.p.) and oral (p.o.) injections. After the TW68 injection plasma, liver, kidney, and ileum tissues were collected at different time points to calculate the concentration of TW68 in a time-dependent manner. The mean concentration-time curves of TW68 in plasma and tissues are shown in **Figure 4.28** and the pharmacokinetic parameters of TW68 were given in **Table 4.4** and **Table 4.5.**

TW68 plasma and tissue concentration reached their maximum at 0.5 hours after injection. The plasma half-life was calculated as 1 hour for intraperitoneal administration and 3.4 hours for oral administration via HPLC and Mass spectrophotometry. Remarkably, orally administered TW68 displayed a higher bioavailability compared to parenteral administration. Thus, we decided to continue with the oral administration of TW68 to evaluate its efficacy.

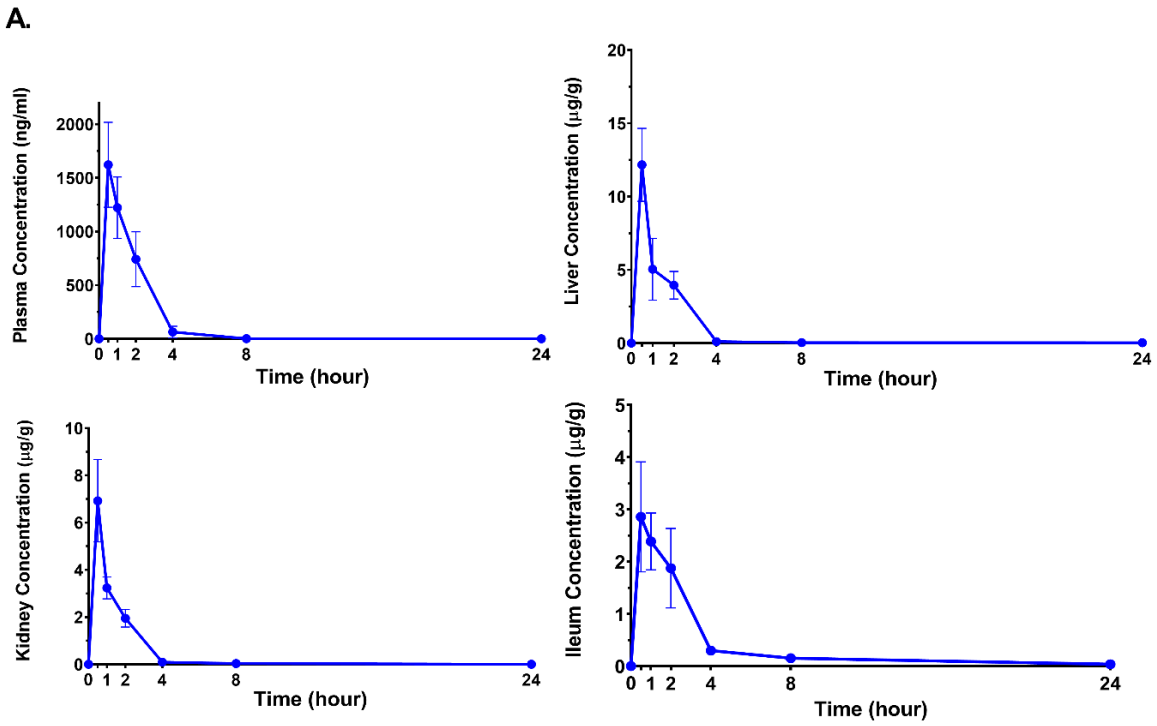

B.

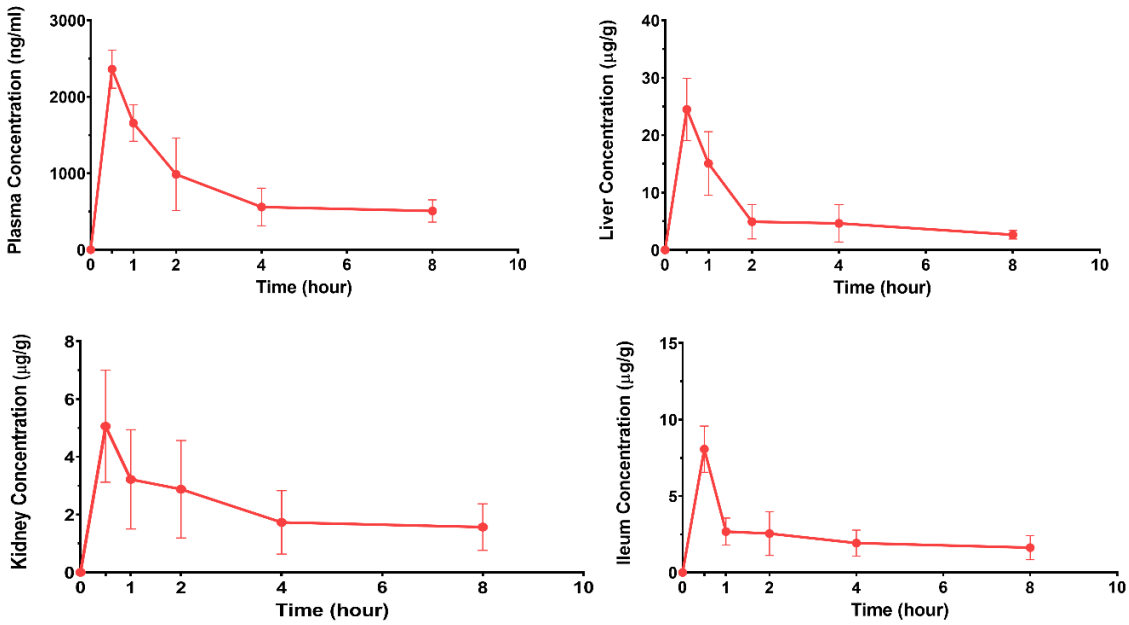

Figure 4. 28: Pharmacokinetics of TW68 in mice A. Mean plasma and tissue concentration-time curve of TW68 administered at a dose of 75 mg/kg intraperitoneally (i.pi) to C57BL/6J mice. Data were expressed as mean ± SEM (n=4 per time point). **B.** Mean plasma and tissue concentration-time curve of TW68 administered at a dose of 75 mg/kg orally (p.o.) to C57BL/6J mice. Data were expressed as mean ± SEM (n=4 per time point).

Table 4. 4: Pharmacokinetic Parameters of Plasma Administered TW68 (75 mg/kg, single dose, n=4 per time point)

Parameters	Plasma (i.p.)	Parameters	Plasma (p.o.)
C_{max} (ng/ml)	1650,22 ± 368,35	**C_{max} (ng/ml)**	2365,13 ± 251,50
t_{max} (h)	0,5	**t_{max} (h)**	0,5
AUC_{0-24} (ng.h/ml)	3046,00 ± 915,70	**AUC_{0-8} (ng.h/ml)**	5464,50 ± 1398,20
$AUC_{0-\infty}$ (ng.h/ml)	3046,00 ± 915,70	**$AUC_{0-\infty}$ (ng.h/ml)**	8503,94 ± 2601,52
$t_{1/2}$ (h)	1,02 ± 0,03	**$t_{1/2}$ (h)**	3,41 ± 0,92
CL (ml/h)	708,58 ± 247,47	**CL/F (ml/h)**	306,12 ± 148,37
Vd (ml)	1072,63 ± 404,63	**Vd/F (ml)**	1066,86 ± 220,49

Table 4. 5: Pharmacokinetic Parameters of Tissue Administered TW68 (75 mg/kg, single dose, n=4 per time point)

Parameters	Liver (i.p.)	Kidney (i.p.)	Ileum (i.p.)	Liver (p.o.)	Kidney (p.o.)	Ileum (p.o.)
C_{max} (ng/ml)	12,16±2,49	6,92±1,75	2,98±1,01	24,47±5,46	5,06±1,94	8,06±1,51
t_{max} (h)	0,5	0,5	0,5	0,5	0,5	0,5
AUC_{0-24} (ng.h/ml)	16,68±4,41	9,42±1,90	8,74±2,56	48,40±22,2	15,78±9,10	17,69±7,33
$AUC_{0-\infty}$ (ng.h/ml)	16,87±4,42	9,42±1,90	8,82±2,63	59,14±24,5	50,90±35,8	43,48±19,92
$t_{1/2}$ (h)	4,814±0,47	0,895±0,17	1,871±0,24	3,49±0,69	8,32±3,01	9,98±5,63

4.12 Effect of TW68 on Fasting-blood glucose level of ob/ob and fat induced diabetic mice

The expression of glucagon-mediated gluconeogenic genes, *Pck1* (Phosphoenolpyruvate Carboxykinase 1) and *G6pc* (Glucose-6-phosphatase), decreased when CRY1 and CRY2 are either stabilized by a small molecule in mouse hepatic cells [160] or overexpressed in diabetic mice [129], as well as reduce the glucose levels in human hepatoblastoma (HepG2) cells [186]. Leptin-deficient transgenic ob/ob mice exhibit high blood glucose levels, obesity and insulin-independent diabetes thus, they are commonly used animal models for studying type II diabetes [191-193].

Next, the effect of TW68 was examined on the blood glucose levels of either transgenic (ob/ob mice) or fat-induced diabetic animals. For fat-induced diabetic mice, wild type C57BL/6J mice were fed with a 60% fat contained diet for 3 months. A body weight higher than 35 g and blood glucose levels higher than 200 mg/dL were classified as diabetic, and the study proceeded with those animals.

Diabetic mice were fasted for 4 hours and 40 mg/kg TW68 was orally administered for 5 days along with control vehicle and pioglitazone molecule. Pioglitazone is a medicine used for the treatment of type 2 diabetes [194, 195]. The blood glucose levels were measured daily after 4 hours of TW68 injection for 5 days. Wild type C57BL/6J used as control to diabetic phenotype. The fasting blood glucose levels were decreased with TW68 administration compared to the control vehicle, similar to pioglitazone administered mice **(Figure 4.29).**

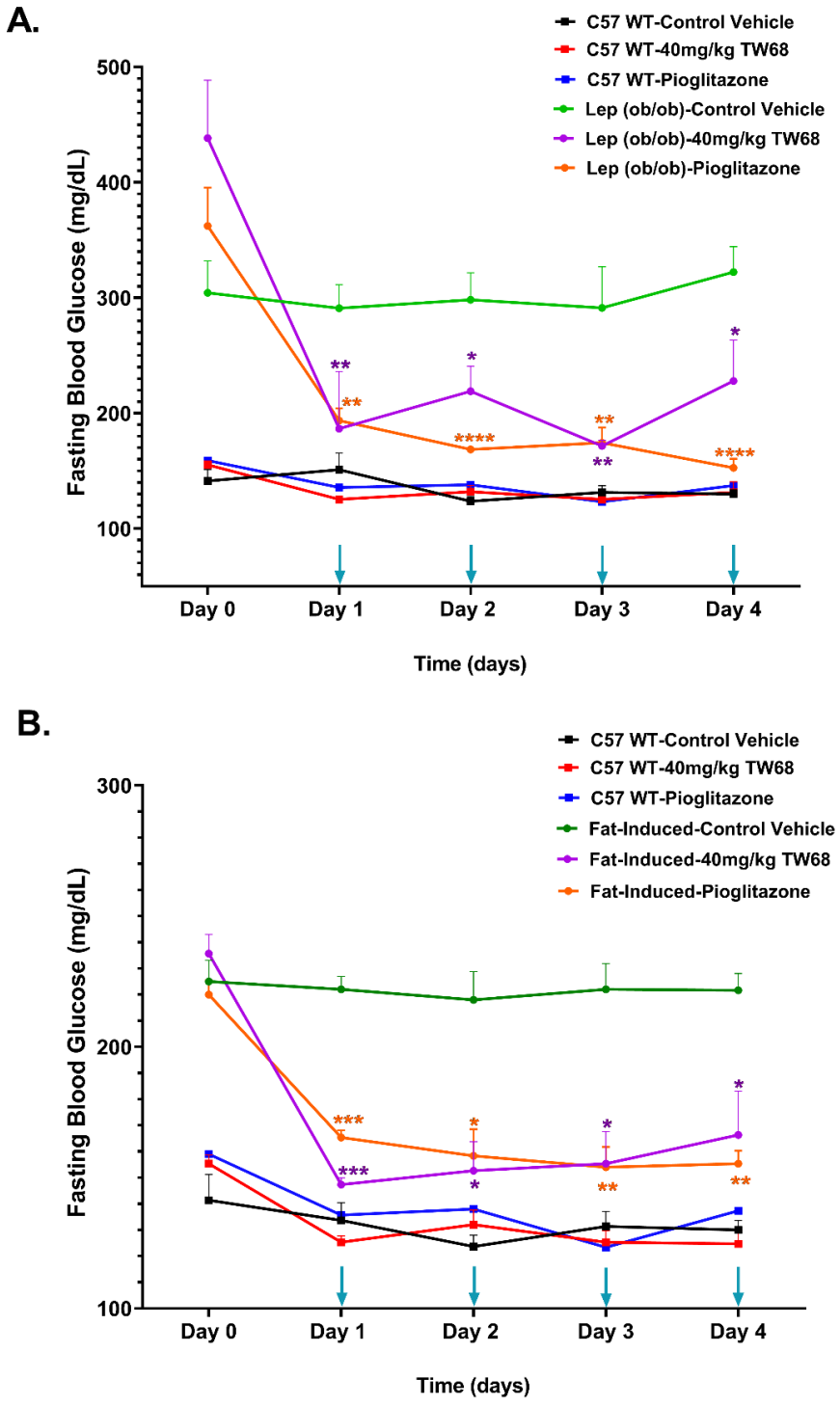

Figure 4. 29: Antidiabetic effect of TW68 on blood glucose level in mice. The effect of TW68 on fasting blood glucose level of **A.** Lep (ob/ob) transgenic diabetic mice and **B.** Fat-induced diabetic mice at 40 mg/kg TW68, 30 mg/kg pioglitazone and control vehicle 4 hours after oral administration. (Data were expressed as mean ± SEM, Statistical analyses were performed by using unpaired t-test, * $p<0.05$, ** $p<0.001$, *** $p<0.005$, **** $p<0.0001$, n=3 for each group).

To confirm that TW68 increases CRY stability, I used the same experimental setup on mice, then isolated liver samples subjected to Western blot and RT-qPCR analysis. Results indicated that the CRY1 protein level increased with TW68 treatment as expected **(Figure 4.30)**, and the transcription levels of gluconeogenic genes *Pck1*, *G6pc* and *Cry1* decreased significantly both in Lep (ob/ob) and C57BL/6J wild-type mice liver which is consistent with in vitro results **(Figure 4.31)**.

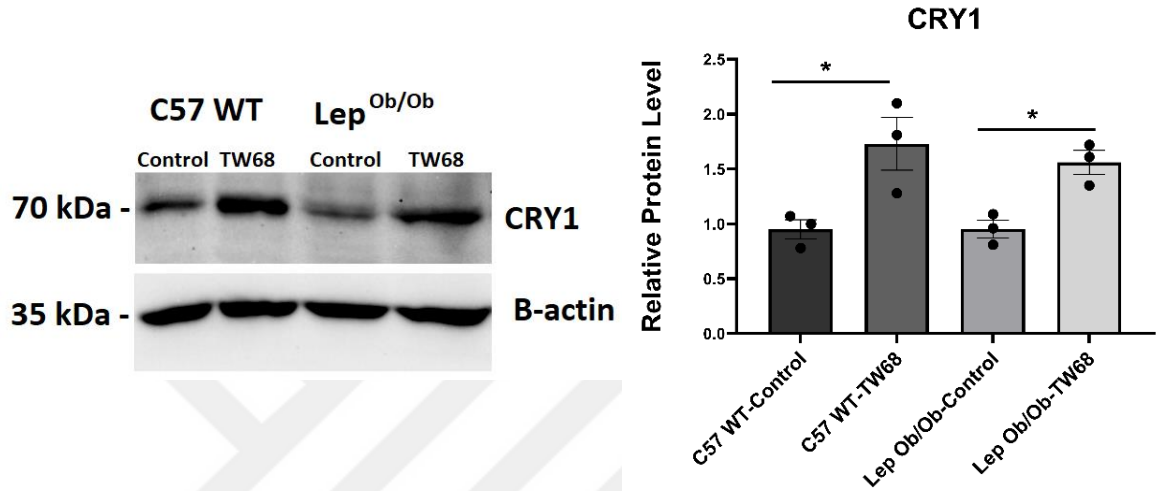

Figure 4. 30: Protein level of CRY1. The effect of TW68 in mice liver (Whole Cell Lysate) 40 mg/kg TW68 or Control vehicle administered (o.p.) to C57BL/6J WT and Lep (ob/ob) mice. 4h after the treatment mice were sacrificed (n = 3). (Data represent the mean ± SEM, n=3, control versus TW68 treated mice by unpaired t-test *p < 0.01).

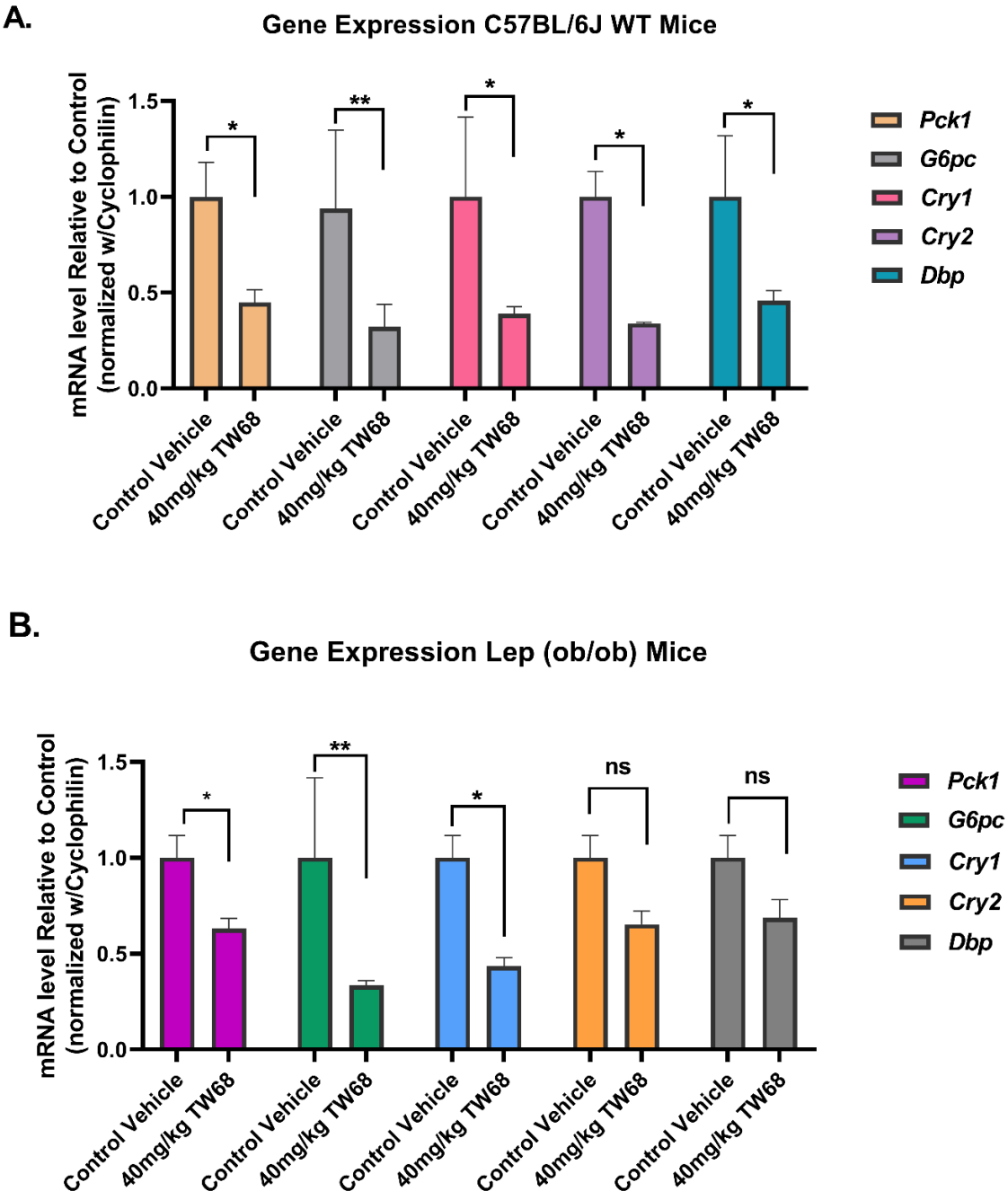

Figure 4. 31: The transcriptional level of *Pck1, G6pc, Cry1, Cry2, Dbp* in C57BL/6J WT and Lep (ob/ob) diabetic mice. 40 mg/kg TW68 or Control vehicle administered (o.p.) to C57BL/6J and Lep (ob/ob) mice. 4h after the treatment mice were sacrificed (n = 3). (Data represent the mean ± SEM, n=3, control versus TW68 treated mice by unpaired t-test *p < 0.01, **p<0.001, ns=non-significant).

Most of the insulin's metabolic activity is mediated by the phosphatidylinositol 3-kinase (PI3K)-AKT pathway. This pathway is activated when the insulin receptor (IR) phosphorylates insulin receptor substrate proteins (IRS proteins) [196]. Therefore, I hypothesized that reducing blood glucose levels by TW68 treatment would result in reducing insulin levels and cause the reduction the AKT phosphorylation.

To test this, plasma insulin levels detected by ELISA analysis from blood samples were collected before TW68 treatment on 1st day, and after 5-days TW68 or pioglitazone oral administration on the 7th day **(Figure 4.32).** The results indicated the TW68 treatment reduced plasma insulin levels in diabetic mice similar to pioglitazone while there was no significant change in C57BL/6J wild type mice. Then, the whole cell lysate of the mice liver was subjected to Western blot analysis using anti-AKT-P and protein levels were normalized by Total-Akt. Results show that the phosphorylation of AKT was reduced in mice treated with TW68 significantly **(Figure 4.33).**

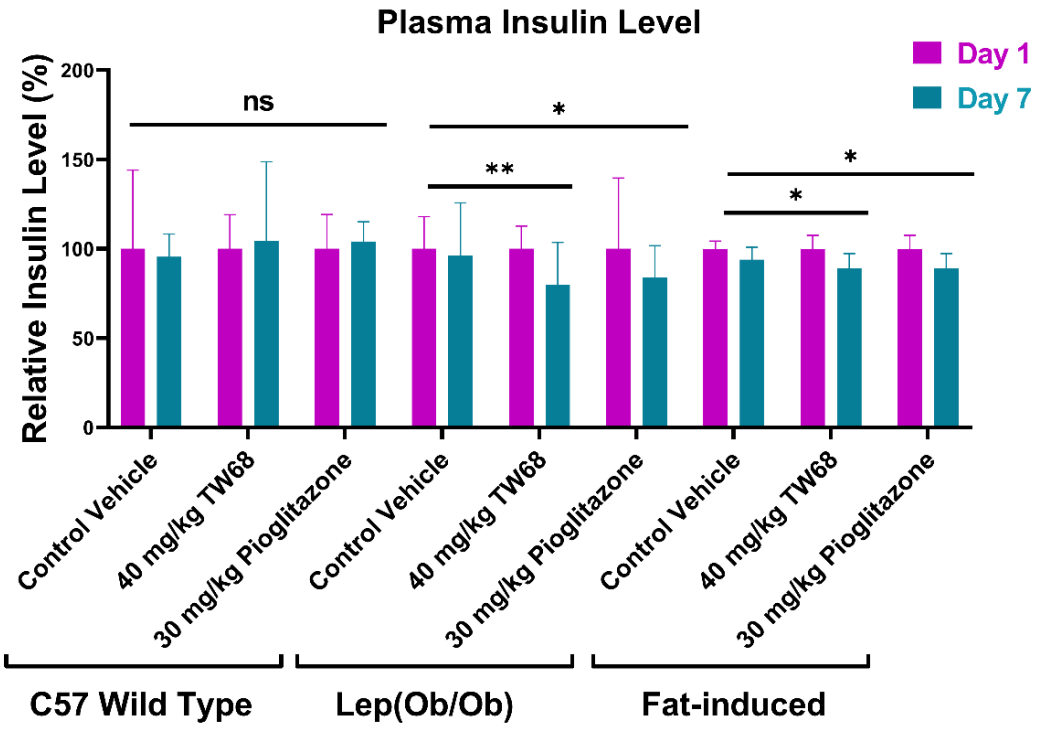

Figure 4. 32: Plasma Insulin levels were determined by ELISA analysis. Blood samples were collected on 1st day before TW68 treatment, and on the 7th day after 5-days TW68 or pioglitazone oral administration. Data are given as mean ± SEM, n=3. Statistical analysis was performed using one-way ANOVA with Dunnett's multiple comparisons test versus the control vehicle (*p<0.05, **p<0.01, ***p<0.001).

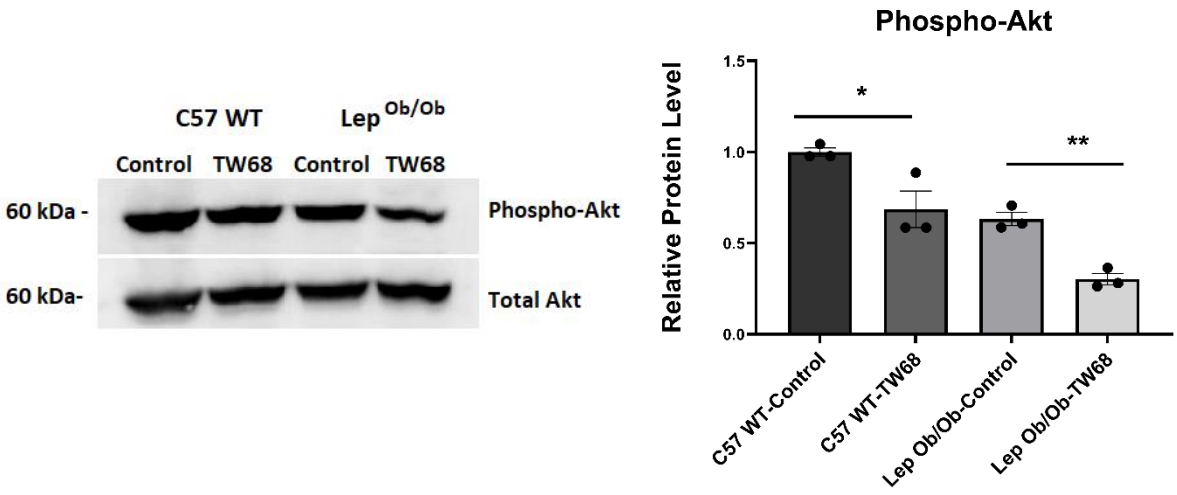

Figure 4. 33: Protein level of Phospho-Akt. The effect of TW68 in mice liver (Whole Cell Lysate) 40 mg/kg TW68 or Control vehicle administered (o.p.) to C57BL/6J WT and Lep (ob/ob) mice. 4h after the treatment mice were sacrificed (n = 3). (Data represent the mean ± SEM, n=3, control versus TW68 treated mice by unpaired t-test *p < 0.01, **p < 0.001).

Next, the oral glucose tolerance test (OGTT) was performed on 18-hour fasted C57BL/6J WT and Lep (ob/ob) diabetic mice to determine whether insulin resistance or the effect of TW68 on glucose tolerance [197]. After overnight fasting, early in the morning TW68 was administered (o.p.) to mice and 2 g/kg glucose was injected 3 hours later than treatment. Fasting blood glucose levels were monitored at 0, 30, 60, 90, 120 and 180 minutes following the glucose administration. OGTT results revealed that the lower blood glucose levels were measured in Lep (ob/ob) diabetic mice with TW68 treatment while there was no significant difference between wild type animals treated with TW68 or control vehicle **(Figure 4.34)**. Overall, in this study I showed that TW68 increases the stability of CRY1/2, reduces the transcription of the *Pck1* and *G6pc* in mice liver subsequently decreases the fasting blood glucose levels in diabetic animals.

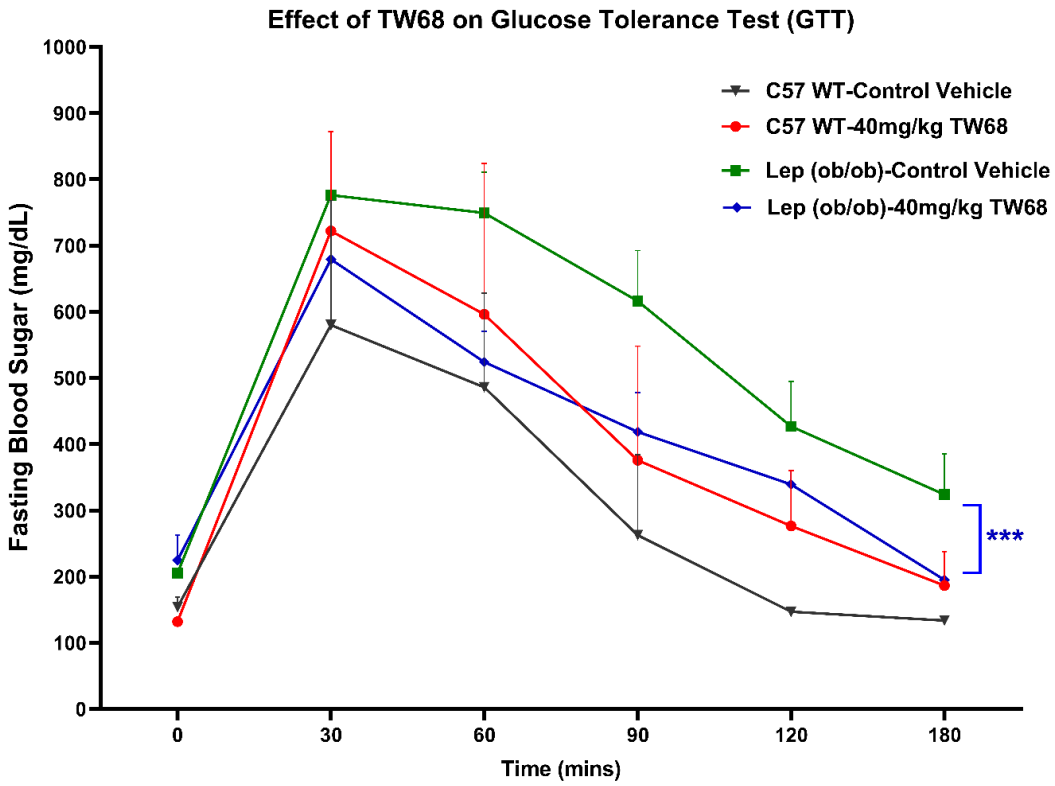

Figure 4. 34: The oral glucose tolerance test (OGTT) was performed for both wild type and ob/ob animals. The effect of TW68 on oral glucose test in animals. Animals were fasted overnight and then 40mg/kg TW68 was administered. Statistical analyses were performed by using the Ordinary two-way ANOVA method by Lep (ob/ob) Control Vehicle versus Lep (ob/ob) TW68, ***$p < 0.0001$. Data represent the mean ± SEM, n=4 for each group).

Chapter 5

DISCUSSIONS

The circadian clock is an endogenous timing system that allows organisms to anticipate and respond to the daily cyclic changes in their environment, including light-dark cycles, temperature, and feeding schedules. Light is the most potent synchronizer of the circadian system. However, modern lifestyle factors, such as artificial lighting, irregular work schedules, and late-night screen use, can disrupt the natural alignment of the circadian clock with the environment [1]. The circadian clock plays a critical role in regulating physiological processes, including sleep, metabolism, and hormone secretion. Proper functioning of the circadian clock ensures optimal performance during daily activities and promotes restorative sleep during the night [34, 198]. Furthermore, the circadian clock not only influences physiological processes but also affects cognitive functions and behavior. The timing of light exposure and the alignment of the circadian clock with the external environment is crucial for maintaining mental well-being [43].

The circadian clock is regulated by a complex network of molecular and genetic mechanisms. At the core of this system are a group of genes known as "clock genes" that oscillate in a rhythmic manner. These clock genes interact with each other and respond to environmental cues to maintain the proper timing of physiological processes [199]. Disruption of circadian synchronization in mammalians may influence the maintenance of the body mass index, glucose, and lipid homeostasis, which are closely associated with risk factors leading to insulin resistance, obesity and type 2 diabetes [38, 200, 201]. The mechanisms underlying these associations are still being studied, but it is believed that disturbances in hormone regulation, particularly hormones involved in gluconeogenesis, metabolism, and appetite control, play a significant role.

The relationship between gluconeogenesis and the circadian clock has been revealed that the core clock protein CRY inhibits glucagon-mediated gluconeogenesis and also reduces blood glucose levels [118]. CRY1 binds to the α subunit of the G protein and effectively inhibits G protein-coupled receptor (GPCR) mediated accumulation at the cAMP level, in this way inhibits gluconeogenesis. Drug discovery studies have recently gained speed with the development of structure-based computational screening methods.

Small molecules have emerged as powerful tools to study and manipulate the circadian clock, offering potential therapeutic strategies for circadian disorders and related diseases [189, 202]. Various small molecules have been identified that regulate the circadian clock by altering the core clock protein activity [159, 167, 203, 204].

In this thesis, we have identified and further characterized a novel small molecule called TW68 that stabilizes both mammalian CRYs. The process started with screening the non-characterized virtual library containing more than 2 million molecules in silico. 90 candidate molecules with small binding free energy were first tested for their cellular toxicity. As a result, 20 small molecules were eliminated due to their toxicity on cells and the effect of non-toxic molecules on CRY1/2 stability and bioluminescence reporter rhythmicity were determined. Among 70 small molecules screened, candidate molecules that significantly affect both CRY1 and CRY2 half-life were further investigated for their dose-dependent effect on CRY stability and circadian rhythm. Observing a dose-response effect is important for identifying small molecules that bind to the target protein.

Here, the best performed molecule TW68, causes the lengthening the period of circadian rhythm in U2OS and NIH3T3 *Bmal1*-d*Luc* cells and increases the stability of the CRY1-LUC and CRY2-LUC (Figure 4.11 and Figure 4.8) dose dependently. The biotinylated TW68 was used in pull down assay to show that physical interaction between TW68 and CRY1/2 through their primary pocket (Figure 4.17) and results were consistent with computational studies. The PHR domain of CRYs is critical for FBXL3 binding to primary pocket, and the stability regulated by ubiquitin-dependent proteasomal degradation [105]. The result of ubiquitinated CRY protein levels revealed that the ubiquitination was decreased with the TW68 treatment (Figure 4.22).

In vivo toxicity experiments have been demonstrated that TW68 can be well tolerated in mice at doses below 50 mg/kg (Figure 4.25). In the following pharmacokinetic analyzes, it was observed that the distribution and bioavailability of TW68 to tissues were optimum, especially when administered orally (Figure 4.28). A previous study highlighted that overexpression or decreasing the rate of the degradation of CRY protein with small molecules leads to the suppression of gluconeogenesis-related pathways [129]. Such molecules could be used as anti-diabetic drugs, which control blood glucose levels.

According to these results then hypothesized that TW68 could effectively lower blood glucose levels in diabetic animals during fasting conditions.

In the subsequent pre-clinical activity analysis, it was observed that TW68 significantly reduced the fasting blood glucose levels in both transgenic and fat-induced diabetic animal models (Figure 4.). Then discovered that TW68 inhibits glucagon-mediated glucogenesis by stabilizing CRY1 and inhibiting the transcription of *Pck1* and *G6pc* gluconeogenetic genes (Figure 4.). Insulin level in blood was reduced upon TW68 treatment of diabetic animals. This is likely due to the blood glucose level reduction, which signals to reduce releasing insulin from the pancreas. These results signify the therapeutic potential of TW68, a CRY stabilizer, on the circadian clock and gluconeogenesis-related metabolic diseases, including type 2 diabetes mellitus.

Type 2 Diabetes Mellitus (T2D) has become a primary health problem next to cancer, and that affects the future of our commonwealth. However, only half of the patients being treated for diabetes respond to current treatment regimens, and only 11% completed their treatment successfully and continued onto a complication-free lifestyle. Hence, research on novel prevention and treatment methods for diabetes is necessary. In order to develop more specific therapeutics that are effective even at lower concentrations, quantitative structure–activity relationship (qSAR) studies can be performed to optimize the TW68 molecule over different side chains by keeping the molecular backbone constant. Derivatives of TW68 can have the potential to improve the efficacy and pharmacokinetic parameters of the drug. At this point, Phase 1 clinical trials can be initiated based on the TW68 pre-clinical studies. The novel CRY1 stabilizer TW68, which we have characterized within this thesis, will open an innovative, unique, and alternative way to treat type 2 diabetes.

BIBLIOGRAPHY

1. Foster, R.G. and T. Roenneberg, *Human responses to the geophysical daily, annual and lunar cycles.* Curr Biol, 2008. **18**(17): p. R784-R794.
2. Loudon, A.S., *Circadian biology: a 2.5 billion year old clock.* Curr Biol, 2012. **22**(14): p. R570-1.
3. Rosbash, M., *The implications of multiple circadian clock origins.* PLoS Biol, 2009. **7**(3): p. e62.
4. Pittendrigh, C.S., *Temporal organization: reflections of a Darwinian clock-watcher.* Annu Rev Physiol, 1993. **55**: p. 16-54.
5. Moser, M., et al., *Why Life Oscillates – from a Topographical Towards a Functional Chronobiology.* Cancer Causes & Control, 2006. **17**(4): p. 591-599.
6. Bass, J., *Circadian topology of metabolism.* Nature, 2012. **491**(7424): p. 348-56.
7. Aschoff, J., *A Survey on Biological Rhythms.* Biological Rhythms, 1981: p. 3-10.
8. Aschoff, J., *Circadian Timing.* Annals of the New York Academy of Sciences, 1984. **423**(1 Timing and Ti): p. 442-468.
9. Young, M.W., Kay, S. A., *Time zones: a comparative genetics of circadian clocks.* Nature Reviews Genetics, 2001. **2**: p. 702-715.
10. von Schantz, M., I. Provencio, and R.G. Foster, *Recent developments in circadian photoreception: more than meets the eye.* Invest Ophthalmol Vis Sci, 2000. **41**(7): p. 1605-7.
11. Botbol, M., et al., *Biological and psychological rhythms: an integrative approach to rhythm disturbances in autistic disorder.* J Physiol Paris, 2013. **107**(4): p. 298-309.
12. Law, S.P., *The regulation of menstrual cycle and its relationship to the moon.* Acta Obstet Gynecol Scand, 1986. **65**(1): p. 45-8.
13. Paul, M.J., I. Zucker, and W.J. Schwartz, *Tracking the seasons: the internal calendars of vertebrates.* Philosophical Transactions of the Royal Society B: Biological Sciences, 2008. **363**(1490): p. 341-361.
14. Brodsky, V.Y., *Ultradian rhythms: introductory remarks.* Cell Biol Int, 2000. **24**(8): p. 499-500.
15. Panda, S., J.B. Hogenesch, and S.A. Kay, *Circadian rhythms from flies to human.* Nature, 2002. **417**(6886): p. 329-35.
16. Welsh, D.K., et al., *Individual neurons dissociated from rat suprachiasmatic nucleus express independently phased circadian firing rhythms.* Neuron, 1995. **14**(4): p. 697-706.
17. Vitaterna, M.H., J.S. Takahashi, and F.W. Turek, *Overview of circadian rhythms.* Alcohol Res Health, 2001. **25**(2): p. 85-93.
18. Koch, J.M., M.H. Hagenauer, and T.M. Lee, *THE RESPONSE OFPER1TO LIGHT IN THE SUPRACHIASMATIC NUCLEUS OF THE DIURNAL DEGU (OCTODON DEGUS).* Chronobiology International, 2009. **26**(6): p. 1263-1271.
19. Krishnaiah, S.Y., et al., *Clock Regulation of Metabolites Reveals Coupling between Transcription and Metabolism.* Cell Metab, 2017. **25**(4): p. 961-974 e4.
20. Welsh, D.K., J.S. Takahashi, and S.A. Kay, *Suprachiasmatic nucleus: cell autonomy and network properties.* Annu Rev Physiol, 2010. **72**: p. 551-77.
21. Stokkan, K.A., et al., *Entrainment of the circadian clock in the liver by feeding.* Science, 2001. **291**(5503): p. 490-3.
22. Dunlap, J.C., *Molecular bases for circadian clocks.* Cell, 1999. **96**(2): p. 271-90.

23. Damiola, F., et al., *Restricted feeding uncouples circadian oscillators in peripheral tissues from the central pacemaker in the suprachiasmatic nucleus.* Genes Dev, 2000. **14**(23): p. 2950-61.
24. Mohawk, J.A., C.B. Green, and J.S. Takahashi, *Central and Peripheral Circadian Clocks in Mammals.* Annual Review of Neuroscience, 2012. **35**(1): p. 445-462.
25. Wever, R.A., *Characteristics of circadian rhythms in human functions.* J Neural Transm Suppl, 1986. **21**: p. 323-73.
26. Bromundt, V., et al., *Circadian sleep-wake cycles, well-being, and light therapy in borderline personality disorder.* J Pers Disord, 2013. **27**(5): p. 680-96.
27. Patke, A., et al., *Mutation of the Human Circadian Clock Gene CRY1 in Familial Delayed Sleep Phase Disorder.* Cell, 2017. **169**(2): p. 203-215.e13.
28. Hood, S. and S. Amir, *The aging clock: circadian rhythms and later life.* Journal of Clinical Investigation, 2017. **127**(2): p. 437-446.
29. Hurd, M.W. and M.R. Ralph, *The significance of circadian organization for longevity in the golden hamster.* J Biol Rhythms, 1998. **13**(5): p. 430-6.
30. Duffy, J.F., K.-M. Zitting, and E.D. Chinoy, *Aging and Circadian Rhythms.* Sleep Medicine Clinics, 2015. **10**(4): p. 423-434.
31. Dunlap, J.C., J.J. Loros, and P.J. DeCoursey, *Chronobiology : biological timekeeping*. 2004, Sunderland, Mass.: Sinauer Associates.
32. Buttgereit, F., et al., *Clocking in: chronobiology in rheumatoid arthritis.* Nat Rev Rheumatol, 2015. **11**(6): p. 349-56.
33. Ripperger, J.A., C. Jud, and U. Albrecht, *The daily rhythm of mice.* FEBS Letters, 2011. **585**(10): p. 1384-1392.
34. Giebultowicz, J., *Chronobiology: biological timekeeping.* Integr Comp Biol, 2004. **44**(3): p. 266.
35. Liu, C. and S.M. Reppert, *GABA synchronizes clock cells within the suprachiasmatic circadian clock.* Neuron, 2000. **25**(1): p. 123-8.
36. Thapan, K., J. Arendt, and D.J. Skene, *An action spectrum for melatonin suppression: evidence for a novel non-rod, non-cone photoreceptor system in humans.* J Physiol, 2001. **535**(Pt 1): p. 261-7.
37. Reid, K.J. and P.C. Zee, *Circadian rhythm disorders.* Semin Neurol, 2009. **29**(4): p. 393-405.
38. Gagliardino, J.J., R.E. Hernandez, and O.R. Rebolledo, *Chronobiological aspects of blood glucose regulation: a new scope for the study of diabetes mellitus.* Chronobiologia, 1984. **11**(4): p. 357-79.
39. Warne, J.P., et al., *Disengaging insulin from corticosterone: roles of each on energy intake and disposition.* Am J Physiol Regul Integr Comp Physiol, 2009. **296**(5): p. R1366-75.
40. Rijo-Ferreira, F. and J.S. Takahashi, *Circadian rhythms in infectious diseases and symbiosis.* Semin Cell Dev Biol, 2022. **126**: p. 37-44.
41. Cermakian, N., et al., *Crosstalk between the circadian clock circuitry and the immune system.* Chronobiology International, 2013. **30**(7): p. 870-888.
42. Kemeny, M.E. and M. Schedlowski, *Understanding the interaction between psychosocial stress and immune-related diseases: A stepwise progression.* Brain, Behavior, and Immunity, 2007. **21**(8): p. 1009-1018.
43. Maiese, K., *Neurodegeneration, memory loss, and dementia: the impact of biological clocks and circadian rhythm.* Front Biosci (Landmark Ed), 2021. **26**(9): p. 614-627.

44. Gerstner, J.R. and J.C.P. Yin, *Circadian rhythms and memory formation.* Nature Reviews Neuroscience, 2010. **11**(8): p. 577-588.
45. Smarr, B.L., et al., *A time to remember: the role of circadian clocks in learning and memory.* Behav Neurosci, 2014. **128**(3): p. 283-303.
46. Kavakli, I.H.S., A., *Circadian-photoreception-in-humans.* 2002.
47. Albrecht, U., *Timing to perfection: the biology of central and peripheral circadian clocks.* Neuron, 2012. **74**(2): p. 246-60.
48. Schibler, U. and P. Sassone-Corsi, *A Web of Circadian Pacemakers.* Cell, 2002. **111**(7): p. 919-922.
49. Wetterberg, L., *Light and biological rhythms.* J Intern Med, 1994. **235**(1): p. 5-19.
50. Nakao, A., Y. Nakamura, and S. Shibata, *The circadian clock functions as a potent regulator of allergic reaction.* Allergy, 2015. **70**(5): p. 467-473.
51. Froy, O., *Circadian Rhythms and Obesity in Mammals.* ISRN Obesity, 2012. **2012**: p. 1-12.
52. Ko, C.H. and J.S. Takahashi, *Molecular components of the mammalian circadian clock.* Hum Mol Genet, 2006. **15 Spec No 2**: p. R271-7.
53. Yang, X., et al., *Nuclear Receptor Expression Links the Circadian Clock to Metabolism.* Cell, 2006. **126**(4): p. 801-810.
54. Shimba, S., *[Regulation of adipose functions by molecular clocks].* Nihon Rinsho, 2006. **64**(10): p. 1955-62.
55. Nakao, A., *Temporal Regulation of Cytokines by the Circadian Clock.* Journal of Immunology Research, 2014. **2014**: p. 1-4.
56. Haspel, J.A., et al., *Perfect timing: circadian rhythms, sleep, and immunity - an NIH workshop summary.* JCI Insight, 2020. **5**(1).
57. Konopka, R.J. and S. Benzer, *Clock Mutants of Drosophila melanogaster.* Proceedings of the National Academy of Sciences, 1971. **68**(9): p. 2112-2116.
58. Reddy, P., et al., *Molecular analysis of the period locus in Drosophila melanogaster and identification of a transcript involved in biological rhythms.* Cell, 1984. **38**(3): p. 701-10.
59. Zehring, W.A., et al., *P-element transformation with period locus DNA restores rhythmicity to mutant, arrhythmic Drosophila melanogaster.* Cell, 1984. **39**(2 Pt 1): p. 369-76.
60. Bargiello, T.A., F.R. Jackson, and M.W. Young, *Restoration of circadian behavioural rhythms by gene transfer in Drosophila.* Nature, 1984. **312**(5996): p. 752-4.
61. Bargiello, T.A. and M.W. Young, *Molecular genetics of a biological clock in Drosophila.* Proceedings of the National Academy of Sciences, 1984. **81**(7): p. 2142-2146.
62. Siwicki, K.K., et al., *Antibodies to the period gene product of Drosophila reveal diverse tissue distribution and rhythmic changes in the visual system.* Neuron, 1988. **1**(2): p. 141-50.
63. Hardin, P.E., J.C. Hall, and M. Rosbash, *Feedback of the Drosophila period gene product on circadian cycling of its messenger RNA levels.* Nature, 1990. **343**(6258): p. 536-540.
64. Vitaterna, M.H., et al., *Mutagenesis and Mapping of a Mouse Gene, Clock , Essential for Circadian Behavior.* Science, 1994. **264**(5159): p. 719-725.

65. King, D.P., et al., *Positional Cloning of the Mouse Circadian Gene.* Cell, 1997. **89**(4): p. 641-653.
66. Turek, F.W., et al., *Obesity and metabolic syndrome in circadian Clock mutant mice.* Science, 2005. **308**(5724): p. 1043-5.
67. Gekakis, N., et al., *Role of the CLOCK protein in the mammalian circadian mechanism.* Science, 1998. **280**(5369): p. 1564-9.
68. Hogenesch, J.B., et al., *Characterization of a Subset of the Basic-Helix-Loop-Helix-PAS Superfamily That Interacts with Components of the Dioxin Signaling Pathway.* Journal of Biological Chemistry, 1997. **272**(13): p. 8581-8593.
69. Hogenesch, J.B., et al., *The basic helix-loop-helix-PAS protein MOP9 is a brain-specific heterodimeric partner of circadian and hypoxia factors.* J Neurosci, 2000. **20**(13): p. Rc83.
70. Bunger, M.K., et al., *Mop3 Is an Essential Component of the Master Circadian Pacemaker in Mammals.* Cell, 2000. **103**(7): p. 1009-1017.
71. Todo, T., et al., *Similarity among the Drosophila (6-4)photolyase, a human photolyase homolog, and the DNA photolyase-blue-light photoreceptor family.* Science, 1996. **272**(5258): p. 109-12.
72. Todo, T., *Functional diversity of the DNA photolyaserblue light receptor family.* 1990.
73. Ishikawa, T., et al., *DCRY is a Drosophila photoreceptor protein implicated in light entrainment of circadian rhythm.* Genes Cells, 1999. **4**(1): p. 57-65.
74. Ahmad, M. and A.R. Cashmore, *Seeing blue: the discovery of cryptochrome.* Plant Molecular Biology, 1996. **30**(5): p. 851-861.
75. Hsu, D.S., et al., *Putative Human Blue-Light Photoreceptors hCRY1 and hCRY2 Are Flavoproteins.* Biochemistry, 1996. **35**(44): p. 13871-13877.
76. Miyamoto, Y. and A. Sancar, *Vitamin B2-based blue-light photoreceptors in the retinohypothalamic tract as the photoactive pigments for setting the circadian clock in mammals.* Proc Natl Acad Sci U S A, 1998. **95**(11): p. 6097-102.
77. Miyamoto, Y. and A. Sancar, *Circadian regulation of cryptochrome genes in the mouse.* Brain Res Mol Brain Res, 1999. **71**(2): p. 238-43.
78. Thresher, R.J., et al., *Role of mouse cryptochrome blue-light photoreceptor in circadian photoresponses.* Science, 1998. **282**(5393): p. 1490-4.
79. Kume, K., et al., *mCRY1 and mCRY2 Are Essential Components of the Negative Limb of the Circadian Clock Feedback Loop.* Cell, 1999. **98**(2): p. 193-205.
80. Okamura, H., et al., *Photic induction of mPer1 and mPer2 in cry-deficient mice lacking a biological clock.* Science, 1999. **286**(5449): p. 2531-4.
81. Vitaterna, *Differential-regulation-of-mammalia.pdf*>. 1999.
82. Dibner, C., U. Schibler, and U. Albrecht, *The mammalian circadian timing system: organization and coordination of central and peripheral clocks.* Annu Rev Physiol, 2010. **72**: p. 517-49.
83. Hastings, M.H., *A clockwork web: circadian timing in brain and periphery, in health and disease.* 2003.
84. Takahashi, J.S., *Finding new clock components; past and future.* 2004.
85. Lowrey, P.L. and J.S. Takahashi, *Mammalian circadian biology: elucidating genome-wide levels of temporal organization.* Annu Rev Genomics Hum Genet, 2004. **5**: p. 407-41.
86. Kavakli, I.H., N. Ozturk, and I. Baris, *Protein interaction networks of the mammalian core clock proteins.* Adv Protein Chem Struct Biol, 2022. **131**: p. 207-233.

87. Reick, M., et al., *NPAS2: An Analog of Clock Operative in the Mammalian Forebrain.* Science, 2001. **293**(5529): p. 506-509.
88. Buhr, E.D. and J.S. Takahashi, *Molecular Components of the Mammalian Circadian Clock*. 2013, Springer Berlin Heidelberg. p. 3-27.
89. Zhang, R., et al., *A circadian gene expression atlas in mammals: Implications for biology and medicine.* Proceedings of the National Academy of Sciences, 2014. **111**(45): p. 16219-16224.
90. Takahashi, J.S., et al., *The genetics of mammalian circadian order and disorder: implications for physiology and disease.* Nat Rev Genet, 2008. **9**(10): p. 764-75.
91. Takahashi, J.S., *Transcriptional architecture of the mammalian circadian clock.* Nature Reviews Genetics, 2017. **18**(3): p. 164-179.
92. Chaves, I., et al., *Functional Evolution of the Photolyase/Cryptochrome Protein Family: Importance of the C Terminus of Mammalian CRY1 for Circadian Core Oscillator Performance.* Molecular and Cellular Biology, 2006. **26**(5): p. 1743-1753.
93. Horst, G.T.J.V.D., et al., *Mammalian Cry1 and Cry2 are essential for maintenance of circadian rhythms.* Nature, 1999. **398**(6728): p. 627-630.
94. Kobayashi, K., et al., *Characterization of photolyase/blue-light receptor homologs in mouse and human cells.* Nucleic Acids Res, 1998. **26**(22): p. 5086-92.
95. Sancar, A., et al., *Photolyase/cryptochrome family blue-light photoreceptors use light energy to repair DNA or set the circadian clock.* Cold Spring Harb Symp Quant Biol, 2000. **65**: p. 157-71.
96. Kang, T.-H., et al., *Circadian control of XPA and excision repair of cisplatin-DNA damage by cryptochrome and HERC2 ubiquitin ligase.* Proceedings of the National Academy of Sciences, 2010. **107**(11): p. 4890-4895.
97. Kang, T.H., J.T. Reardon, and A. Sancar, *Regulation of nucleotide excision repair activity by transcriptional and post-transcriptional control of the XPA protein.* Nucleic Acids Res, 2011. **39**(8): p. 3176-87.
98. Kavakli, I.H., et al., *The Photolyase/Cryptochrome Family of Proteins as DNA Repair Enzymes and Transcriptional Repressors.* Photochemistry and Photobiology, 2017. **93**(1): p. 93-103.
99. Griffin, E.A., Jr., D. Staknis, and C.J. Weitz, *Light-independent role of CRY1 and CRY2 in the mammalian circadian clock.* Science, 1999. **286**(5440): p. 768-71.
100. Czarna, A., et al., *Quantitative Analyses of Cryptochrome-mBMAL1 Interactions.* Journal of Biological Chemistry, 2011. **286**(25): p. 22414-22425.
101. Hirano, A., et al., *FAD Regulates CRYPTOCHROME Protein Stability and Circadian Clock in Mice.* Cell Rep, 2017. **19**(2): p. 255-266.
102. Mure, L.S., et al., *Diurnal transcriptome atlas of a primate across major neural and peripheral tissues.* Science, 2018. **359**(6381).
103. Ozturk, N., et al., *Loss of cryptochrome reduces cancer risk in p53 mutant mice.* Proceedings of the National Academy of Sciences, 2009. **106**(8): p. 2841-2846.
104. Kavakli, I.H., N. Ozturk, and S. Gul, *DNA repair by photolyases*. 2019, Elsevier. p. 1-19.
105. Busino, L., et al., *SCFFbxl3 controls the oscillation of the circadian clock by directing the degradation of cryptochrome proteins.* Science, 2007. **316**(5826): p. 900-4.

106. Godinho, S.I., et al., *The after-hours mutant reveals a role for Fbxl3 in determining mammalian circadian period.* Science, 2007. **316**(5826): p. 897-900.
107. Siepka, S.M., et al., *Circadian Mutant Overtime Reveals F-box Protein FBXL3 Regulation of Cryptochrome and Period Gene Expression.* Cell, 2007. **129**(5): p. 1011-1023.
108. Hirano, A., et al., *FBXL21 Regulates Oscillation of the Circadian Clock through Ubiquitination and Stabilization of Cryptochromes.* Cell, 2013. **152**(5): p. 1106-1118.
109. Xing, W., et al., *SCFFBXL3 ubiquitin ligase targets cryptochromes at their cofactor pocket.* Nature, 2013. **496**(7443): p. 64-68.
110. Nangle, S.N., et al., *Molecular assembly of the period-cryptochrome circadian transcriptional repressor complex.* Elife, 2014. **3**: p. e03674.
111. Schmalen, I., et al., *Interaction of Circadian Clock Proteins CRY1 and PER2 Is Modulated by Zinc Binding and Disulfide Bond Formation.* Cell, 2014. **157**(5): p. 1203-1215.
112. Khan, S.K., et al., *Identification of a Novel Cryptochrome Differentiating Domain Required for Feedback Repression in Circadian Clock Function.* Journal of Biological Chemistry, 2012. **287**(31): p. 25917-25926.
113. Koike, N., et al., *Transcriptional Architecture and Chromatin Landscape of the Core Circadian Clock in Mammals.* Science, 2012. **338**(6105): p. 349-354.
114. Lamia, K.A., et al., *AMPK Regulates the Circadian Clock by Cryptochrome Phosphorylation and Degradation.* Science, 2009. **326**(5951): p. 437-440.
115. Kurabayashi, N., et al., *DYRK1A and Glycogen Synthase Kinase 3β, a Dual-Kinase Mechanism Directing Proteasomal Degradation of CRY2 for Circadian Timekeeping.* Molecular and Cellular Biology, 2010. **30**(7): p. 1757-1768.
116. Ma, X., et al., *RBP4 functions as a hepatokine in the regulation of glucose metabolism by the circadian clock in mice.* Diabetologia, 2016. **59**(2): p. 354-62.
117. Allaman-Pillet, N., et al., *Circadian regulation of islet genes involved in insulin production and secretion.* Mol Cell Endocrinol, 2004. **226**(1-2): p. 59-66.
118. Hatori, M. and S. Panda, *CRY links the circadian clock and CREB-mediated gluconeogenesis.* Cell Research, 2010. **20**(12): p. 1285-1288.
119. Ruiter, M., et al., *The daily rhythm in plasma glucagon concentrations in the rat is modulated by the biological clock and by feeding behavior.* Diabetes, 2003. **52**(7): p. 1709-15.
120. La, F., et al., *A Suprachiasmatic Nucleus Generated Rhythm In Basal Glucose Concentrations.* Journal of Neuroendocrinology, 2001. **11**(8): p. 643-652.
121. Barnea, M., Z. Madar, and O. Froy, *High-fat Diet Followed by Fasting Disrupts Circadian Expression of Adiponectin Signaling Pathway in Muscle and Adipose Tissue.* Obesity, 2010. **18**(2): p. 230-238.
122. Ahima, R.S., D. Prabakaran, and J.S. Flier, *Postnatal leptin surge and regulation of circadian rhythm of leptin by feeding. Implications for energy homeostasis and neuroendocrine function.* Journal of Clinical Investigation, 1998. **101**(5): p. 1020-1027.
123. Bagnasco, M., et al., *Leptin Expression in Hypothalamic PVN Reverses Dietary Obesity and Hyperinsulinemia but Stimulates Ghrelin*.* Obesity Research, 2003. **11**(12): p. 1463-1470.
124. Kalsbeek, A., et al., *The suprachiasmatic nucleus generates the diurnal changes in plasma leptin levels.* Endocrinology, 2001. **142**(6): p. 2677-85.

125. von Gall, C., et al., *Rhythmic gene expression in pituitary depends on heterologous sensitization by the neurohormone melatonin.* Nat Neurosci, 2002. **5**(3): p. 234-8.
126. Lamia, K.A., et al., *Cryptochromes mediate rhythmic repression of the glucocorticoid receptor.* Nature, 2011. **480**(7378): p. 552-556.
127. Jang, H., et al., *SREBP1c-CRY1 signalling represses hepatic glucose production by promoting FOXO1 degradation during refeeding.* Nat Commun, 2016. **7**: p. 12180.
128. Toledo, M., et al., *Autophagy Regulates the Liver Clock and Glucose Metabolism by Degrading CRY1.* Cell Metab, 2018. **28**(2): p. 268-281.e4.
129. Zhang, E.E., et al., *Cryptochrome mediates circadian regulation of cAMP signaling and hepatic gluconeogenesis.* Nat Med, 2010. **16**(10): p. 1152-6.
130. Oishi, K., et al., *Genome-wide expression analysis of mouse liver reveals CLOCK-regulated circadian output genes.* J Biol Chem, 2003. **278**(42): p. 41519-27.
131. Griebel, G., et al., *Mice Deficient in Cryptochrome 1 (Cry1−/−) Exhibit Resistance to Obesity Induced by a High-Fat Diet.* Frontiers in Endocrinology, 2014. **5**.
132. Barclay, J.L., et al., *High-fat diet-induced hyperinsulinemia and tissue-specific insulin resistance in Cry-deficient mice.* Am J Physiol Endocrinol Metab, 2013. **304**(10): p. E1053-63.
133. Marcheva, B., et al., *Circadian Clocks and Metabolism*. 2013, Springer Berlin Heidelberg. p. 127-155.
134. Auger, R.R., et al., *Clinical Practice Guideline for the Treatment of Intrinsic Circadian Rhythm Sleep-Wake Disorders: Advanced Sleep-Wake Phase Disorder (ASWPD), Delayed Sleep-Wake Phase Disorder (DSWPD), Non-24-Hour Sleep-Wake Rhythm Disorder (N24SWD), and Irregular Sleep-Wake Rhythm Disorder (ISWRD). An Update for 2015: An American Academy of Sleep Medicine Clinical Practice Guideline.* J Clin Sleep Med, 2015. **11**(10): p. 1199-236.
135. Onat, O.E., et al., *Human CRY1 variants associate with attention deficit/hyperactivity disorder.* Journal of Clinical Investigation, 2020. **130**(7): p. 3885-3900.
136. Solheim, B., et al., *Cognitive performance in DSWPD patients upon awakening from habitual sleep compared with forced conventional sleep.* J Sleep Res, 2019. **28**(5): p. e12730.
137. Nesbitt, A.D., *Delayed sleep-wake phase disorder.* Journal of Thoracic Disease, 2018. **10**(S1): p. S103-S111.
138. Abbott, S.M., *Non-24-hour Sleep-Wake Rhythm Disorder.* Neurol Clin, 2019. **37**(3): p. 545-552.
139. Sun, S.Y. and G.H. Chen, *Treatment of Circadian Rhythm Sleep-Wake Disorders.* Curr Neuropharmacol, 2022. **20**(6): p. 1022-1034.
140. Pradhan, G., S.L. Samson, and Y. Sun, *Ghrelin.* Current Opinion in Clinical Nutrition and Metabolic Care, 2013. **16**(6): p. 619-624.
141. Labra, F.A., P.A. Marquet, and F. Bozinovic, *Scaling metabolic rate fluctuations.* Proceedings of the National Academy of Sciences, 2007. **104**(26): p. 10900-10903.
142. Serin, Y. and N. Acar Tek, *Effect of Circadian Rhythm on Metabolic Processes and the Regulation of Energy Balance.* Annals of Nutrition and Metabolism, 2019. **74**(4): p. 322-330.

143. Avidan, A. and C. Colwell, *Jet lag syndrome: circadian organization, pathophysiology, and management strategies.* Nature and Science of Sleep, 2010: p. 187.
144. Ferrannini, E., et al., *Dapagliflozin monotherapy in type 2 diabetic patients with inadequate glycemic control by diet and exercise: a randomized, double-blind, placebo-controlled, phase 3 trial.* Diabetes Care, 2010. **33**(10): p. 2217-24.
145. Galicia-Garcia, U., et al., *Pathophysiology of Type 2 Diabetes Mellitus.* International Journal of Molecular Sciences, 2020. **21**(17): p. 6275.
146. Khandelwal, D., et al., *Sleep Disorders in Type 2 Diabetes.* Indian J Endocrinol Metab, 2017. **21**(5): p. 758-761.
147. Ali, O., *Genetics of type 2 diabetes.* World Journal of Diabetes, 2013. **4**(4): p. 114.
148. Scheiermann, C., Y. Kunisaki, and P.S. Frenette, *Circadian control of the immune system.* Nature Reviews Immunology, 2013. **13**(3): p. 190-198.
149. Dallmann, R., A. Okyar, and F. Lévi, *Dosing-Time Makes the Poison: Circadian Regulation and Pharmacotherapy.* Trends in Molecular Medicine, 2016. **22**(5): p. 430-445.
150. Chen, Z., S.H. Yoo, and J.S. Takahashi, *Small molecule modifiers of circadian clocks.* Cell Mol Life Sci, 2013. **70**(16): p. 2985-98.
151. Oshima, T., et al., *C□H Activation Generates Period-Shortening Molecules That Target Cryptochrome in the Mammalian Circadian Clock.* Angewandte Chemie International Edition, 2015. **54**(24): p. 7193-7197.
152. Chun, S.K., et al., *Identification and validation of cryptochrome inhibitors that modulate the molecular circadian clock.* ACS Chem Biol, 2014. **9**(3): p. 703-10.
153. Wallach, T. and A. Kramer, *Chemical chronobiology: Toward drugs manipulating time.* FEBS Lett, 2015. **589**(14): p. 1530-8.
154. Grant, D., et al., *GSK4112, a Small Molecule Chemical Probe for the Cell Biology of the Nuclear Heme Receptor Rev-erbα.* ACS Chemical Biology, 2010. **5**(10): p. 925-932.
155. Shimozaki, K., *REV-ERB Agonist SR9009 Regulates the Proliferation and Neurite Outgrowth/Suppression of Cultured Rat Adult Hippocampal Neural Stem/Progenitor Cells in a Concentration-Dependent Manner.* Cellular and Molecular Neurobiology, 2022. **42**(6): p. 1765-1776.
156. Wang, Y., et al., *Identification of SR1078, a Synthetic Agonist for the Orphan Nuclear Receptors RORα and RORγ.* ACS Chemical Biology, 2010. **5**(11): p. 1029-1034.
157. Keenan, C.R., et al., *Casein Kinase 1δ/ε Inhibitor, PF670462 Attenuates the Fibrogenic Effects of Transforming Growth Factor-β in Pulmonary Fibrosis.* Front Pharmacol, 2018. **9**: p. 738.
158. Wu, Y., et al., *GSK3 inhibitors CHIR99021 and 6-bromoindirubin-3'-oxime inhibit microRNA maturation in mouse embryonic stem cells.* Scientific Reports, 2015. **5**(1): p. 8666.
159. Doruk, Y.U., et al., *A CLOCK-binding small molecule disrupts the interaction between CLOCK and BMAL1 and enhances circadian rhythm amplitude.* Journal of Biological Chemistry, 2020. **295**(11): p. 3518-3531.
160. Hirota, T., et al., *Identification of Small Molecule Activators of Cryptochrome.* Science, 2012. **337**(6098): p. 1094-1097.
161. Nangle, S., W. Xing, and N. Zheng, *Crystal structure of mammalian cryptochrome in complex with a small molecule competitor of its ubiquitin ligase.* Cell Research, 2013. **23**(12): p. 1417-1419.

162. Lee, J.W., et al., *Development of Small-Molecule Cryptochrome Stabilizer Derivatives as Modulators of the Circadian Clock.* ChemMedChem, 2015. **10**(9): p. 1489-1497.
163. Öztürk, N., et al., *Structure and Function of Animal Cryptochromes.* Cold Spring Harbor Symposia on Quantitative Biology, 2007. **72**(1): p. 119-131.
164. Czarna, A., et al., *Structures of Drosophila Cryptochrome and Mouse Cryptochrome1 Provide Insight into Circadian Function.* Cell, 2013. **153**(6): p. 1394-1405.
165. Parico, G.C.G. and C.L. Partch, *The tail of cryptochromes: an intrinsically disordered cog within the mammalian circadian clock.* Cell Communication and Signaling, 2020. **18**(1).
166. Cal-Kayitmazbatir, S., et al., *CRY1-CBS binding regulates circadian clock function and metabolism.* The FEBS Journal, 2021. **288**(2): p. 614-639.
167. Gul, S., et al., *Discovery of a small molecule that selectively destabilizes Cryptochrome 1 and enhances life span in p53 knockout mice.* Nature Communications, 2022. **13**(1).
168. Bicker, J., et al., *Timing in drug absorption and disposition: The past, present, and future of chronopharmacokinetics.* British Journal of Pharmacology, 2020. **177**(10): p. 2215-2239.
169. Lu, D., et al., *Circadian Clock–Controlled Drug Metabolism: Implications for Chronotherapeutics.* Drug Metabolism and Disposition, 2020. **48**(5): p. 395-406.
170. Ozturk, N., et al., *Molecular Aspects of Circadian Pharmacology and Relevance for Cancer Chronotherapy.* International Journal of Molecular Sciences, 2017. **18**(10): p. 2168.
171. Phillips, J.C., et al., *Scalable molecular dynamics with NAMD.* Journal of Computational Chemistry, 2005. **26**(16): p. 1781-1802.
172. MacKerell, A.D., Jr., et al., *All-Atom Empirical Potential for Molecular Modeling and Dynamics Studies of Proteins.* The Journal of Physical Chemistry B, 1998. **102**(18): p. 3586-3616.
173. Pettersen, E.F., et al., *UCSF Chimera?A visualization system for exploratory research and analysis.* Journal of Computational Chemistry, 2004. **25**(13): p. 1605-1612.
174. Trott, O. and A.J. Olson, *AutoDock Vina: Improving the speed and accuracy of docking with a new scoring function, efficient optimization, and multithreading.* Journal of Computational Chemistry, 2009: p. NA-NA.
175. DeLano, W.L., *PyMOL Molecular Graphics System*. Schrödinger, LLC.
176. Case, D.A., et al., *The Amber biomolecular simulation programs.* Journal of Computational Chemistry, 2005. **26**(16): p. 1668-1688.
177. Van Meerloo, J., G.J.L. Kaspers, and J. Cloos, *Cell Sensitivity Assays: The MTT Assay*. 2011, Humana Press. p. 237-245.
178. Zhou, P., *Determining protein half-lives.* Methods Mol Biol, 2004. **284**: p. 67-77.
179. Zielinski, T., et al., *Strengths and Limitations of Period Estimation Methods for Circadian Data.* PLoS ONE, 2014. **9**(5): p. e96462.
180. Lee, D.H. and A.L. Goldberg, *Proteasome inhibitors: valuable new tools for cell biologists.* Trends Cell Biol, 1998. **8**(10): p. 397-403.
181. Kiyohara, Y.B., et al., *The BMAL1 C terminus regulates the circadian transcription feedback loop.* Proceedings of the National Academy of Sciences, 2006. **103**(26): p. 10074-10079.

182. Ramanathan, C., et al., *Monitoring Cell-autonomous Circadian Clock Rhythms of Gene Expression Using Luciferase Bioluminescence Reporters.* Journal of Visualized Experiments, 2012(67).
183. Solanas, G. and P.S. Welz, *Circadian Regulation: Methods and Protocols*. 2022: Springer US.
184. Koteshwar P, S.R., Francis D, Gupta SK. , *Drug Discovery and Clinical Research*. Chapter 1. New Drug Development. 2011: New Delhi: Jaypee Brothers Medical Publishers.
185. Campbell JE, C.D., *A Pharmacognosy Perspective*. Chapter 26: Pharmacodynamics. 2017: Pharmacognosy.: Academic Press.
186. Ergun, C., *Discovery and characterization of small molecules stabilizing the cryptochrome in the mammalian circadian clock,* in *Chemistry and Biology Engineering*. 2019, Koç University: Istanbul, Turkey.
187. St. John, P.C., et al., *Spatiotemporal separation of PER and CRY posttranslational regulation in the mammalian circadian clock.* Proceedings of the National Academy of Sciences, 2014. **111**(5): p. 2040-2045.
188. Hadadi, E., et al., *Identification of valid reference genes for circadian gene-expression studies in human mammary epithelial cells.* Chronobiology International, 2018. **35**(12): p. 1689-1701.
189. Hirota, T., et al., *High-Throughput Chemical Screen Identifies a Novel Potent Modulator of Cellular Circadian Rhythms and Reveals CKIα as a Clock Regulatory Kinase.* PLoS Biology, 2010. **8**(12): p. e1000559.
190. Mellacheruvu, D., et al., *The CRAPome: a contaminant repository for affinity purification–mass spectrometry data.* Nature Methods, 2013. **10**(8): p. 730-736.
191. Stachura, A., et al., *Wound Healing Impairment in Type 2 Diabetes Model of Leptin-Deficient Mice—A Mechanistic Systematic Review.* International Journal of Molecular Sciences, 2022. **23**(15): p. 8621.
192. Hayden, M.R. and W.A. Banks, *Deficient Leptin Cellular Signaling Plays a Key Role in Brain Ultrastructural Remodeling in Obesity and Type 2 Diabetes Mellitus.* International Journal of Molecular Sciences, 2021. **22**(11): p. 5427.
193. Murphy, J.E., et al., *Long-term correction of obesity and diabetes in genetically obese mice by a single intramuscular injection of recombinant adeno-associated virus encoding mouse leptin.* Proceedings of the National Academy of Sciences, 1997. **94**(25): p. 13921-13926.
194. Tentolouris, A., et al., *SGLT2 Inhibitors: A Review of Their Antidiabetic and Cardioprotective Effects.* International Journal of Environmental Research and Public Health, 2019. **16**(16): p. 2965.
195. Eleftheriadou, I., et al., *Update on Cardiovascular Effects of Older and Newer Anti-diabetic Medications.* Curr Med Chem, 2018. **25**(13): p. 1549-1566.
196. Avruch, J., *Insulin signal transduction through protein kinase cascades.* Mol Cell Biochem, 1998. **182**(1-2): p. 31-48.
197. Heikkinen, S., et al., *Evaluation of Glucose Homeostasis.* Current Protocols in Molecular Biology, 2007. **77**(1).
198. Bell-Pedersen, D., et al., *Circadian rhythms from multiple oscillators: lessons from diverse organisms.* Nat Rev Genet, 2005. **6**(7): p. 544-56.
199. Shearman, L.P., et al., *Interacting molecular loops in the mammalian circadian clock.* Science, 2000. **288**(5468): p. 1013-9.
200. Oster, M.H., et al., *Circadian rhythm of corticosterone in diabetic rats.* Life Sciences, 1988. **43**(20): p. 1643-1645.

201. Shimomura, Y., et al., *Different effects of insulin administration time in streptozotocin-induced diabetic rats.* Exp Clin Endocrinol, 1990. **96**(3): p. 296-300.
202. Roenneberg, T. and M. Merrow, *The Circadian Clock and Human Health.* Curr Biol, 2016. **26**(10): p. R432-43.
203. Kavakli, I.H., S. Gul, and M. Turkay, *Identification of novel small molecules targeting core clock proteins to regulate circadian rhythm.* Current Opinion in Chemical Engineering, 2022. **35**: p. 100730.
204. Gul, S., et al., *Structure-based design and classifications of small molecules regulating the circadian rhythm period.* Scientific Reports, 2021. **11**(1).
205. Laskowski, R.A. and M.B. Swindells, *LigPlot+: Multiple Ligand–Protein Interaction Diagrams for Drug Discovery.* Journal of Chemical Information and Modeling, 2011. **51**(10): p. 2778-2786.

APPENDIX A: SUPPLEMENTARY DATA

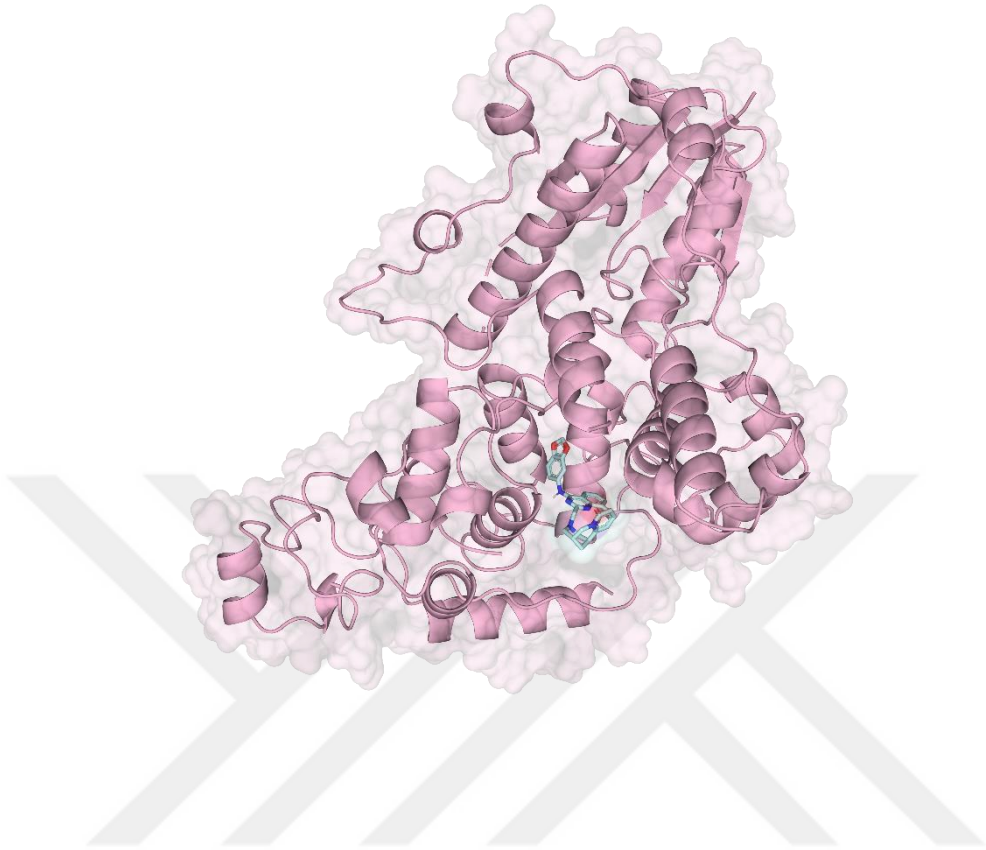

Figure A. 1: Binding pose of TW68 on the equilibrated CRYs. TW68 docked into primary pocket of mCRY2 PHR domains (PDB ID: 6KX8) using Autodock Vina.The protein structure is shown in surface.

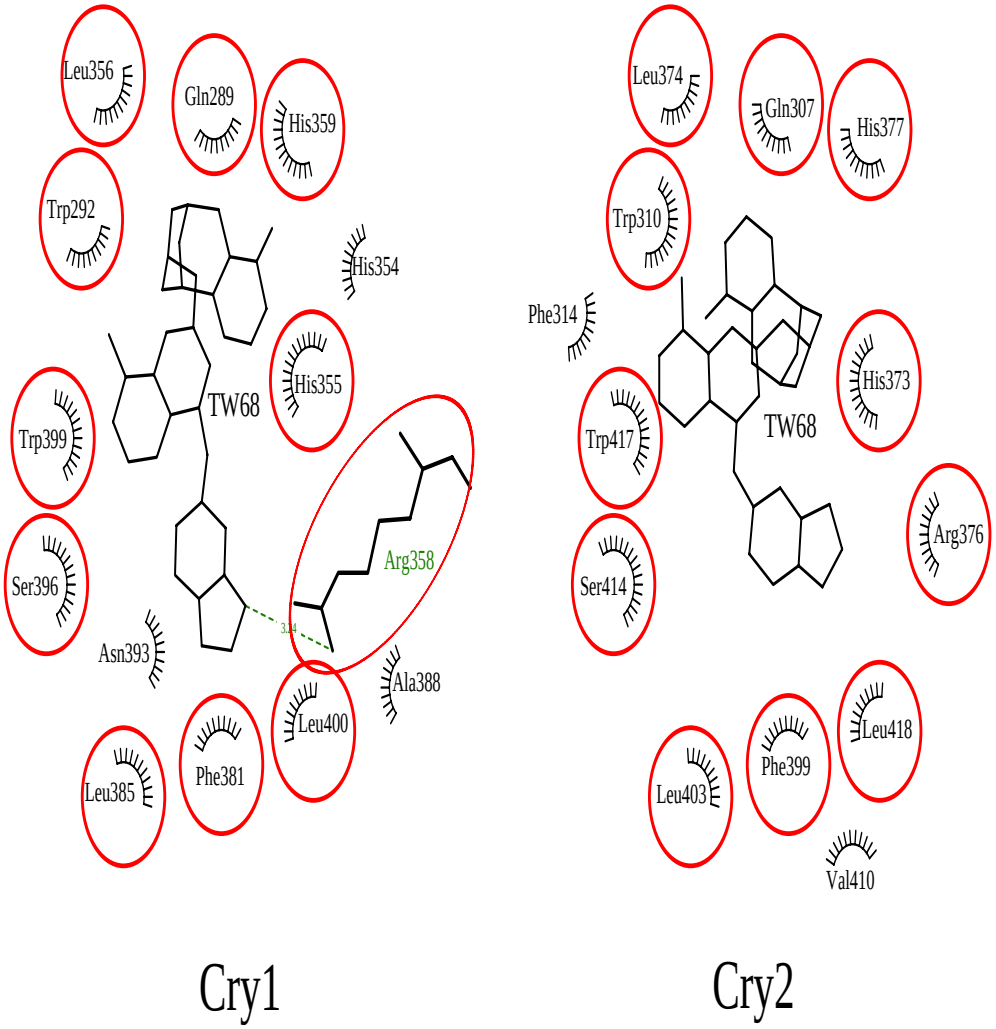

Figure A. 2: 2D interraction diagram of TW68 with CRY1(left) and CRY2(right) plotted in LigPlot+ [205]. Equvalent residues that are in interaction with TW68 in both CRY1 and CRY2 are encircled in red. ΔG values are respective scores from molecular docking in Autodock Vina.

A.

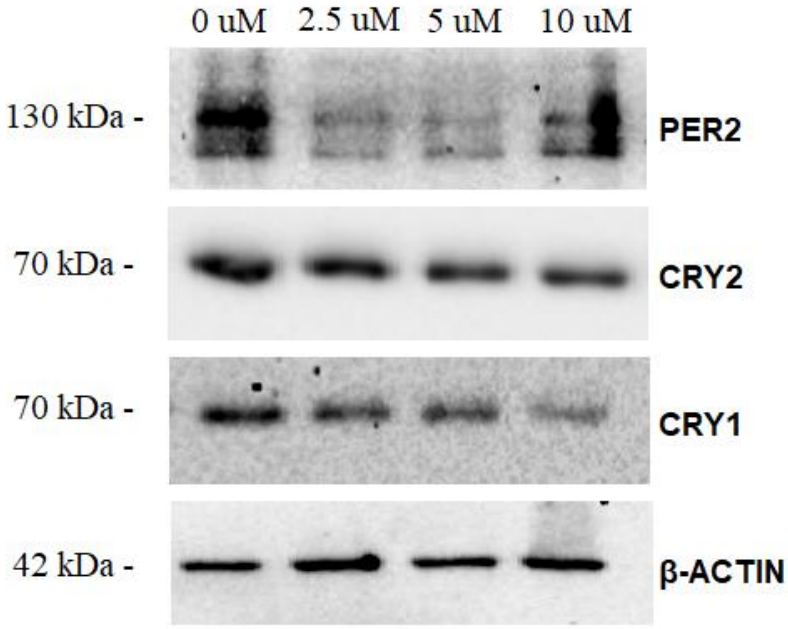

B.

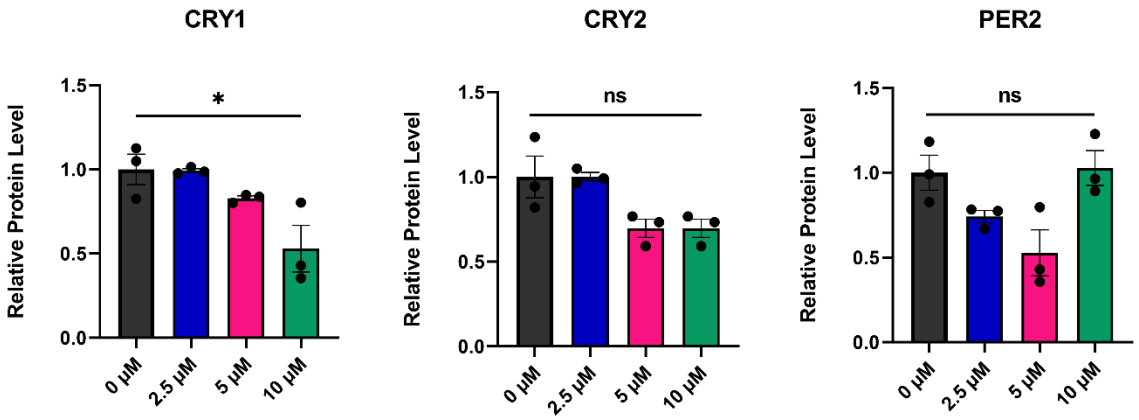

Figure A. 3: Western blot analysis of unsynchronized U2OS cells treated with CP53. **A.** CRY1, CRY2 and PER2 proteins, and **B.** Protein levels normalized with β-ACTIN, relative to DMSO (0 uM) control. Data are given as mean ± SEM, n=3. Statistical analysis performed using one-way ANOVA with Dunnett's multiple comparisons test (*p<0.05, ns = non-significant).

APPENDIX B: PLASMID MAPS

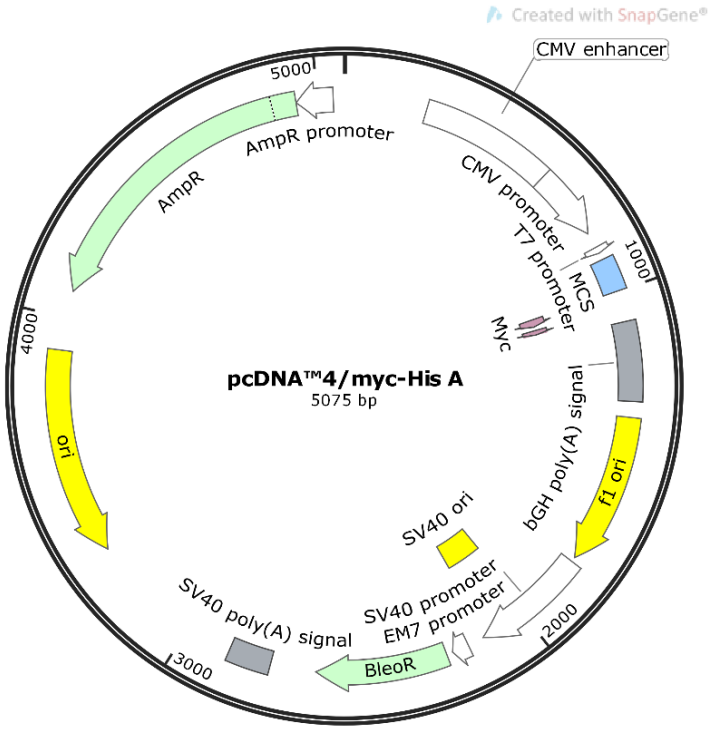

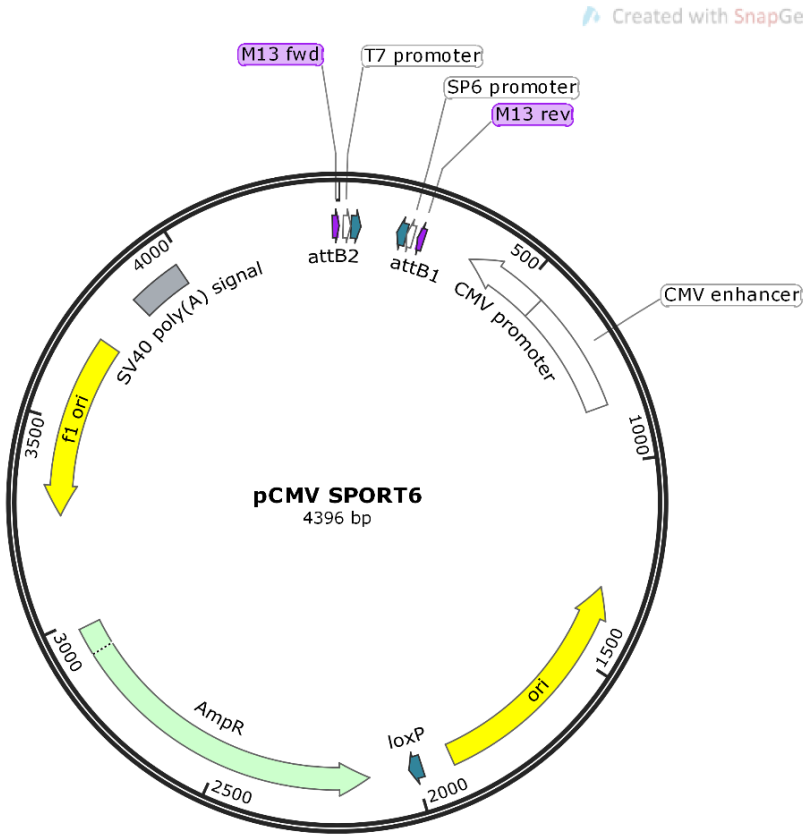

APPENDIX C: PRIMER SEQUENCES

RT-qPCR Primers

Primer Name*	Sequence
Hs-CRY1-RT-fwd	ACAGGTGGCGATTTTTGCTTC
Hs-CRY1-RT-rev	TCCAAAGGGCTCAGAATCATACT
Hs-CRY2-RT-fwd	CGTGTTCCCAAGGCTGTTCA
Hs-CRY2-RT-rev	CTCCGTCACTACTTCCACACC
Hs-PER2-RT-fwd	CCTCTTCCAGGATGTGGATGAA
Hs-PER2-RT-rev	CAACTGCAGAATCTTCTTGTGGA
Hs-DBP-RT-fwd	GAGGAACTTAAGCCCCAGCC
Hs-DBP-RT-rev	CTCGTTGTTCTTGTACCGCC
Hs-BMAL1-RT-fwd	GCCCATTGAACATCACGAGTAC
Hs-BMAL1-RT-rev	CCTGAGCCTGGCCTGATAGTAG
Hs-CLOCK-RT-fwd	GGCACCACCCATAATAGGGTA
Hs-CLOCK-RT-rev	TGTTGCCCCTTAGTCAGGAAC
Hs-RORa-RT-fwd	ACTACACACCAGCATCAGGC
Hs-RORa-RT-rev	GCAGGTTTCCAGATGCGATT
Hs-REV-ERBa-RT-fwd	AGACATGACGACCCTGGACT
Hs- REV-ERBa-RT-rev	ATGGTGGGAAGTAGGTGGGA
Hs-RPLP0-RT-fwd	TGTGGGAGCAGACAATGTGG
Hs-RPLP0-RT-rev	CATTCCCCCGGATATGAGGC
m-Pck1-RT-fwd	AGGTGTCACCATCACGTCCT
m-Pck1-RT-rev	AGGTCTACGGCCTCCAAAGA
m-G6pc-RT-fwd	TTCAGGAAGCTGTGGGCATT
m- G6pc-RT-rev	CTTTCCCTGGTCCAGTCTCAC
m-Cry1-RT-fwd	CAACGTGGGCATCAACAGG
m-Cry1-RT-rev	GATGTTCCATTCCTTGAAAAGCC
m-Cry2-RT-fwd	TCGTCTGTGGGCATCAACC
m-Cry2-RT-rev	CCCATTCCTTGAACAGCCTT
m-Dbp-RT-fwd	GCTGCTTGGGCTGAGGAG
m-Dbp-RT-rev	TGAGGGCAGAGTTGCCTTG

*** Hs: Homo sapiens, m: Mouse, RT: Real-Time, fwd: Forward, rev: Reverse**

APPENDIX D: PROTEIN AND DNA MARKERS

DNA Size Marker: Thermo Scientific™ O'GeneRuler 1 kb DNA Ladder, Ready-to-Use- 250-10,000 bp

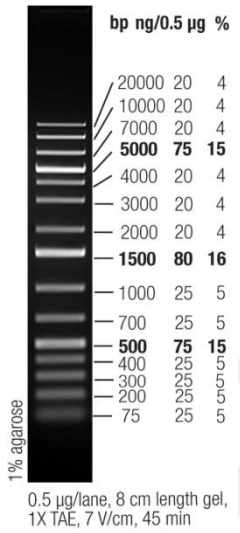

Protein Molecular Weight Marker: Thermo Scientific™ PageRuler™ Prestained Protein Ladder, 10 to 180 kDa

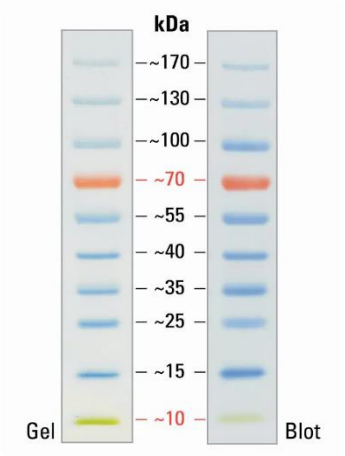

Biotinylated Molecules:

1. Biotinylated-TW68, Amb19577708, MW: 481.546, Formula:C28H27N5O3. (https://www.ambinter.com/molecule/19577708)
2. CP53, Amb3466646, MW: 568.442, Formula:C25H22BrN5O4S. (https://www.ambinter.com/molecule/3466646)
3. Biotinylated-CP53, Amb35883646, MW: 809.752, Formula:C35H37BrN8O6S2. (https://www.ambinter.com/molecule/35883646)

APPENDIX E: PERMISSIONS

For **Figure 2.3** the permission to reuse material was obtained from “Springer Nature” [91].

SPRINGER NATURE LICENSE TERMS AND CONDITIONS

Jun 14, 2023

This Agreement between Ms. Saliha Surme ("You") and Springer Nature ("Springer Nature") consists of your license details and the terms and conditions provided by Springer Nature and Copyright Clearance Center.

License Number	5567570365775
License date	Jun 14, 2023
Licensed Content Publisher	Springer Nature
Licensed Content Publication	Nature Reviews Genetics
Licensed Content Title	Transcriptional architecture of the mammalian circadian clock
Licensed Content Author	Joseph S. Takahashi
Licensed Content Date	Dec 19, 2016
Type of Use	Thesis/Dissertation
Requestor type	non-commercial (non-profit)
Format	print and electronic
Portion	figures/tables/illustrations
Number of figures/tables/illustrations	1
Would you like a high resolution image with your order?	no
Will you be translating?	no
Circulation/distribution	50000 or greater
Author of this Springer Nature content	no

Title	Discovery of Small Molecule: Regulates the Cryptochrome Stability and Controls Blood Glucose Levels in Diabetic Mice
Institution name	Koç University
Expected presentation date	Jul 2023
Portions	Figure 2.
	Ms. Saliha Surme Koç University, Sariyer, Istanbul
Requestor Location	
	Istanbul, 34550 Turkey Attn: Ms. Saliha Surme
Total	0.00 USD

For **Figure 2.4** the permission to reuse material was obtained from “ELSEVIER” [86].

ELSEVIER LICENSE TERMS AND CONDITIONS

Jul 04, 2023

This Agreement between Ms. Saliha Surme ("You") and Elsevier ("Elsevier") consists of your license details and the terms and conditions provided by Elsevier and Copyright Clearance Center.

License Number	5581920550064
License date	Jul 04, 2023
Licensed Content Publisher	Elsevier
Licensed Content Publication	Elsevier Books
Licensed Content Title	Advances in Protein Chemistry and Structural Biology
Licensed Content Author	Ibrahim Halil Kavakli,Nuri Ozturk,Ibrahim Baris
Licensed Content Date	Jan 1, 2022
Licensed Content Pages	27
Start Page	207
End Page	233
Type of Use	reuse in a thesis/dissertation
Portion	figures/tables/illustrations
Number of figures/tables/illustrations	1
Format	both print and electronic
Are you the author of this Elsevier chapter?	No
Will you be translating?	No
Title	Discovery of Small Molecule: Regulates the Cryptochrome Stability and Controls Blood Glucose Levels in Diabetic Mice
Institution name	Koç University

Expected presentation date	Jul 2023
Portions	Figure 3
	Ms. Saliha Surme
	Koç University, Sariyer, Istanbul
Requestor Location	
	Istanbul, 34550
	Turkey
	Attn: Ms. Saliha Surme
Publisher Tax ID	GB 494 6272 12
Total	0.00 USD

APPENDIX F: LABORATORY EQUIPMENT

Autoclaves:	CL-40S/SDP (60L) ALP autoclave
Centrifuges:	Microfuge 1-14K, Sigma Laboratory Microfuge 1-16K (refrigerated), Sigma Laboratory Allegra X-15R, Beckman Coulter
Deep freezes and refrigerators:	Premium U570 Ultra-Low Temperature Freezer, New Brunswick Scientific 1061 M refrigerator, Arcelik
Electrophoresis equipment:	Mini-Sub Cell GT, Bio-Rad. Mini-PROTEAN 3 Cell and Single-Row AnyGel Stand, Catalog # 165-3321, Bio-Rad
Gel documentation system:	ChemiDoc Touch Imaging System, Bio-Rad BlueLight Table (LED transilluminator), SERVA
Ice Machine:	AF 10, Scotsman.
Shaker:	Innova 4300 incubator shaker
Magnetic stirrer:	Heidolph MR 3001
Pipettes:	Finnpipette F1 1-10µl, F1 10-100µl, F1 100-1000µl, ThermoScientific
pH meter:	SevenCompact pH/Ion meter S220, Mettler Toledo
Power supply:	PowerPac Basic (300V, 400mA, 75W), Bio-Rad
Pure water systems:	DV25 Pure Lab Option, ELGA GenPure ultrapure water system, ThermoScientific
Microplate Reader:	Synergy H1 Hybrid Multi-Mode Microplate Reader, BioTek
Vortex machine:	Reax Top, Heidolph
CO2 Incubator:	Memmert INC108med
Incubator:	Incucell 111
Lumicycle:	LumiCycle 32 luminometer (Actimetrics)